

New Insights in Cellular Biochemistry
Owing to the Use of
Fluorescence Microspectroscopy

Jan Willem Borst

Promotor:

Prof. Dr. A.J.W.G. Visser

Hoogleraar in de Biochemische Microspectroscopie

Wageningen Universiteit

Samenstelling promotiecommissie:

Prof. Dr. P.I.H. Bastiaens (EMBL, Heidelberg Germany)

Prof. Dr. J. Feijo (Gulbenkian Institute, Oeiras Portugal)

Dr. A.B. Houtsmuller (Josephine Nefkens Institute, Erasmus Universiteit Rotterdam)

Prof. Dr. T. Bisseling (Wageningen Universiteit)

Prof. Dr. H. van Amerongen (Wageningen Universiteit)

Dit onderzoek is uitgevoerd binnen de onderzoekschool EPS

New Insights in Cellular Biochemistry Owing to the Use of Fluorescence Microspectroscopy

Jan Willem Borst

Proefschrift
ter verkrijging van de graad van doctor
op gezag van de rector magnificus
van Wageningen Universiteit,
Prof.dr. M.J. Kropff
in het openbaar te verdedigen
op woensdag 20 september 2006
des namiddags te half twee in de Aula.

New Insights in Cellular Biochemistry Owing to the Use of Fluorescence Microspectroscopy

Borst, Jan Willem

Thesis Wageningen University, The Netherlands

With references – With summary in Dutch

ISBN 90-8504-474-X

Voor mijn ouders

Aan Tanja, Anne en Thomas

Contents

Chapter 1	General Introduction	9
Chapter 2	Oxidation of Unsaturated Phospholipids in Membrane Bilayer Mixtures is accompanied by Membrane Fluidity Changes	27
Chapter 3	Imaging of Oxidative Stress in Plant Cells by Quantitative Fluorescence Microscopy and Spectroscopy	45
Chapter 4	Multiphoton Microspectroscopy in Living Plant Cells	55
Chapter 5	Heterodimerization and Endocytosis of <i>Arabidopsis</i> Brassinosteroid Receptors BRI1 and AtSERK3 (BAK1)	65
Chapter 6	Effects of Refractive Index and Viscosity on Fluorescence and Anisotropy Decays of Enhanced Cyan and Yellow Fluorescent Proteins	77
Chapter 7	Polarized Resonance Energy Transfer Spectroscopy reveals Structural Changes in the Calcium Sensor YC3.60	91
Chapter 8	Summarizing Discussion	103
	References	109
	Nederlandse Samenvatting	120
	List of Abbreviations	125
	Dankwoord	126
	Curriculum Vitae	129
	List of Publications	130

Chapter 1

General Introduction

1.1 Why microspectroscopy?

A living cell consists of a very complicated network of molecules. Actually, it can be viewed as a factory that contains an elaborate network of interlocking assembly lines composed of many protein machines (Alberts 1998). The internal organization of such a biomolecular network is dependent on the exchange of substances and information with its environment primarily via protein-protein or receptor-ligand interactions.

The field of genomics and proteomics can provide us with information about molecular compositions of cellular systems by using techniques like DNA sequencing, yeast two/three hybrid methods, immunoprecipitation, affinity chromatography, mass spectrometry and DNA/protein arrays. However, these techniques lack information about the dynamic assembly of the molecular machinery in living cells and organisms. To understand how a living cell processes information in response to external stimuli leading to, for example, cell proliferation, differentiation or programmed cell death, we need to gain insight in the spatial and temporal properties of biomolecular networks. This is exactly one of the main objectives of systems biology research. Systems biology aims to understand biology at the system level (Kitano 2002). To obtain insight in cellular function, research must then be shifted from isolated parts of the cell to structure and dynamics of biomolecular networks in the cell as a whole. Microspectroscopic techniques, which combine fluorescence spectroscopy with optical microscopy, are the methods of choice for this purpose. These techniques and methods can provide direct information on molecular interactions and dynamic events involving biological molecules with minimal perturbation of cellular integrity and function.

The dimensions of protein machines and signaling domains vary from 5 to 50 nm covering the experimental range of electron microscopy and, partly, optical microscopy. Electron microscopy has the highest spatial resolution, but is an invasive technique only applicable to fixed, specially prepared cells and tissues. On the other hand, fluorescence microscopy including the genetically encoded visible fluorescent protein (VFP) technology in particular, has all non-invasive capabilities for real-time live cell imaging. Although the resolution of optical microscopy is light-diffraction limited (~ 250 nm), it is sufficient to observe many features of live cells, but not to disclose structural features of individual biomolecules in their natural habitat. The success of system biology research depends very much on the technological progress in the development of microspectroscopic contrast schemes to image networks of molecules in living systems (Kitano 2002).

During the last decade we have observed a revolutionary development in state-of-the-art microspectroscopic techniques. The applications of these technologies in cell biology

have yielded new, detailed information on biomolecular interactions and their roles in signal transduction networks. Existing spectroscopic methods such as fluorescence lifetime measurements and Förster resonance energy transfer (FRET) have been introduced in fluorescence microscopy to realize fluorescence lifetime imaging microscopy (FLIM) for the observation of FRET. The distance range for FRET is 1-10 nm providing spatial information about two proteins that is 200-20x better than the diffraction limit of optical microscopy. FRET is very suitable to measure protein-protein interactions via the shortening of the donor excited-state lifetime in supra-molecular protein machines such as transcription factors, oligomeric receptors, signal-transducing assemblies, ribosomes, molecular motors, etc. Furthermore, the development of optical biosensors based on FRET technology can provide information about intracellular biochemical processes such as caspase activity, phosphorylation state of signaling proteins, or the detection of calcium concentrations. Advances in confocal microscopy techniques have resulted in single-molecule sensitivity as applied in fluorescence correlation spectroscopy (FCS). Molecular interactions of longer range than FRET can then be measured with a two-color cross-correlation variant of FCS (FCCS), when pairs of labeled proteins move synchronously through a confocal volume element of a focused laser beam.

The purpose of this chapter is to give an introduction to different microspectroscopic techniques and their applications starting with basic principles of fluorescence, a survey of available fluorescent probes and details of time-resolved fluorescence spectroscopy and microscopy.

1.2 Basic principles and parameters of fluorescence

1.2.1 Jablonski diagram

The phenomenon of fluorescence was first described by Sir George Gabriel Stokes in 1852 (Stokes 1852). Stokes reported on the shift of the fluorescence spectrum to lower energy relative to the absorption spectrum, now better known as the ‘Stokes shift’. In that time sunlight was used as excitation source and the fluorescence light intensity was measured via color glass filters. Nowadays, fluorescence spectroscopy is often used in chemistry, physics and biology because this technique can supply unique information about molecular properties and behaviour. It is a very sensitive technique and the temporal dynamic range of fluorescence overlaps with the time range of molecular interactions and chemical reactions. Fluorescence is a process that occurs in certain molecules (poly-aromatic hydrocarbons and/or heterocyclic compounds). In general these molecules are called fluorophores or fluorescent dyes. These molecules are able to absorb light (and are therefore called chromophores) to raise an electron to an excited state. The excess of energy can be converted to the emission of light or fluorescence. The principle can be illustrated with the Jablonski energy diagram (see Fig. 1.1) where the (relative) energy scale is in a vertical direction and transitions between the different energetic states are depicted with arrows. The Jablonski diagram is a helpful scheme for illustrating the pathways, kinetics and spectra of light absorption, fluorescence and phosphorescence (Lakowicz 1999; Valeur 2002; Jiskoot *et al* 2005). The absorption-fluorescence process is cyclic, unless the fluorophore is irreversibly destroyed by continuous light excitation. The long-lived triplet state provides ample opportunity for fluorophores to

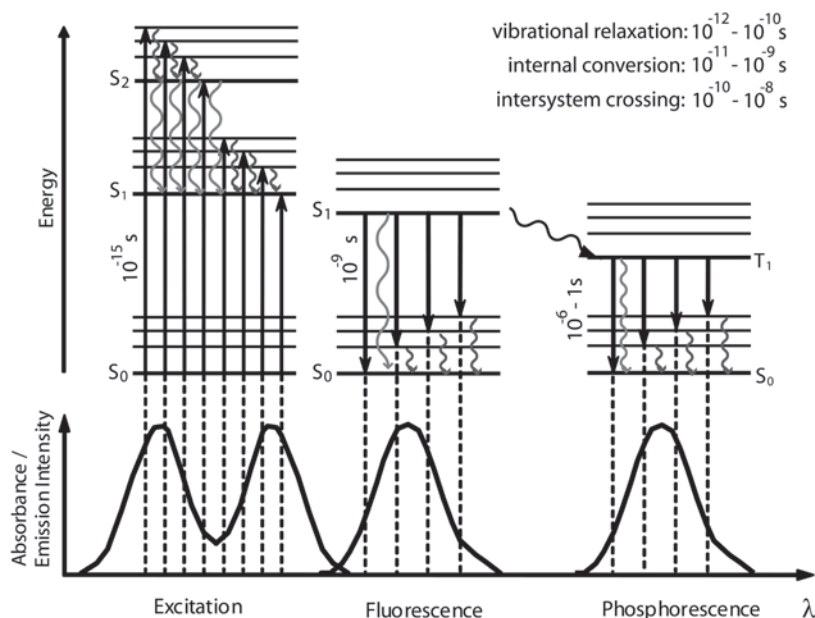


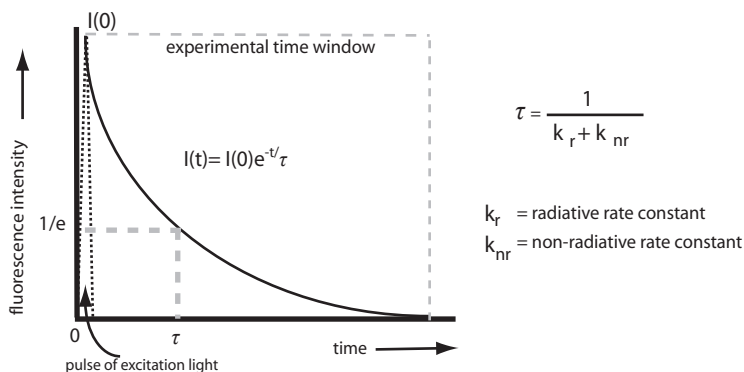
Figure 1.1: The Jablonski energy diagram (top) and schematic illustration of the relative positions of absorption, fluorescence and phosphorescence spectra (bottom). Light absorption and emission are represented by vertical, black arrows. Vibrational relaxation, internal conversion and intersystem crossing are indicated by light gray undulated arrows. In this particular diagram the electronic states are shown for an arbitrary aromatic molecule: the singlet ground state second electronic excited states (S_1 and S_2) and the triplet state (T_1), respectively. Typical time scales of the different processes are indicated. The absorption of a photon results in the transition to a vibronic excited state of either S_1 or S_2 . Vibrational relaxation occurs within each electronic state. Internal conversion is a non-radiative process from one higher energy electronic state to a lower one. The emission of a longer wavelength photon of the molecule starting from the lowest vibrational level of S_1 and ending in one of the vibrational levels of S_0 is known as fluorescence. An electron in the S_1 state can also undergo a spin conversion accompanied by transfer to the T_1 state (intersystem crossing). Emission from T_1 , known as phosphorescence, is generally shifted to longer wavelengths relative to the fluorescence and only detectable in vitrified solutions.

interact with other molecules to produce irreversible covalent modifications. This process, also called photobleaching, is induced under high intensity illumination conditions. In addition, when oxygen is present, triplet state energy can be transferred to oxygen producing highly reactive singlet oxygen. The most effective remedy to reduce photobleaching is to maximize the detection sensitivity and to reduce excitation power in any experiment.

1.2.2 Quantum yield and fluorescence lifetime

Two important and measurable parameters in fluorescence are the fluorescence quantum yield (Q) and the fluorescence lifetime (τ) of a potentially fluorescent molecule. The quantum yield can be defined as the ratio between the number of emitted photons and the number of absorbed photons. The quantum yield gives the probability of light emission relative to that of energy losses and varies between zero and one. The most commonly used fluorescent molecules have quantum yields between 0.2 and 0.9. For instance, green fluorescent protein (GFP) has a quantum yield of about 0.7. In general, for microspectroscopy applications it is desirable to use fluorophores with high quantum yields and high molecular extinction coefficients at the excitation wavelength.

- A) The fluorescence lifetime (τ) provides a time window for the detection of dynamic processes



- B) Dynamic processes that compete with fluorescence

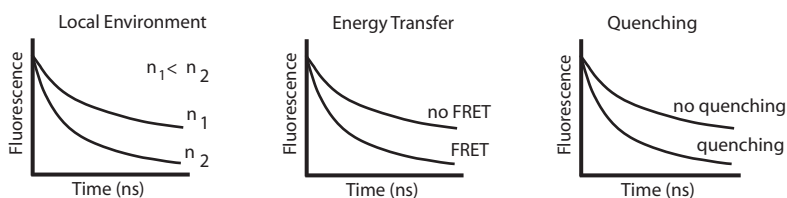


Figure 1.2: A. Fluorescence intensity decay (solid line) after excitation with a light pulse (dotted curve). The lifetime (τ) is indicated as the time, when fluorescence intensity reaches $1/e$ of its initial value. The fluorescence lifetime is determined by interplay of radiative and non-radiative decay rates where k_r is the radiative rate constant and k_{nr} the non-radiative rate constant. B. The fluorescence lifetime can be affected by changes in local environment (e.g. differences in refractive index of the solvent) or dynamic processes such as energy transfer and quenching.

The other parameter is the fluorescence lifetime (τ), which can be defined as the characteristic time that a fluorophore resides in the excited state before returning to the ground state while emitting a photon. Depending on nature and photophysical properties, each fluorophore has a typical fluorescence lifetime in the range of 100 ps - 100 ns. The fluorescence lifetime can be affected by the local environment (for instance refractive index (Suhling *et al* 2002a; Borst *et al* 2005)) or by interactions with other molecules through collisions (quenching) or FRET (Suhling *et al* 2005) (see Fig. 1.2). Therefore, fluorescence lifetime measurements will yield information about these processes and local conditions. Fluorescence lifetimes can be determined by experiments in either a cuvette or a light microscope. The latter technique is called fluorescence lifetime imaging microscopy, which combines a fluorescence lifetime measurement with the spatial resolution of a microscope.

1.2.3 Fluorescence anisotropy and depolarization

Fluorescence anisotropy makes use of polarized light excitation and detection of polarized fluorescence. The amount of depolarization of the emitted light is expressed in the value of the fluorescence anisotropy. Fluorescence anisotropy measurements supply information about molecular dynamics and energy transfer of fluorescent molecules. When the excitation light is linearly polarized, the fluorophores with the absorption dipole moment aligned parallel to the polarization plane of the incident light are preferentially excited. This is called photoselection. The extent of polarization of the fluorescence emission can be best described in terms of anisotropy (r) (Lakowicz 1999; Valeur 2002).

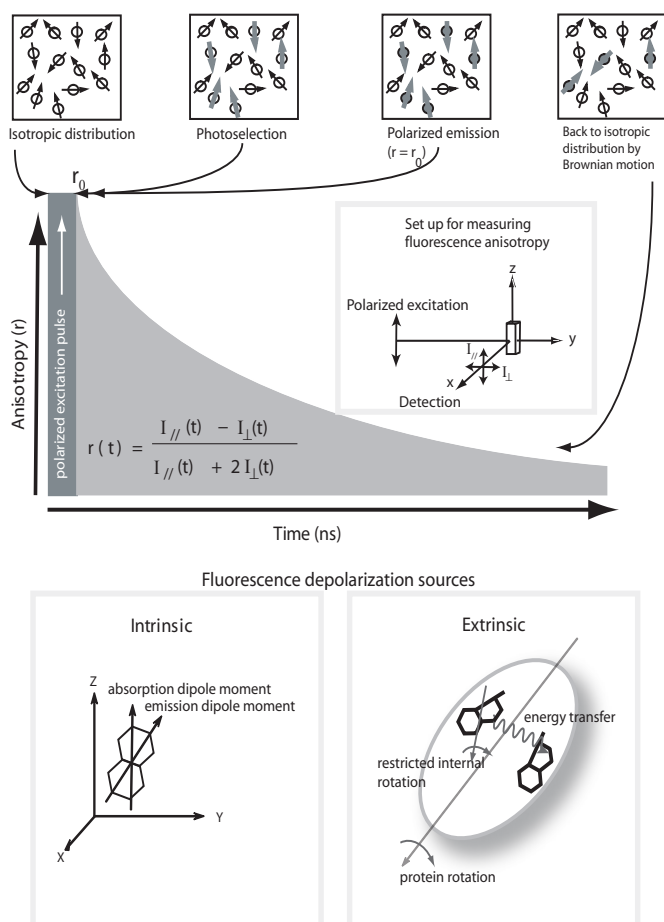


Figure 1.3: Fluorescence anisotropy decay after excitation with a polarized light pulse (top). Only a fraction of the isotropically distributed fluorophores can be excited by linearly polarized light (a process called photoselection). The fluorophores having the absorption dipoles parallel to the electric field of the excitation light are most probably excited. The immediately created emission is also polarized. The extent of polarization is expressed by a quantity known as the fluorescence anisotropy (r), which is measurable and defined as indicated. The fundamental anisotropy (r_0) is reached immediately after pulse excitation. Rotational motions of the fluorophores during the excited-state lifetime lead to a loss of memory of being photoselected, return to isotropic distribution and a decrease of anisotropy. Schematic illustration of intrinsic and extrinsic fluorescence depolarization processes (bottom).

Fluorescence anisotropy is defined as the ratio of the difference between the fluorescence emission intensity parallel (I_{\parallel}) to the polarization of the electric vector of the exciting light and that perpendicular (I_{\perp}) to that vector ($I_{\parallel} - I_{\perp}$) divided by the total intensity ($I_T = I_{\parallel} + 2 I_{\perp}$) (see Fig. 1.3).

The rotational motion of a fluorescent molecule taking place during the lifetime of the excited state is one source of depolarization and will influence the observed anisotropy. The rate of rotation is dependent on size and shape of the fluorescent molecule or protein complexes and the viscosity of the environment. In time-resolved measurements in case of spherically shaped molecules the fluorescence anisotropy can be described as a single exponential decay process with rotational correlation time ϕ as the characteristic time. Internal restricted molecular reorientation and energy transfer between identical molecules are other sources of depolarization. Under constant illumination conditions the steady-state fluorescence anisotropy of a fluorophore is related to the Perrin equation ($r_0/r = 1 + \tau/\phi$, where r_0 is the limiting anisotropy, ϕ the rotational correlation time and τ the fluorescence lifetime of the probe).

1.2.4 Förster Resonance Energy Transfer (FRET)

The quantification of molecular interactions or conformational changes can be conveniently studied by using FRET as a spectroscopic ruler. During FRET energy is transferred from a donor to an acceptor molecule when they are in close proximity as illustrated in figure 1.4.

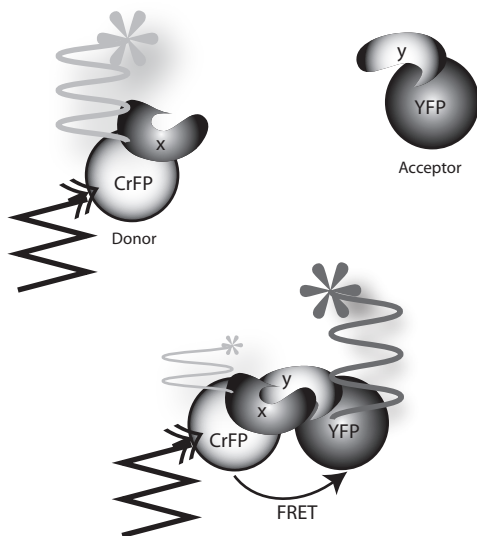


Figure 1.4: Pictorial view of the FRET principle. When two protein molecules labeled with one fluorescent donor protein (CrFP) and one fluorescent acceptor protein (YFP) are in close proximity (<10 nm) resonance energy transfer can occur. This results in a decrease in fluorescence emission intensity of the donor and sensitized emission of the acceptor.

Resonance energy transfer was first correctly described by Theodor Förster (1948) as a photophysical process where the excited-state energy from a donor molecule is transferred non-radiatively to an acceptor molecule via weak dipole-dipole interactions (Förster 1948). One condition for the occurrence of FRET is spectral overlap between the fluorescence emission spectrum of a donor molecule and the absorption spectrum of an acceptor molecule. Therefore a proper selection of donor and acceptor molecules is crucial. Furthermore, energy transfer will only occur, when the donor and acceptor are within a small distance from each other (typically <10 nm). The energy transfer efficiency is proportional to the reciprocal of the sixth power of the intermolecular distance (R). The so-called critical (or Förster) radius (R_0) is the distance between donor and acceptor, at which the energy transfer efficiency is 50%. Because FRET is based upon dipolar interactions, both distance and orientation between donor and acceptor transition dipoles are determining factors. The concepts of FRET and relevant equations are summarized in figure 1.5.

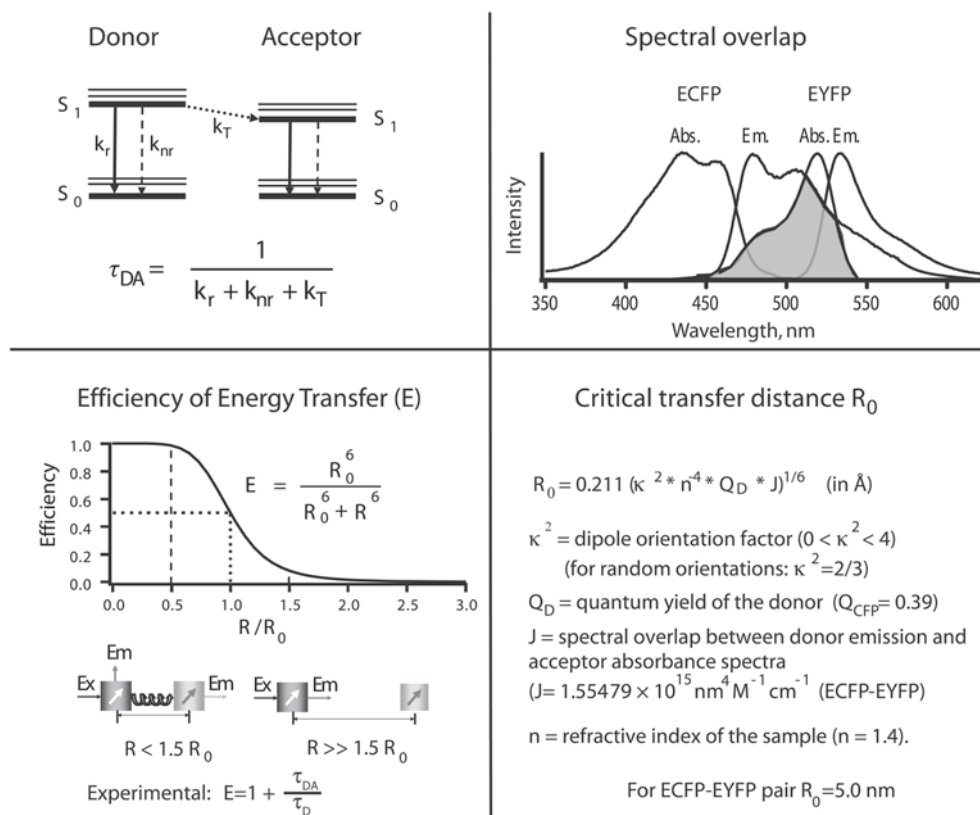


Figure 1.5: Summary of FRET principles. When a donor and acceptor are in close proximity energy transfer can take place leading to an additional relaxation pathway (k_T) (top left). Some prerequisites for FRET are spectral overlap between donor emission and acceptor absorption spectra (top right), small distance between donor and acceptor and finite dipole orientation factor. These parameters determine the critical transfer distance (R_0), which is characteristic for each FRET pair (bottom right). The efficiency of energy transfer can be related to relative distance and experimentally determined from lifetime measurements (bottom left).

1.3 Fluorescent probes

1.3.1 Synthetic fluorescent probes

At present many fluorescent probes have been designed and synthesized to follow specific processes in cellular systems (<http://probes.invitrogen.com/handbook>). The choice for an appropriate fluorescent probe depends on the particular system and purpose of the experiment. In addition, selection of the proper fluorescent dye combination allows multicolor detection by staining multiple targets in the same sample. Several synthetic probes are not only used for the staining of DNA, membranes or proteins in cells, but can also report on physiological and other parameters. In chapters 2 and 3 of this thesis some examples of the effect of lipid oxidation on some properties of artificial and natural membrane bilayers are presented.

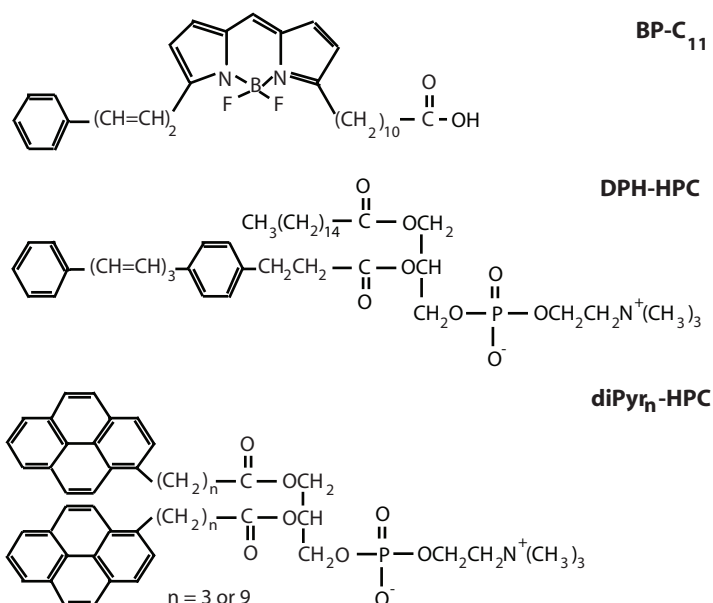


Figure 1.6: Chemical structures of the fluorescent probes used in research described in chapters 2 and 3.

For the detection of the oxidation rates of the unsaturated lipids, the lipid probe BODIPY-C11 (Fig. 1.6) was used (Pap *et al* 1999). This probe can be conveniently excited in the visible range using readily available laser lines. Upon oxidation of one of the double bonds in the probe the fluorescence emission shifts from red to green. Other fluorescent lipid probes like pyrenyl- and diphenylhexatriene (DPH) labeled phospholipids can give detailed information about microfluidity in artificial membranes (Fig. 1.6). Pyrene-containing phospholipids can report on lateral mobility of lipids because of the ability of forming excimers between one pyrene molecule in the excited state (Pyr*) and another one in the ground state (Pyr) (Förster and Kasper 1955). The excimer (Pyr-Pyr*) fluorescence is at longer wavelengths than the monomer fluorescence. The ratio of excimer to monomer emission intensities (E/M) is a measure of the rate of excimer

formation, which is determined by the frequency of collisions between pyrene moieties and hence can be related to parameters describing membrane dynamics and organization. DPH is also a lipophilic probe and has been proven to be very sensitive for probing membrane fluidity. A whole palette of fluorescent biosensors and indicators is now available. These indicators can be equipped with a reactive group to label proteins, DNA or be integrated in membranes. Proteins can be genetically extended with a tetracysteine motif for labeling with fluorescent bi-arsenical dyes (Griffin *et al* 1998; Martin *et al* 2005). Another development in fluorescent probes is the introduction and further optimization of quantum dots. Quantum dots are small colloidal semiconductor nanocrystals. The size and shape of these crystals, which can be precisely controlled, determine the absorption and emission properties. The main advantages of quantum dots are i) a very narrow emission bandwidth, ii) non-toxicity because of a protecting polymeric shell, iii) superior photo-stability and iv) the suitability for two-photon excitation (reviewed in Michalet *et al* 2005). The main disadvantages are the size of the probe (about 2-20 nm) and the coupling of specific peptides or proteins to the quantum dot requiring very specific and elaborate chemical synthesis.

1.3.2 GFP technology

A genetically encoded fluorescent probe is the green fluorescent protein (GFP) from the jellyfish *Aequorea victoria*. The application of the GFP technology has been of crucial importance for imaging of intracellular proteins (Tsien 1998). Several differently colored GFP mutants have now been developed and have found widespread application as natural, brightly fluorescent markers in cell biology. Currently, fluorescent proteins, also from coral species, emitting from violet to red are available (Shaner *et al* 2004; Verkhusha and Lukyanov 2004; Shaner *et al* 2005) enabling to track differently labeled proteins simultaneously in the cell.

Different pairs of the fluorescent proteins are widely used as donor-acceptor pairs in FRET applications. So far, the enhanced forms of cyan fluorescent protein (ECFP) and yellow fluorescent protein (EYFP) are the most commonly used FRET pair in cell biology. Recently, a monomeric and improved version of ECFP, mCerulean, has been developed, which is 2.5 times brighter than ECFP (Rizzo *et al* 2004). In combination with the improved YFP version called 'Venus', mCerulean-Venus is then an improved FRET pair for imaging protein-protein interactions *in vivo*. Another frequently used combination is EGFP and the *Discosoma* (from coral species) red fluorescent protein, DsRED, or related red fluorescent protein (RFP). The disadvantage of DsRED as an acceptor is the maturation time, which is about four times longer than for EGFP and its tendency to form tetramers (Baird *et al* 2000). Furthermore, DsRED has a 'green' absorption band, which overlaps with the absorption band of EGFP. Direct excitation of DsRED will then perturb intensity-based FRET imaging. Several different red fluorescent proteins, dimer and monomer versions of DsRED have been cloned even extending the color to the near-infrared (Campbell *et al* 2002; Zhang *et al* 2002; Shaner *et al* 2004; Shaner *et al* 2005). Studies of proteins tagged with EGFP and monomeric RFP (mRFP) have already shown that this is a good pair for FRET-FLIM applications (Peter *et al* 2005). At this moment the current selection of fluorescent proteins contains bright, monomeric, spectral variants that can be used in future studies of multi-color imaging and FRET detection (Chapman *et al* 2005).

Different biosensors based on GFP technology were developed, like the ‘cameleons’ for *in vivo* measurements of calcium concentrations. These genetically encoded fluorescent calcium indicators do not require any cofactors and are targetable to specific intracellular locations (Miyawaki *et al* 1997; Miyawaki *et al* 1999). Calcium is a very important ion in cellular signalling, since it acts as an essential second messenger. Ca^{2+} signals are found in the cytosol and different organelles, but these signals are often difficult to measure. To overcome this problem the so-called cameleon (YCam) was developed consisting of a tandem fusion of ECFP, a calmodulin domain having four calcium binding sites, a calmodulin binding peptide M13 and EYFP (Miyawaki *et al* 1997; Varadi and Rutter 2002). The level of intramolecular FRET is dependent on the extent of Ca^{2+} binding to the calmodulin. Binding of calcium ions makes calmodulin wrap around the M13 domain resulting in an increase of the FRET efficiency. The dynamic Ca^{2+} concentration range of these cameleons vary from 10^{-8} to 10^{-2} M. Several variants of the cameleon sensors are currently available and are continuously improved. The latest versions are pH independent and consist of the brighter EYFP variant Venus (Evanko and Haydon 2005). The important benefit of YCams is that EYFP and ECFP fluorescence intensities can be measured simultaneously in two different detection channels of a fluorescence microscope. This enables ratio imaging so that relative calcium concentration changes can be measured in real time.

Motional dynamics and chemical reaction kinetics of proteins equipped with fluorescent proteins in living cells can be investigated using techniques like fluorescence recovery after photobleaching (FRAP) and fluorescence correlation spectroscopy (FCS) (Lippincott-Schwartz *et al* 2001; Hess *et al* 2002). FCS will be briefly addressed later in paragraph 1.5.4.

The engineering of photoactivatable (PA) or photoswitchable GFP variants have led to new selective methods for studying dynamic processes in living cells. Photoactivation is the rapid conversion of initially ‘dark’ molecules to a fluorescent state by intense irradiation (Patterson and Lippincott-Schwartz 2002). The first PA-GFP appears to be almost non-fluorescent, but after illumination with 405-nm laser light the protein becomes activated resulting in bright green fluorescence upon 488 nm excitation. Using this photoactivation methodology cellular trafficking of the fluorescent PA-GFP can be monitored in time when the protein is photoactivated in a specific region of the cell. There are now several different PA-GFP’s available. One of the variants is the photoswitchable fluorescent protein ‘DRONPA’. This protein can be switched ‘on’ and ‘off’ by using illumination of either 405 or 488 nm laser light (Ando *et al* 2004). In single-molecule detection measurements of DRONPA the switching process could be performed more than 100 times (Habuchi *et al* 2005). There are also photoconvertible proteins like ‘Kaeda’. This protein emits green fluorescence by illumination with 488-nm light but can be converted to red fluorescence after illumination with 561-nm laser light. The latter process is irreversible after irradiation 561-nm laser light. Recently it has been shown that PA-GFP can also be activated by two-photon excitation (Post *et al* 2005; Chen *et al* 2006).

1.4 Instruments and Methods

1.4.1 Fluorescence lifetime measurements

There are two different techniques for measuring fluorescence lifetimes, phase and pulse fluorometry (for principles and details see: (Lakowicz 1999; Valeur 2002)). One popular pulse-based technique for the determination of fluorescence lifetimes is time-correlated single photon counting (TCSPC). This method has been introduced in the late 1960s and further optimized thereafter for measuring fluorescence decays with high time resolution and sensitivity (O'Connor and Phillips 1984; Becker *et al* 2004; Becker 2005).

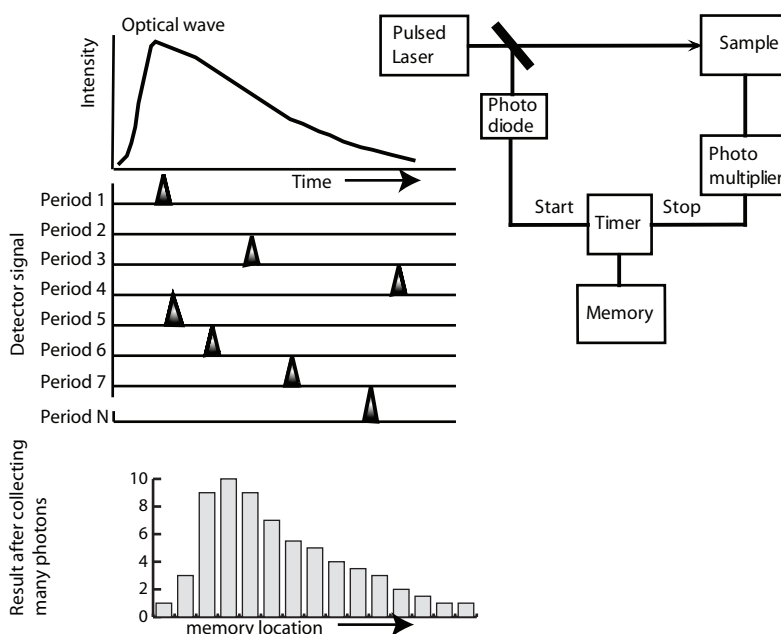


Figure 1.7: Time-correlated single photon counting principle. The detector-arrival times of the first emitting photons are recorded as a function of time with respect to the corresponding laser pulse. Many arrival times are measured after accumulation of photon events in sequential periods. The measured times are addressed in a histogram of arrival times per memory location. This is equivalent to the fluorescence intensity versus time curve.

Currently, the technique makes use of high-frequency, ultra-short laser pulses from mode-locked lasers for excitation, while the arrival times of single fluorescent photons are repeatedly detected with respect to the corresponding laser excitation pulse. Many arrival-time events are registered and stored in computer memory resulting in the reconstruction of a histogram of fluorescence intensity versus time (see Fig. 1.7). The fluorescence photons pass through a specific emission filter and are detected with a very sensitive microchannel-plate photomultiplier having high time resolution. The photon pulses from the detector are collected by a special data acquisition card, which is synchronized by the input of the laser pulses. The single-photon timing principle can also be applied in combination with a confocal laser scanning microscope, so that the fluorescence lifetimes will be spatially resolved.

1.4.2. One- and two-photon excitation

Upon the absorption of a photon the electronic configuration of a chromophore changes from the lower-energy configuration (ground state) to that of the excited state (see Fig. 1.1). The energy necessary to make this transition possible can be provided by a single photon, but as Maria Göppert-Mayer (1931) has shown theoretically, it is also possible to create this transition by the quasi-simultaneous absorption of two photons with approximately half of the energy (Göppert-Mayer 1931; Zipfel *et al* 2003). To fulfil two-photon excitation (TPE) processes, the photon density must be sufficiently high, requiring compression of photons in time and space, which can be achieved with ultra-short, high-energy light pulses in a sharply focussed laser beam. For this reason TPE was introduced for the first time in an optical microscope (Denk *et al* 1990).

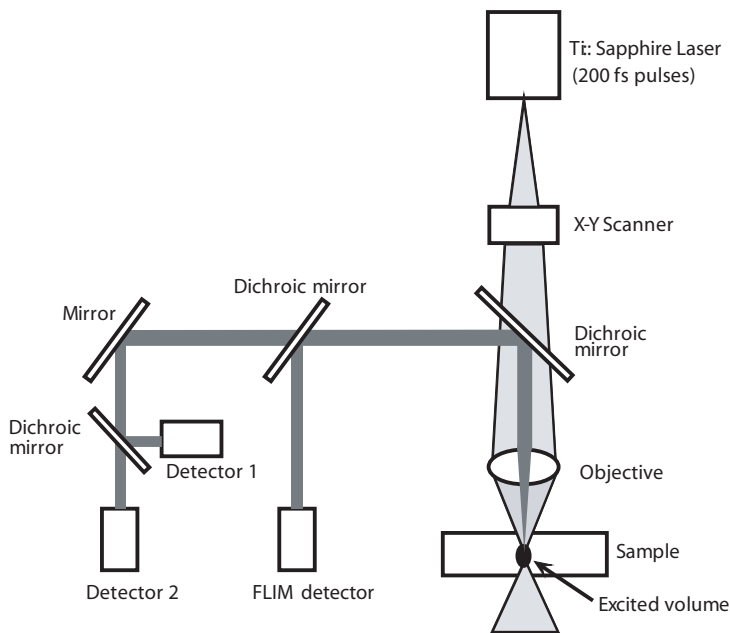


Figure 1.8: Schematic representation of a two-photon excitation microscope in combination with fluorescence lifetime imaging. The excitation path is indicated in light gray, the emission path is in dark gray.

In a TPE microscope fluorescence is only induced in the diffraction-limited spot where the excitation event takes place (see Fig. 1.8). In a regular confocal microscope using one-photon excitation (OPE) the fluorescence spot is focussed through a pinhole blocking the out-of-focus light. At first glance the optical resolution of a TPE microscope seems to be worse by a factor of two as compared to OPE confocal microscopy, because the excitation light is at twice the wavelength. However, since the pinhole opening in a confocal microscope is not infinitely small but is opened to a certain extent, the resolution difference for the two cases becomes less noticeable (Booth and Wilson 2001). The effective spatial resolution achieved is a function of many parameters leading to a TPE microscopic resolution close to the one obtained with a OPE confocal microscope (Gerritsen and De Grauw 1999; Zipfel *et al* 2003,

Cox and Sheppard 2004). TPE microscopy has some major advances over OPE confocal microscopy. First, the penetration of the near-infrared light used for TPE is much deeper than that of visible light used in OPE confocal microscopy. TPE of thick biological samples allows imaging to a depth of more than 200 μm whereas OPE confocal microscopy is limited to depths of approximately 50 μm (Piston 1999). Furthermore, TPE occurs only in the focal spot and therefore the amount of photobleaching out of that region is strongly suppressed. In addition, long-wavelength excitation scattering is much less than in OPE microscopy.

1.5 Monitoring molecular interaction *in situ*

The question, whether the oligomeric state of a protein is monomeric, dimeric, or multimeric can be addressed and answered by several approaches. The phage display method and/or yeast two-hybrid system are the most significant examples (Causier and Davies 2002; Burch *et al* 2004). However, these methods have the disadvantage that they lack spatial information, because they cannot be applied to proteins in their natural habitat. The introduction of high-resolution confocal microscopy gave the opportunity to investigate the co-expression of different proteins in their natural environment. The optical resolution of a microscope allows detection of fluorescent molecules at sub-cellular level. At most, co-localization of two proteins equipped with two different fluorophores can be established, but physical interactions between proteins on nanometer scale cannot be determined. One possibility to go beyond that optical limitation is to apply FRET microscopy. FRET can be visualized by confocal or wide-field fluorescence lifetime imaging microscopy (FLIM).

1.5.1 Intensity-based FRET imaging in a microscope

The combination of optical microscopy with FRET spectroscopy provides quantitative, temporal and spatial information about binding and interaction of proteins *in vivo* (Herman 1998; Wallrabe *et al* 2003). FRET can be quantified using steady-state or time-resolved fluorescence techniques. In the steady-state approach the fluorescence intensities of fluorescent donor and fluorescent acceptor are monitored in a fluorescence microscope. This steady-state approach relies on the observation that the fluorescence intensity of the donor is reduced and that of the acceptor is enhanced when energy transfer takes place. The disadvantage of this approach is that the signals are highly dependent on the local concentrations of donor and acceptor molecules. Photobleaching needs to be avoided, because it alters the effective donor and acceptor concentrations. Artefacts like bleed-through of the donor fluorescence in the acceptor detection channel and direct excitation of the acceptor also need to be taken into account for quantitative analysis. In several publications corrected FRET imaging methods have been demonstrated and further improved (Gordon *et al* 1998; Xia and Liu 2001; Hoppe *et al* 2002).

1.5.2 Acceptor photobleaching

Acceptor photobleaching (APB) is an alternative method in which FRET can be used to examine intracellular molecular interactions between proteins. The method has been applied in several studies (Lippincott-Schwartz *et al* 2001). APB is not only restricted to intensity-based fluorescence microscopy, but can also be applied to fluorescence lifetime imaging microscopy (FLIM) (Wouters and Bastiaens 1999).

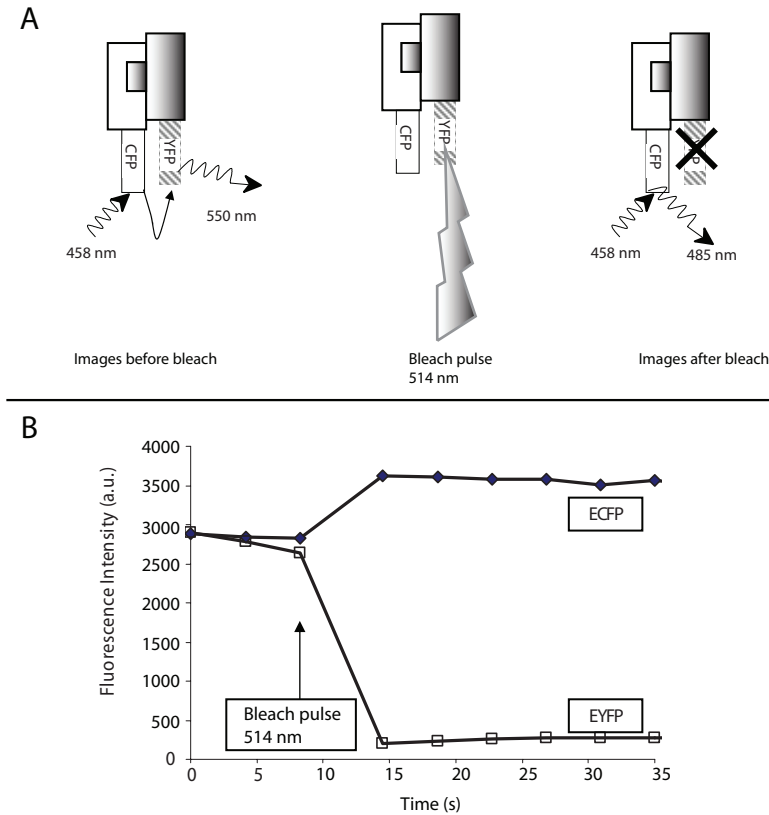


Figure 1.9: Acceptor photobleaching principle. A. Fluorescence intensity images are taken before and after a strong photobleach pulse, which irreversibly destroys the acceptor molecule (EYFP). B. Plot of measured integrated fluorescence intensities of donor (ECFP) and acceptor (EYFP). The energy transfer efficiency (E) before the bleaching can be calculated according to $E = (I_{DA} - I_{DB}) / I_{DA}$ where I_{DB} is the fluorescence intensity of the donor before bleaching and I_{DA} is the fluorescence intensity after bleaching.

APB is often employed to prove the occurrence of FRET. APB measurements in a confocal microscope have been critically assessed by Karpova and colleagues (Karpova *et al* 2003). They describe APB experiments using a confocal laser scanning microscope, which is not only able to selectively excite both fluorophores, but can also selectively photobleach the acceptor fluorophore. The fluorescence intensities of donor and acceptor are determined before and after applying a highly intense laser pulse that irreversibly photobleaches the acceptor fluorophore. When donor and acceptor molecules interact, the destruction of the acceptor fluorophore will result in increased donor fluorescence intensity, since the energy cannot

be transferred any more to the acceptor molecule (see Fig. 1.9). The measurement of FRET efficiencies by the APB approach requires several checkpoints. First, selective bleaching of the acceptor is required, because bleaching of the donor will result in underestimation of donor dequenching (Lippincott-Schwartz *et al* 2001; Voss *et al* 2005). Second, APB is still an intensity-based approach and therefore it is sensitive for donor and acceptor concentrations. By using a FRET indicator where only one ECFP and one EYFP molecule are connected by a linker this problem can be avoided. Third, the method is very often confined to fixed cells because of rapid diffusion of fresh acceptor molecules in the bleached area and rapid recovery of acceptor fluorescence.

1.5.3 Fluorescence Lifetime Imaging Microscopy (FLIM)

For the quantification of protein-protein interactions by means of FRET several methods are available. In paragraph 1.5.1 and 1.5.2 the intensity-based methodologies are described. However, these methods show severe disadvantages because the results are very much dependent on differences in local probe concentrations and removal of experimental artefacts addressed in previous paragraphs. An alternative method is fluorescence lifetime imaging microscopy (FLIM), which measures the fluorescence lifetime pixel by pixel in a fluorescence image. FLIM overcomes problems of intensity-based methods, since only the fluorescence lifetime of the donor molecule is determined. Molecular interaction between donor and acceptor will result in the quenching of donor fluorescence. This donor fluorescence quenching will result in a decrease of the fluorescence lifetime, since energy transfer will introduce an additional relaxation path from the excited state to the ground state (see Fig. 1.5). The amount of reduction is directly correlated with the FRET efficiency E via $E = 1 - \tau_{DA}/\tau_D$ where τ_{DA} is the fluorescence lifetime of the donor in the presence of acceptor and τ_D is the fluorescence lifetime of the donor alone. FLIM combines fluorescence lifetime measurements with microscopic resolution resulting in spatially resolved fluorescence lifetimes.

1.5.4 Fluorescence Correlation Spectroscopy (FCS)

In previous paragraphs microspectroscopic approaches like FRET or fluorescence anisotropy have been described that provide information on protein-protein interactions and protein dynamics. Fluorescence fluctuation techniques, such as fluorescence correlation spectroscopy (FCS) and photon counting histogram (PCH) analysis, have been developed as complementary methods to measure dynamics and brightness distribution of fluorescently labelled molecules under equilibrium conditions (Hink *et al* 2003a; Hink 2002). FCS experiments are performed using a confocal microscope equipped with an objective of high numerical aperture in combination with a very sensitive photodetector (for instance an avalanche photodiode) (Hink *et al* 2000). The focused laser beam illuminates a sub-femtoliter volume element. Due to Brownian motion, single molecules will move in and out of this volume element resulting in fluctuations of the fluorescence intensity. The observed intensity traces are autocorrelated over time and analyzed with appropriate model functions. The fluorescence intensities can be detected from nanomolar amounts of molecules, which make this technique ideal to study molecules under physiological conditions. FCS operates at the single-molecule detection level. Several review articles and a book are available describing theory and applications of

FCS in large detail (Rigler and Elson 2001; Hess *et al* 2002; Schwille and Haustein 2002). FCS is increasingly applied in living cells (Hink 2002; Engel 2005 and references therein). Most studies are concerned with the determination of diffusion constants of fluorescent proteins, since this quantity may reflect its aggregation state or microviscosity. In addition, the absolute concentration of fluorescent molecules can be determined. Careful analysis of the autocorrelation curves even allows measuring rates of chemical reactions or conformational relaxations. To increase the selectivity for interacting molecules the standard one-detector configuration of a FCS setup, can be extended to a two-channel FCS instrument. When each of the interacting molecules is now labeled with different dyes two-color intensity traces can be simultaneously detected and cross-correlated. The amplitude of the cross-correlation curve can be directly related to the number of interacting species (Hink *et al* 2003a).

1.6 Outline of this thesis

New developments in the detection of biological processes in combination with fluorescence microspectroscopy give deeper insight in the spatio-temporal behaviour of molecular components in the cell. Classical biochemical approaches have been proven to be valuable for identification and physical isolation of proteins. The localization of these proteins in cells can be established using standard fluorescence immuno-staining techniques. Real-time live cell imaging provides the time as an additional dimension and has evolved as an important approach in cell biology to monitor cell dynamics (Lippincott-Schwartz *et al* 2001; Hink *et al* 2002). Nowadays, localization and dynamics can be connected with cellular properties like active state and mobility of proteins, oxygen, calcium or proton fluxes. In this way many different biological questions can be addressed (Wouters *et al* 2001). To visualize and quantify proteins of interest, advanced spectroscopic techniques are combined with microscopy and biosensors, so that specific molecular information of cells can be retrieved (Bunt and Wouters 2004). These applications were stimulated by the visible fluorescent protein technology (Tsien 1998; Matz *et al* 1999). GFP can be coupled to the protein of interest via genetic approaches. The fluorescence of the transcribed proteins can be detected within several hours after transfection. This thesis describes several microspectroscopic applications in order to detect and probe molecular interactions and biochemical processes *in situ*. To obtain quantitative information on *in situ* interactions and dynamics of biological molecules, it was also required to conduct cuvette-type of fluorescence experiments of the purified fluorophores and fluorescent proteins in well-defined model systems.

The specific outline of the remainder of this thesis is as follows. In **chapter 2**, lipid oxidation in model membrane bilayers made from single unilamellar vesicles (SUV's) of dioleoylphosphatidylcholine (DOPC) mixed with increasing amounts of 1-stearoyl-2-arachidonoylphosphatidylcholine (SAPC) using the BP-C11 probe (see paragraph 1.3.1) is studied. Furthermore, the associated dynamical and structural changes in these bilayers are investigated using steady-state and time-resolved fluorescence spectroscopy of membrane probes like pyrene and diphenylhexatriene (DPH) lipid derivatives. The formation of reactive oxygen species (ROS) is the result of oxidative bursts in plant cells. Two aspects of ROS detection are described in **chapter 3**, namely lipid oxidation and hydrogen peroxide

production. In **chapter 4** the application of two-photon excitation microscopy is described for the *in vivo* detection of molecular interactions. The study of MADS box transcription factor interactions in living plant cells show the advantage of using FLIM in combination with FRET. **Chapter 5** reports on the study of the heterodimerization and endocytosis of the *Arabidopsis* brassinosteroid receptors BRI1 and AtSERK3 (BAK1) at the plasma membrane of cowpea protoplasts using the FRET-FLIM methodology. Chapters 4 and 5 have shown the advantages of FRET-FLIM in living cells. In **chapter 6** it is illustrated that FLIM can be potentially used to characterize the molecular environment of fluorescent proteins. The fluorescence lifetime of visible fluorescent proteins is dependent on the local environment such as the refractive index of the medium. In **chapter 7** a detailed time-resolved polarized fluorescence study of the purified calcium sensor Yellow Cameleon 3.60 is presented. The enhanced FRET efficiency of the calcium bound form of YC3.60 is verified using time-correlated fluorescence and fluorescence anisotropy measurements. Analyses of these experiments resulted in estimations of the dipole orientation factor and the actual energy transfer rates between the donor and acceptor moieties in presence and absence of calcium. Based on these results a structural model of YC 3.60 has been developed. In **chapter 8** the research topics described in this thesis are summarized and discussed. Implications and future developments of fluorescence microspectroscopy techniques for *in situ* studies are emphasized.

Chapter 2

Oxidation of Unsaturated Phospholipids in Membrane Bilayer Mixtures is Accompanied by Membrane Fluidity Changes

Abstract

Steady-state and time-resolved fluorescence spectroscopy have been used to obtain information on oxidation processes and associated dynamical and structural changes in model membrane bilayers made from single unilamellar vesicles (SUV's) of dioleoylphosphatidylcholine (DOPC) mixed with increasing amounts of 1-stearoyl-2-arachidonoylphosphatidylcholine (SAPC). The highly unsaturated arachidonoyl chain containing four double bonds is prone to oxidation. Lipid oxidation was initiated chemically by a proper oxidant and could be followed on line via the fluorescence changes of an incorporated fluorescent lipophilic fatty acid (4,4-difluoro-5-(4-phenyl-1,3-butadienyl)-4-bora-3a,4a-diaza-s-indacene-3-undecanoic acid: BP-C11). The oxidation rate increases with increasing amount of SAPC. Size measurements of different SUV's incorporated with a trace amount of a phosphatidylcholine analogue of BP-C11 using fluorescence correlation spectroscopy have demonstrated that an increase of lipid unsaturation results in smaller sized SUV's and therefore to a larger curvature of the outer bilayer leaflet. This suggests that the lipid-lipid spacing has increased and that the unsaturated fatty acyl chains are better accessible for the oxidant. Oxidation results in some characteristic physical changes in membrane dynamics and structure, as indicated by the use of specific fluorescence probes. Fluorescence measurements of both dipyrenyl- and diphenylhexatriene labeled PC introduced in non-oxidized and oxidized DOPC/SAPC membranes clearly show that the microfluidity (local fluidity at the very site of the probes) significantly decreases when the oxidized SAPC content increases in the lipid mixture. A similar effect is observed from the lateral diffusion experiments using monopyrenyl PC in the same membrane systems: the lateral diffusion is distinctly slower in oxidized membranes.

This chapter has been published as:

J. W. Borst, N. V. Visser, O. Kouptsova, A. J. W. G. Visser. (2000). "Oxidation of unsaturated phospholipids in membrane bilayer mixtures is accompanied by membrane fluidity changes" *Biochim. Biophys. Acta.* **1487**: 61-73.

2.1 Introduction

Phospholipids play an important role in cellular processes by self-organizing in a membrane bilayer, which forms together with intrinsic membrane proteins a permeable barrier of cells and organelles (Dowhan 1997). The primary events in intracellular signaling take place at the very site of the plasma membrane. Natural membranes are composed of phospholipids consisting of both saturated and poly-unsaturated fatty acyl chains. In food industry oxidation of (phospho-) lipids composed of poly-unsaturated fatty acids forms a major problem, since oxidation leads to the loss of quality of food products. Foods containing high levels of unsaturated lipids, such as vegetables and fish, lend themselves readily to oxidative deterioration. Hence they are prone to lipid oxidation, which leads to generation of undesirable flavours and odours and changes in appearance and texture (Hsieh and Kinsella 1989). It is therefore desirable to understand membrane oxidation processes at a molecular level. For instance, the question can be addressed whether the dynamical structure of the membrane will undergo alterations upon oxidation. To obtain an answer to this question, one has to understand first how model membranes will behave upon oxidation. Artificial membranes such as liposomes offer clear advantages over biological membranes. Liposomes or, more specific, small unilamellar vesicles (SUV's) of a defined lipid composition constitute a simple and convenient system for studying lipid oxidation and its inhibition by antioxidants without ambiguities, which are introduced by native enzymes or anti-oxidants that may be present in biological membranes (Vigo-Pelfrey and Nguyen 1991; Lasic 1995). With the aid of fluorescence spectroscopy both the oxidation level and changes in bilayer dynamics of liposomes upon oxidation can be studied.

The most commonly known and widely used membrane fluorescent probes for following oxidation in cells and in liposomes are *cis*- and *trans*-parinaric acids (Kuypers *et al* 1987; McGuire *et al* 1997). Despite the unique chemical and physical properties, these probes are not suitable for fluorescence microscopy, as the required UV excitation will elicit an overwhelming amount of autofluorescence. In this contribution, taking in account our future plans of using fluorescence microscopy techniques, we made use of newly discovered oxidation probe called BP-C11 (Naguib 1998; Pap *et al* 1999). This probe is a BODIPY[®] analogue that contains at position 3 of the BODIPY[®] ring system a fatty acyl chain of 11 carbon atoms and at position 5 a 4-phenyl-1,3-butadienyl group (Fig. 2.1). The BODIPY[®]- and the butadienyl groups form a conjugated electronic system and absorb light of low energy (581 nm). When the double bonds of the butadienyl group are chemically oxidized, the electron conjugation breaks up and a shift in the absorption maximum to higher energy is observed (488 nm). Concomitantly, the fluorescence spectral maximum changes from 591 nm (non-oxidized) to 520 nm (oxidized) (Pap *et al* 1999).

Pyrene-containing phospholipids in membranes report on lateral mobility of lipids, because of the ability of forming excimers between one pyrene molecule in the excited state (Pyr*) and another one in the ground state (Pyr) (Förster and Kasper 1955). The excimer (Pyr-Pyr*) fluorescence is at longer wavelengths than the monomer fluorescence. The ratio of excimer to monomer emission intensities (E/M) is a measure of the rate of excimer formation, which is determined by the frequency of collisions between pyrene moieties

and hence can be related to parameters describing membrane dynamics and organisation (Galla and Sackmann 1974). Changes in fluidity of membranes upon oxidation can be detected via the intramolecular collision frequency of two pyrene molecules bound at the *sn*1- and *sn*2-positions of a phospholipid such as in dipyrenylphosphatidylcholine (diPyr_n-PC). The excimer/monomer fluorescence intensity (E/M) ratio gives local information on the fluidity in a bilayer (Vauhkonen *et al* 1990; Sassaroli *et al* 1993; Pap *et al* 1995). In the following with “fluidity” is actually meant “microfluidity”, since the used dipyrenyl probes

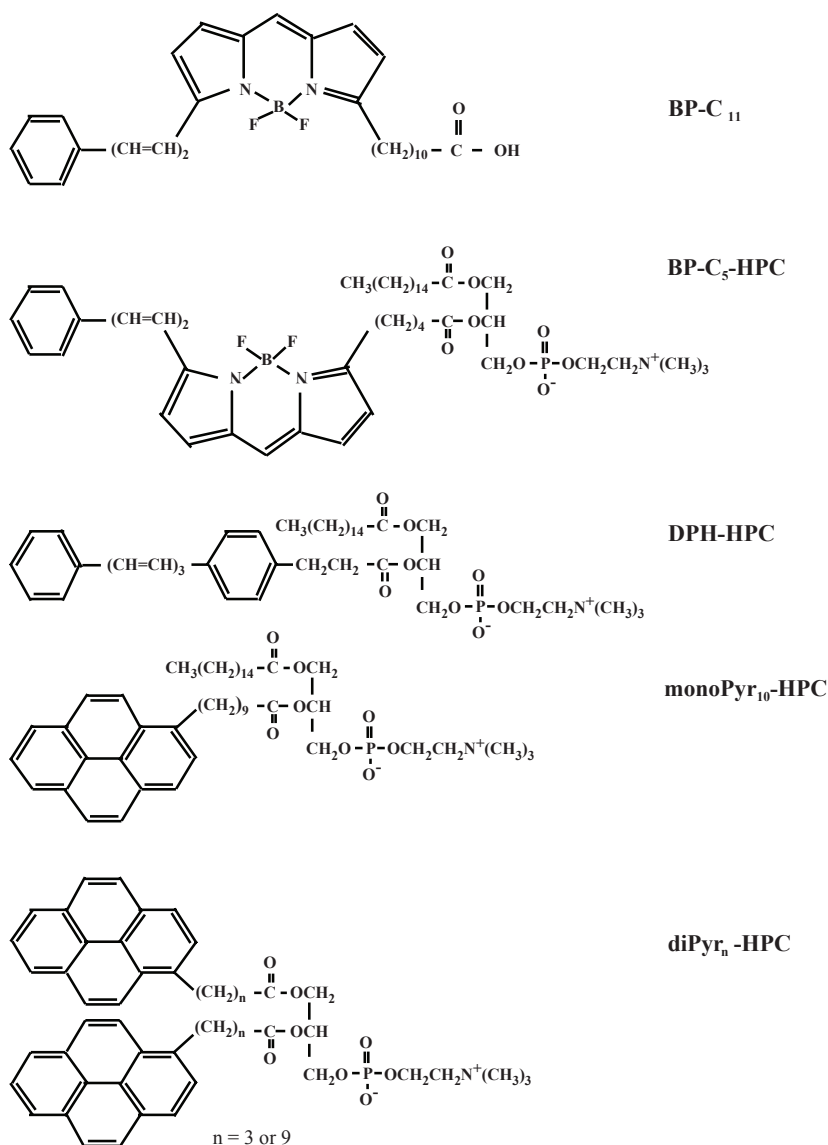


Figure 2.1: Structures of the used fluorescent probes.

report on the dynamic properties of the local probe environment. These probes are highly sensitive to constraints imposed by their environment and can therefore be used as fluidity sensors for interior regions of bilayer membranes. By using both pyrenyl groups at different depths with respect to the glycerol moiety of the phospholipid the fluidity can be measured at different depths in the membrane.

Historically, fluorescence polarization measurements of the lipophilic probe diphenylhexatriene (DPH) have proven to be a very sensitive technique for monitoring membrane fluidity (again better “microfluidity” see Lentz (1993) for a review). A systematic study of the effect of molecular order and dynamics - determined using polarized time-resolved fluorescence of DPH - in membrane bilayers consisting of symmetrically and mixed-chain polyunsaturated phospholipids has been published (Mitchell and Litman 1998). DPH itself is often used as a membrane probe, but the disadvantage is that it can be located in various domains of the membrane bilayer thereby hampering an unambiguous interpretation (van der Heide *et al* 1996). Therefore DPH-HPC is chosen, because the DPH is incorporated in the *sn*2-position of the phospholipid (Fig. 2.1). In this way the fluorescent probe is located at a fixed distance from the phospholipid-water interface. Lateral diffusion over the 2-dimensional membrane surface can be measured via the excimer formation of monopyrene phospholipids (Fig. 2.1), when these probe lipids are introduced in the bilayer membrane at increasing relative concentrations. The measured monomer fluorescence intensity (relative to one obtained at infinite dilution) can be plotted against the increase of probe-to-total lipid concentration ratio, which is followed by recovery of the relevant parameters (Sassaroli *et al* 1990; Pap *et al* 1995).

In the present study we have investigated membrane dynamics monitoring oxidation and fluidity in artificial membranes composed of liposomes containing different amounts of polyunsaturated phospholipids using the fluorescence approaches sketched above. The membrane system consisted of dioleoylphosphatidylcholine (DOPC) in combination with increasing fractional amounts of 1-stearoyl-2-arachidonoylphosphatidylcholine (SAPC). It is known that the polyunsaturated fatty acid arachidonic acid is very sensitive for lipid oxidation both as free fatty acid as well as in phospholipids (Kuypers *et al* 1987).

Using fluorescence spectroscopy one must realize that there is always a compromise between the sensitivity of the method (which is superior as compared to other spectroscopic methods) and the local perturbation induced by the (sometimes bulky) probe on the membrane structure in its immediate vicinity. Fluorescence methods do reflect observable changes, when the physical properties of the surrounding lipids are altered, and are therefore very suitable in comparative studies. Other spectroscopic methods such as ^2H NMR lead to more quantitative results of, for instance, the effect of acyl chain polyunsaturation on acyl chain order (Separovic and Gawrisch 1996; Koenig *et al* 1997), but are less sensitive - higher concentrations of lipid are required - and more elaborate in execution and analysis.

2.2 Materials and Methods

2.2.1 Materials

The phospholipids dioleoylphosphatidylcholine (DOPC), 1-stearoyl-2-arachidonyl-phosphatidylcholine (SAPC), dimyristoylphosphatidylcholine (DMPC) and the oxidant cumene hydroperoxide were purchased from Sigma (Zwijndrecht, The Netherlands). Hemin was obtained from Aldrich (Zwijndrecht, The Netherlands). The fluorescent probes BP-C11, BP-C5-HPC, DPH-HPC, monoPyr₁₀-HPC, diPyr_n-PC (n is 4 or 10) were purchased from Molecular Probes (Leiden, The Netherlands). Specific details on the use of these probes can be found in (Haugland 1996). The diPyr_n-PC has the same structure of the phospholipid headgroup as monoPyr₁₀-HPC, but both acyl chains contain a pyrene moiety at position 4 or 10. All chemicals were used without further purification.

2.2.2 Liposomes

Phospholipids and fluorescent probes were dissolved in spectroscopic grade ethanol and SUV's were prepared by injection of a few microliters of this mixture into 0.5 ml PBS (Batzri and Korn 1973). With this procedure the fluorescent molecules are located both at the inner and outer membrane leaflet of the liposomes (Pap *et al* 1995). Injection and gentle vortexing was carried out at room temperature. Phospholipid mixtures were prepared with molar percentages 0%, 25%, 50% and 100% of SAPC with respect to DOPC. These liposomes were all in the liquid-crystalline phase, because the transition temperatures (from the gel to liquid-crystalline phase) of the used phospholipids were below 0 °C in the non-oxidized state (-20 °C for DOPC and -13 °C for SAPC) (Koynova and Caffrey 1998). The total phospholipid concentration was kept at 50 or 100 µM depending on the type of experiments (see below).

2.2.3 Oxidation

The oxidation study was performed by using the fluorescent probe BP-C11. The molar ratio of BP-C11 probe and phospholipid was 1:4000. The excitation wavelength was set at 488 nm and the emission intensity ratio between oxidized (520 nm) and non-oxidized (591 nm) was followed in time. Oxidation was introduced by adding 150 µM cumene hydroperoxide and 0.5 µM hemin under gently stirring.

2.2.4 Fluidity

Membrane fluidity has been determined following two approaches. The first approach utilised the excimer/monomer fluorescence intensity (E/M) ratio of dipyrenylphosphatidylcholines (diPyr_n-PC, in which n is either 4 or 10). Liposomes were prepared as described above and oxidation was introduced by adding 250 µM cumene hydroperoxide and 1 µM hemin. The E/M ratio was followed in time using a fixed excitation wavelength of 345 nm and alternating emission wavelengths of 480 nm (excimer emission) and 377 nm (monomer emission). The slit width of the excitation monochromator was chosen small (0.2 nm) in order to minimise photo-oxidation of pyrene, while the slit width of the emission monochromator was fixed at 4 nm. The total diPyr_n-PC concentration is kept at 0.1 µM, so that only the intramolecular collision frequency reflects the local membrane fluidity.

The second approach for measuring membrane fluidity was via steady-state and time-resolved fluorescence anisotropy of DPH-HPC. The anisotropy experiment with DPH-HPC differs from the one using E/M ratio with diPyr_n-PC. It turned out that DPH, in contrast to pyrene, is easily oxidized by the cumene hydroperoxide/hemin couple and then becomes non-fluorescent. The liposomes without DPH-HPC were oxidized overnight with 250 μ M cumene hydroperoxide and 1 μ M hemin. After oxidation, the phospholipids were extracted with chloroform:methanol (2:1 v/v) (Bligh and Dyer 1959) and the phospholipid content was estimated via a phosphorus determination (Rouser *et al* 1970). The phospholipids were dried, dissolved in ethanol and liposomes were prepared as described before. The samples were excited with polarized light of 360 nm (monochromator slit width 1.5 nm) and the vertically and horizontally polarized fluorescence intensities of DPH-HPC were detected through cut-off filters > 399 nm (Schott, Mainz, Germany). The steady state anisotropy r was then determined using equation 1.

$$r = (I_{VV} - GI_{Vh}) / (I_{Vh} + 2GI_{vh}) \quad (1)$$

where I_{VV} and I_{Vh} are the vertically and horizontally polarized fluorescence intensities at the vertically polarized excitation beam; $G = I_{hv}/I_{hh}$ is the G-factor, which accounts for the different responses of the two emission light paths in the T-format setup (see below). The fluorescence intensities I_{hv} and I_{hh} were measured with horizontally polarized excitation. Polarized background emission arising from liposomes without DPH-HPC was measured separately and subtracted from all polarized intensities. Time-resolved polarized fluorescence experiments of DPH-HPC in various membrane bilayers have been carried out exactly as described elsewhere (Pap *et al* 1996). The fluorescence anisotropy decay profiles were analyzed using a general Brownian diffusion model (Ameloot *et al* 1984; Szabo 1984; Van der Meer *et al* 1984) with the intuitive assumption that the DPH moiety is Gaussian distributed parallel with respect to the direction of the phospholipid acyl chains (see (Ameloot *et al* 1984) for details).

Lateral diffusion was determined by measuring the normalized monomer fluorescence of monoPyr₁₀-HPC at increasing molar ratio of probe-host phospholipid as described before (Pap *et al* 1995). Usually 5 to 7 different samples with increasing probe concentration were measured first. The samples were then incubated with oxidant for 20 minutes and subsequently measured. Fluorescence decay times of the monomer fluorescence of monoPyr₁₀-HPC were determined in various liposomes at a probe/phospholipid molar ratio of 1:1000 to ensure that no excimer emission was observed. As previously (Pap *et al* 1995) the predominant long-lived component has been selected.

2.2.5 Instruments

The oxidation experiments using the BP-C11 probe, the fluidity experiments using diPyr_n-PC and lateral diffusion experiments with monoPyr₁₀-HPC were carried out on a Spex Fluorolog 3.2.2 spectrofluorometer. Fluorescence anisotropy measurements using DPH-HPC were performed on a home built T-format fluorometer using a dual channel photon counting setup, which allows to simultaneously measure the I_{VV} , I_{Vh} and I_{hv} , I_{hh} pairs.

Fluorescence Correlation Spectroscopy (FCS) measurements were performed on a Zeiss-Evotec ConfoCor instrument. SUV's were loaded with BP-C5-HPC at a probe-host phospholipid concentration ratio of 1:100000. The excitation was performed with a He-Ne laser emitting at 543 nm and the emission was detected via a bandpass filter transmitting light between 550 and 600 nm. Both instrument and data processing have been described previously (Hink and Visser 1998; Hink *et al* 1999).

Time-resolved fluorescence experiments were measured by use of the time-correlated single photon counting set-up as described in detail elsewhere (Pap *et al* 1995; Pap *et al* 1996). For DPH-HPC in the various membranes the excitation wavelength was 340 nm and the emission wavelength was selected with a KV370 cut-off filter (Schott, Mainz, Germany) and a 402.3 nm line filter (Baird Atomic, USA). For monopyr₁₀-HPC the excitation wavelength was 343 nm and the emission was selected with a KV370 cut-off filter and a 374.6 nm line filter (Schott). The dynamical instrumental response of the setup was obtained with POPOP in fluorescent grade ethanol having a lifetime of 1.35 ns. Data analysis was performed with software described elsewhere (Digris *et al* 1999)

Unless stated otherwise, all experiments were carried out at 295 K.

2.3 Results and Discussion

2.3.1 Size measurements of liposomes

Fluorescence correlation spectroscopy (FCS) has emerged as an ultrasensitive technique operating at the level of single fluorescent molecules diffusing in and out of the confocal volume created by a focussed laser beam (Rigler 1995; Maiti *et al* 1997).

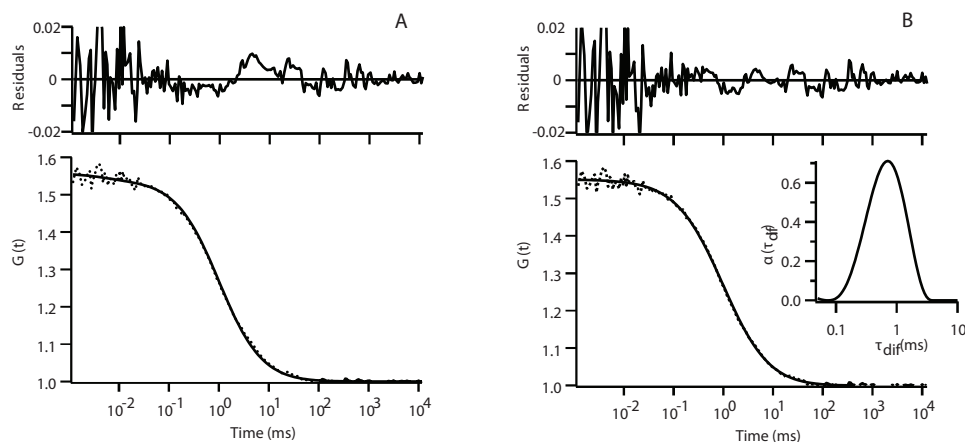


Figure 2.2: Example of analysis of the autocorrelation function of the burst of fluorescence photons emitted by BP-C5-HPC incorporated in SUV's consisting of DOPC. The top panel (A) presents the analysis in a single diffusion time. The dotted curve is the experimental curve whereas the solid line is the fitted curve. The lower panel (B) presents the analysis of the same experiment to a distribution of characteristic times on a logarithmic time axis. This analysis results in a better fit as can be concluded from the plots of the residuals in the range between 0.1-10 ms. In the inset the recovered distribution of diffusion times between 0.1 and 10 ms is shown. From this distribution the weighted diffusion time τ_{diff} is determined from $\sum \alpha(i) \cdot \tau_{diff}(i) / \sum \alpha(i)$, where the sum is taken from the starting and final time of the distribution (0.1 and 10 ms in the example).

At these low molecular concentrations the fluorescence intensity shows fluctuations which are on-line autocorrelated. Analysis of the autocorrelation function yields parameters such as the number of molecules in the detection volume and the residence or diffusion time of the molecule in the confocal volume, which is inversely proportional to the translational diffusion constant. Sizes of the liposomes were estimated using fluorescence correlation spectroscopy. Since the analysis of the autocorrelation functions in single diffusion times did not result in optimal fits (see (Hink and Visser 1998)), the data were analyzed in a distribution of diffusion times (Provencher 1982). An example of such analysis has been given in figure 2.2. All results have been collected in figure 2.3. The data presented in figure 2.3 show that an increase of the relative amount of SAPC in the phospholipid mixture leads to smaller sized liposomes (see the recovered hydrodynamic radii R_h in Fig. 2.3).

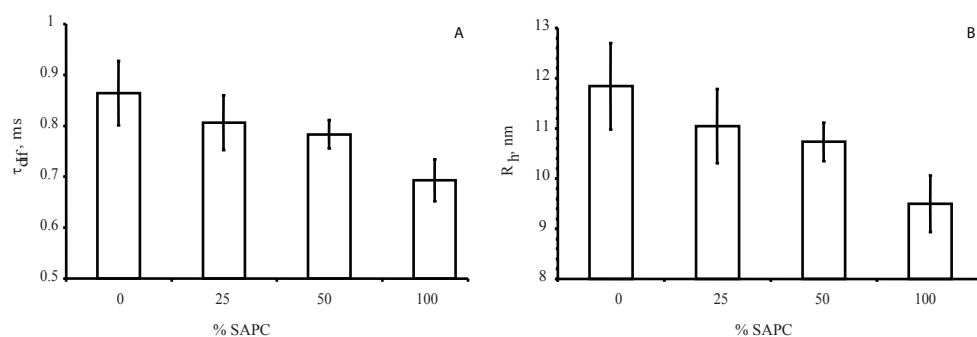


Figure 2.3: Top panel (A): Bar diagram of weighted diffusion times (see legend to Fig. 2.2) of BP-C5-HPC incorporated in SUV's consisting of DOPC with increasing amounts of SAPC. The standard errors result from the analysis of at least 10 autocorrelation traces. Lower panel (B): Hydrodynamic radii of the same lipid mixtures as for panel A as determined according to (Hink *et al* 1999).

From these results it can be concluded that the curvature in the outer leaflet of the latter SUV's is higher, so that the headgroups occupy a larger area and hence more space is created between them. Increasing the amount of unsaturated phospholipid in the mixture leads therefore to different packing of the inner and outer leaflet of the membrane. All four double bonds of SAPC in the SUV's are in the “*cis*” form, which introduces a kink in the carbon chain that disturbs the ordered packing of the adjacent DOPC chains (Stanley 1991).

2.3.2 Oxidation of BP-C11

In figure 2.4 the fluorescence ratio of oxidized and non-oxidized form of the BP-C11 probe incorporated in liposomes is detected in time, when the probe was chemically oxidized by adding cumene hydroperoxide (oxidant) and hemin (catalyst). Compounds like cumene hydroperoxide and *t*-butylhydroperoxide decompose in the presence of hemin with concomitant addition of a hydroperoxide to the unsaturated double bond of a polyunsaturated acyl chain. These oxidizing agents are often used for studying oxidative processes in membranes (van den Berg *et al* 1992). Optimal concentrations for oxidation of BP-C11 were 150 μ M cumene hydroperoxide and 0.5 μ M hemin. From the results presented in figure 2.4 it is clear that the rate of oxidation is dependent on the fractional amount of SAPC in the mixed SUV's. An increase of the fractional concentration of polyunsaturated fatty acyl chains in

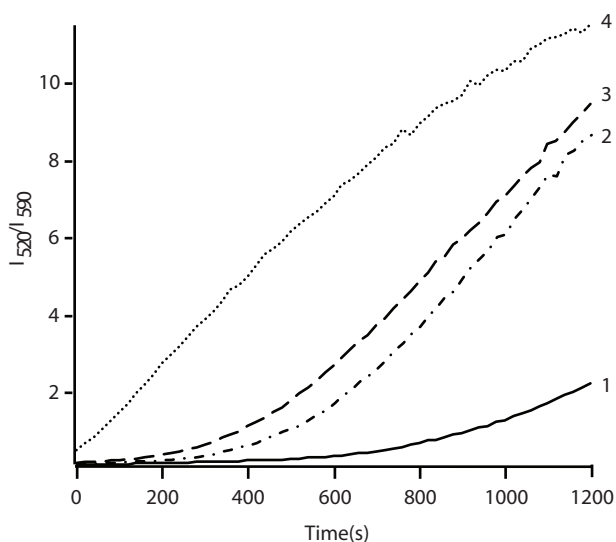


Figure 2.4: Time dependence of oxidation of BP-C11 (25 nM), expressed as the intensity ratio $(I_{520})_{\text{oxidized}} / (I_{590})_{\text{non-oxidized}}$ in liposomes containing different amounts of SAPC in DOPC. Final phospholipid concentration in the liposomes was 100 μM . Oxidation was started at $t = 0$ s. Curves are labeled as follows: 0% SAPC (1), 25% SAPC (2), 50% SAPC (3) and 100% SAPC (4).

the liposome system leads to an increase in the initial oxidation rate measured through the fluorescence ratio of BP-C11. After addition of cumene hydroperoxide and hemin a lag phase in the oxidation traces was seen for all liposomes except the ones consisting of 100 % SAPC. However, when a twofold higher probe concentration was used, the lag phase was much shorter and tended to vanish (results not shown). Therefore, the lag phase is related to the low probe concentration implying a finite time of the reactants to find each other and yield reaction. Probably because of the higher curvature in the outer leaflet of the liposomes (see previous section) penetration of cumene hydroperoxide and hemin can more easily occur in liposomes with higher amounts of polyunsaturated fatty acids, so that oxidation can take place more rapidly. It has been shown that oxidation of BP-C11 occurs on the same time scale as oxidation of arachidonic acid (Pap *et al* 1999). Therefore the fluorescence changes of BP-C11 indirectly reflect the oxidation of unsaturated fatty acids in lipid bilayers. On the other hand, it can not be ruled out that the oxidation of an increasing amount of SAPC has an accelerating effect on the oxidation of BP-C11.

2.3.3 Fluidity: Excimer/monomer ratio of diPyr_n-PC

Figure 2.5 shows the time dependence of the E/M ratio of diPyr₄-PC and diPyr₁₀-PC in different liposome mixtures upon chemical oxidation. The initial E/M ratio of diPyr₄-PC is higher than the one of diPyr₁₀-PC in the different liposomes. The location of diPyr₄-PC can be expected in the center of a leaflet of the bilayer, while diPyr₁₀-PC is located more in the center of a bilayer. The conclusion can be drawn that initially the collision frequency of pyrene moieties with a longer acyl chain (diPyr₁₀-PC) is less than

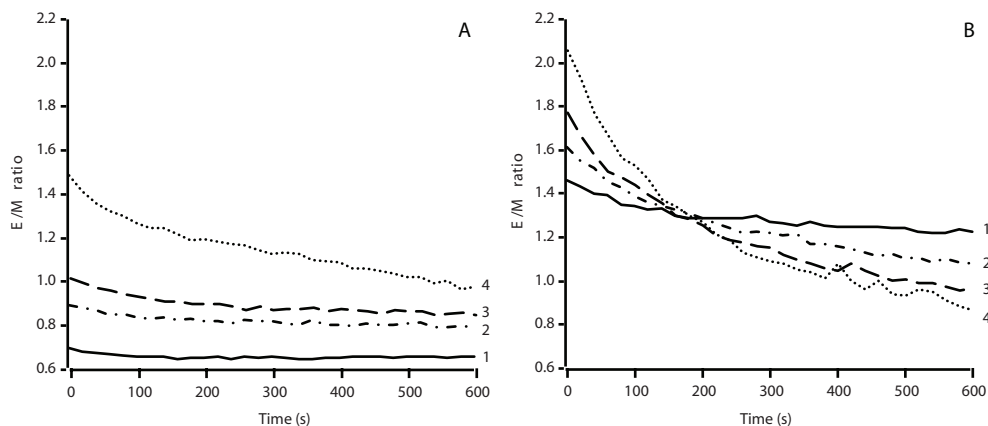


Figure 2.5: Time dependence of E/M ratio of diPyr₁₀-PC (A) and diPyr₄-PC (B) in liposomes containing different amounts of SAPC in DOPC. The probe concentration was 0.1 μ M and the final phospholipid concentration in the liposomes was 50 μ M. Oxidation was started at $t = 0$. Curves are labeled as follows: 0% SAPC (1), 25% SAPC (2), 50% SAPC (3) and 100% SAPC (4).

that for those with a shorter chain (diPyr₄-PC). It should be noted, however, that this difference can also be caused by the relatively unfavourable orientation of both pyrene moieties in the diPyr₁₀-PC. The E/M ratio of diPyr₁₀-PC does not change much upon oxidation, except for 100 % SAPC, where it is shown that the ratio decreases by approximately 25 % (see Fig. 2.5A). Apparently, in the center of the bilayer hardly any fluidity changes are detected when oxidation takes place. On the other hand, oxidation of the double bonds of the phospholipids results in a distinct lowering of the E/M ratio when diPyr₄-PC is incorporated in the liposome (Fig. 2.5B). The effect becomes larger when the unsaturated fatty acyl chain content in the liposome increases. At this level of the bilayer (about halfway of one leaflet) liposomes with a high level of unsaturation become distinctly more rigid (or less fluid) after oxidation. A similar decrease in fluidity of mixed PC/PE vesicles after lipid peroxidation has been reported previously (Dobretsov *et al* 1977).

Although the pyrene moiety seems much less prone to oxidation than the DPH moiety (see next section), additional control experiments have been carried out. First, we have followed the time dependence of the E/M ratio of diPyr_n-PC (n is 4 or 10) in DMPC vesicles (at probe: phospholipid molar ratio of 1:500) at 30 °C (fluid membranes) in the presence of 1 μ M hemin and 250 μ M cumene hydroperoxide (Fig. 2.6). In this case the pyrene moieties are the only targets for oxidation. The effects on the E/M ratio are absent in case of diPyr₄-PC and minor in case of diPyr₁₀-PC. This observation suggests that the time-resolved traces in figure 2.5 really reflect fluidity changes in the vicinity of the pyrene probe and not effects of pyrene oxidation. In a second experiment, we have added the pyrene probe to pre-oxidized lipids, similarly as described for the experiments with DPH-HPC (see below). The E/M ratios were measured for both oxidized and non-oxidized membranes and the results (expressed as relative E/M: $(E/M)_{\text{non-oxidized}}/(E/M)_{\text{oxidized}}$) have been included in Table 2.1. For comparison we have listed the same relative values that were obtained from the time-dependent traces in figure 2.5 (note that the oxidation may not be complete after 600 s). The conclusion is obvious: all oxidized

membranes exhibit smaller E/M values as compared to non-oxidized ones and are therefore less fluid than non-oxidized membranes. The rate of decrease in fluidity (or E/M ratio) is larger for increasing unsaturation of the phospholipid mixture. This effect is more pronounced for diPyr₄-PC (Fig. 2.5B), where the largest degree of unsaturation finally leads to the lowest E/M ratio and thus to a more rigid local structure. Another remarkable result is that for SUV's consisting of 100% SAPC the rate of decrease in fluidity parallels the rate of oxidation (Fig. 2.4).

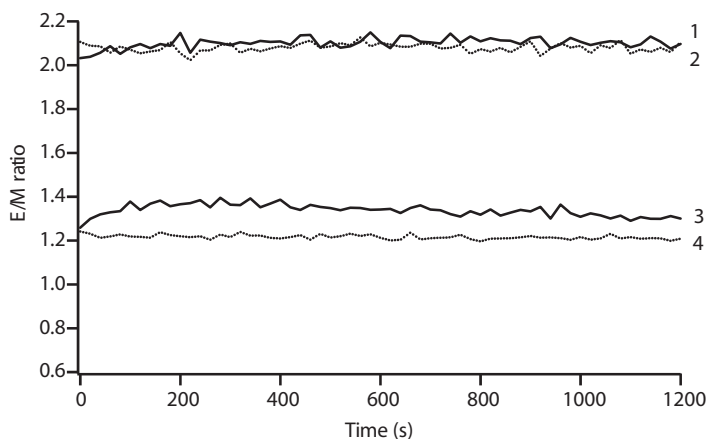


Figure 2.6: Time dependence of E/M ratio of diPyr₄-PC (curves 1 and 2) and diPyr₁₀-PC (curves 3 and 4) in liposomes containing DMPC at 30°C. The probe concentration was 0.1 μM and the final phospholipid concentration in the liposomes was 50 μM. Oxidation was started at t = 0. Curves 2 and 4 represent the situation when no oxidants were added.

For the SUV's consisting of mixed DOPC and SAPC no distinct lag phase is observed in the time-dependence of the E/M ratio in contrast to the observed lag phase in the oxidation experiments. Note, however, that the diPyr_n-PC concentration (n is 4 or 10) is about eight times higher than the BP-C11 concentration.

What is the physical significance of the different E/M values in the different lipid systems and can these values be related to kinetic constants? In principle, one can estimate the rate constant (k_2) of excimer formation of two neighbouring pyrene moieties in a single phospholipid (one pyrene is in the ground state and the other one in the excited state) from (Sassaroli *et al* 1990):

$$k_2 = [(E/M)_2 / (E/M)_1(x_0)] \cdot \tau_m^{-1} \quad (2)$$

where $(E/M)_2$ is the excimer to monomer fluorescence ratio of the dipyrene-containing lipids and $(E/M)_1(x_0)$ that of monopyrene lipids at the critical mole fraction x_0 (Vauhkonen *et al* 1990). At this critical molar ratio of probe lipid and host lipid, the rate of excimer formation is equal to the monomer fluorescence decay rate τ_m^{-1} . To give an order of magnitude it was found previously that $k_2 = 1.13 \times 10^7 \text{ s}^{-1}$ for the system diPyr₁₀-PC and monoPyr₁₀-HPC in DOPC SUV's (Pap *et al* 1995). Without giving absolute values of k_2 it is immediately apparent from the data presented in figure 2.5, that k_2 (which is proportional to the E/M ratio, see equation 2)

increases with increasing saturation (see Fig. 2.5A) and is considerably larger for diPyr₄-PC (see Fig. 2.5B). For the latter probe lipid the rate of excimer formation becomes much less, when SAPC is oxidized.

Table 2.1: The ratio $(E/M)_{\text{non-oxidized}} / (E/M)_{\text{oxidized}}$ for diPyr₄-PC and diPyr₁₀-PC in SUV's prepared from different DOPC/SAPC mixtures^a.

Molar % SAPC	diPyr ₄ -PC		diPyr ₁₀ -PC	
	Lipid extraction after oxidation	On-line oxidation	Lipid extraction after oxidation	On-line oxidation
0% SAPC	2.0	1.2	1.2	1.0
25% SAPC	1.6	1.5	1.5	1.1
50% SAPC	2.1	1.9	1.4	1.2
100% SAPC	3.0	2.4	1.6	1.5

^a See text for details.

2.3.4 Fluidity: Fluorescence anisotropy of DPH-HPC

In figure 2.7 the fluorescence anisotropy values of DPH-HPC in different SUV's have been summarized. The grey bars present the fluorescence anisotropy of DPH-HPC in liposomes prior to oxidation whereas the white bars give the anisotropy of DPH-HPC in liposomes after phospholipid oxidation. The control experiment consists of SUV's made from DMPC, which does not contain any unsaturated carbon bonds in the fatty acyl chains. Indeed, there is no

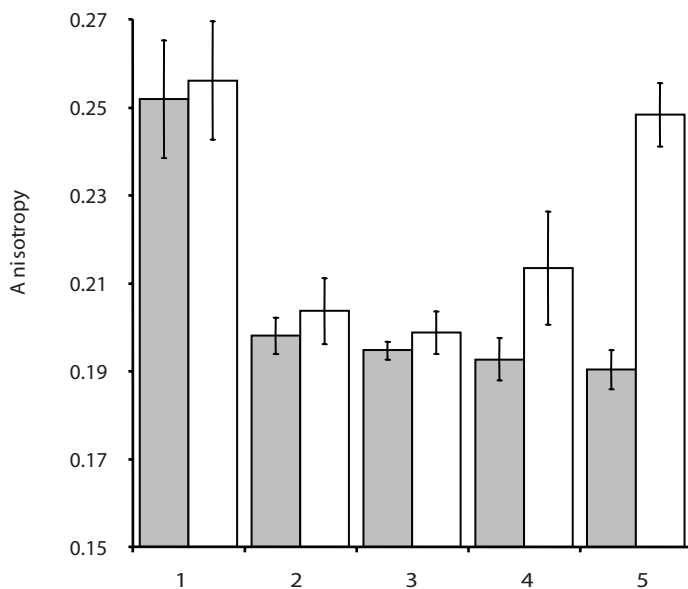


Figure 2.7: Fluorescence anisotropy values of DPH-HPC (0.1 μM) in liposomes containing different amounts of SAPC in DOPC. Oxidation of the liposomes was carried out overnight by incubation with 250 μM cumene hydroperoxide and 1 μM hemin, which was followed by lipid extraction, phospholipid concentration determination and preparation of labeled liposomes. The final phospholipid concentration in the liposomes was always 50 μM . The grey bars denote the anisotropy values of DPH-HPC prior to oxidation whereas the white bars denote the ones after oxidation. The numbering of the pair of bars is as follows: DMPC (1), 0% SAPC (2), 25% SAPC (3), 50% SAPC (4) and 100% SAPC (5). The standard errors are determined from at least 10 experiments.

effect seen. In all other cases oxidation leads to a decrease in fluidity, because the fluorescence anisotropy significantly increases. The largest effect is observed in liposomes made from SAPC where oxidation leads to a fluidity that is comparable to that observed in DMPC. These results are in full agreement with those obtained with the E/M ratio measurements of diPyr₄-PC. In this respect it should be noted that the DPH moiety is located at approximately the same distance from the headgroup as the corresponding pyrene in diPyr₄-PC. No time-dependent effects could be observed, since DPH-HPC is very readily oxidized and in this respect resembles the parinaric acid probes used previously (Kuypers *et al* 1987; McGuire *et al* 1997).

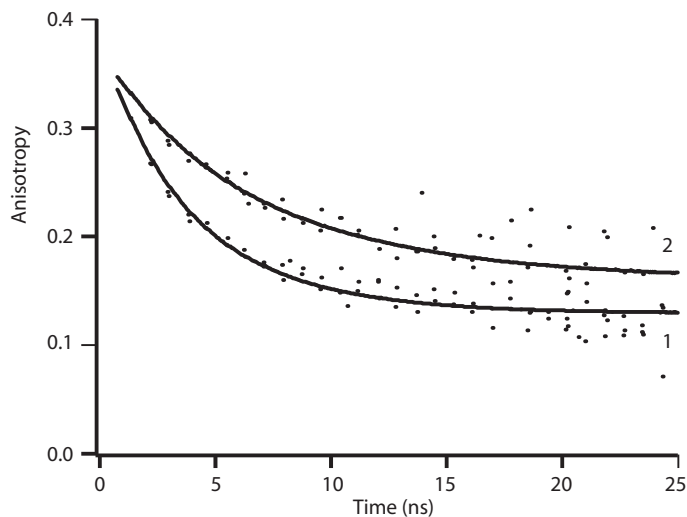


Figure 2.8: Fluorescence anisotropy decay of DPH-HPC in liposomes prepared from non-oxidized SAPC (curve 1) and oxidized SAPC (curve 2). The experimental points are the dotted ones, while the calculated curves (solid lines) correspond with fits to the Brownian diffusion model (see text for details). The optimized parameters are collected in Table 2.2.

From time-resolved fluorescence anisotropy and application of a Brownian rotational diffusion model, one can retrieve information on the local rotational dynamics and order of DPH-HPC. A typical example of experimental fluorescence anisotropy decays of DPH-HPC in oxidized and non-oxidized liposomes is given in figure 2.8. The smooth curves through the data points represent the optimized fits according to the general diffusion model with the assumption that the orientation distribution of DPH-HPC is Gaussian shaped. The used model adequately fits the decay curves.

This approach offers the advantage of a minimal number of adjustable parameters: the initial anisotropy (r_0), the rotational diffusion coefficient of the symmetry axis of DPH (D_{\perp}) and the Gaussian distribution width (θ_g). In addition, an intuitively correct probe orientation is assumed (for details concerning the analysis according to this model and the rigorous error analysis see (Pap *et al* 1996)). All optimized parameters have been collected in Table 2.2. After inspection of the results in Table 2.2, one can notice the following trends. The rotational diffusion coefficient becomes larger upon an increase in the fractional concentration of SAPC

in the mixed bilayer system SAPC/DOPC, whereas the width of the orientation distribution is much less affected. This result is in full agreement with results obtained by Mitchell and Litman (1998) using time-resolved fluorescence methods of DPH in different symmetrically substituted phosphatidylcholines (such as DOPC) and mixed-chain phosphatidylcholines with a saturated *sn*-1 chain and various double bonds in the *sn*-2 chain (such as SAPC). The latter authors found that unsaturation of both acyl chains did not produce a bilayer environment that affords DPH as much rotational mobility as high levels of polyunsaturation at only the *sn*-2 acyl chain. Mitchell and Litman (1998) also found a bimodal orientation distribution function for DPH in membranes, which is in agreement with results obtained previously (van der Heide *et al* 1996), but is not physically realistic with a phospholipid containing DPH in the *sn*-2 chain (Pap *et al* 1996). The other striking feature from the data in Table 2.2 is that oxidation leads to a significant decrease in rotational mobility and a narrower rotational distribution width.

Table 2.2: Optimized parameters from anisotropy decay analysis of DPH-HPC in SUV's prepared from different DOPC/SAPC mixtures^a

Molar % SAPC	Non-oxidized			Oxidized		
	r_0 (-)	θ_g (rad)	D_{\perp} (μs^{-1})	r_0 (-)	θ_g (rad)	D_{\perp} (μs^{-1})
0%	0.35 (0.336-0.361)	0.671 (0.650-0.699)	26.6 (23.9-29.7)	0.357 (0.343-0.369)	0.636 (0.612-0.660)	25.9 (22.8-29.1)
25%	0.346 (0.339-0.355)	0.644 (0.630-0.665)	28.9 (25.6-33.1)	0.355 (0.341-0.367)	0.635 (0.615-0.662)	27.0 (24.0-30.5)
50%	0.345 (0.331-0.356)	0.653 (0.628-0.678)	29.9 (26.9-33.4)	0.361 (0.347-0.373)	0.621 (0.591-0.653)	23.4 (20.5-26.7)
100%	0.337 (0.320-0.355)	0.574 (0.556-0.598)	29.3 (25.3-33.3)	0.348 (0.337-0.362)	0.516 (0.465-0.594)	13.8 (10.5-18.0)

^a See text for details. The values within parentheses are the confidence limits taken at the 67% level (for details, see (Digris *et al* 1999)).

2.3.5 Lateral diffusion measurements

The use of increasing concentrations of monopyrene phospholipid analogues provides information on the lateral mobility of phospholipids over the two-dimensional surface of a bilayer membrane (Galla and Sackmann 1974; Eisinger *et al* 1986; Vauhkonen *et al* 1989). The formation of excimers is very well modeled with the so-called Milling-Crowd model (Eisinger *et al* 1986), which considers lipid probes migrating in a trigonal lattice of lipids by exchanging positions with one of their six nearest neighbours. In this way the overall rate of intermolecular excimer formation of monopyrene lipids (k_{exc}) can be expressed in terms of the frequency of lipid exchange in the trigonal matrix (f) and the average number of lipid exchanges (n) required before an excimer is formed (Eisinger *et al* 1986). Details on how k_{exc} depends on the various rate constants and on how f and n can be evaluated are given in Pap *et al* (1995).

Briefly, the minimum diffusion frequency f_{min} in all lipid systems can be obtained by fitting the data to the following equation (Eisinger *et al* 1986):

$$I_m/I'_m = (1 + \tau_m \cdot k_{exc})^{-1} = (1 + \tau_m \cdot f_{min}/(n(l,x)))^{-1} \quad (3)$$

where I_m corresponds to the observed monomer fluorescence intensity, while I'_m refers to the monomer fluorescence intensity at very low mole fraction of pyrene lipid; τ_m is the average fluorescence lifetime of the monomer and $n(l,x)$ (n depends on the molar ratio of pyrene lipid and total phospholipid and it is assumed that the probability of a nearest neighbour pair to form an excimer in the time interval f^{-1} is equal to one) has been obtained by random walk simulations of pyrene lipids in a trigonal lipid matrix (Pap *et al* 1995). The (minimum) lateral diffusion coefficient can be calculated according to (Eisinger *et al* 1986):

$$D_{lat} = f_{min} \cdot \lambda^2/4 \quad (4)$$

where λ corresponds to the lipid-lipid spacing in the bilayer membrane. A surface area $\lambda^2 = 0.68 \text{ nm}^2$ for phospholipids has been used before (Vauhkonen *et al* 1989).

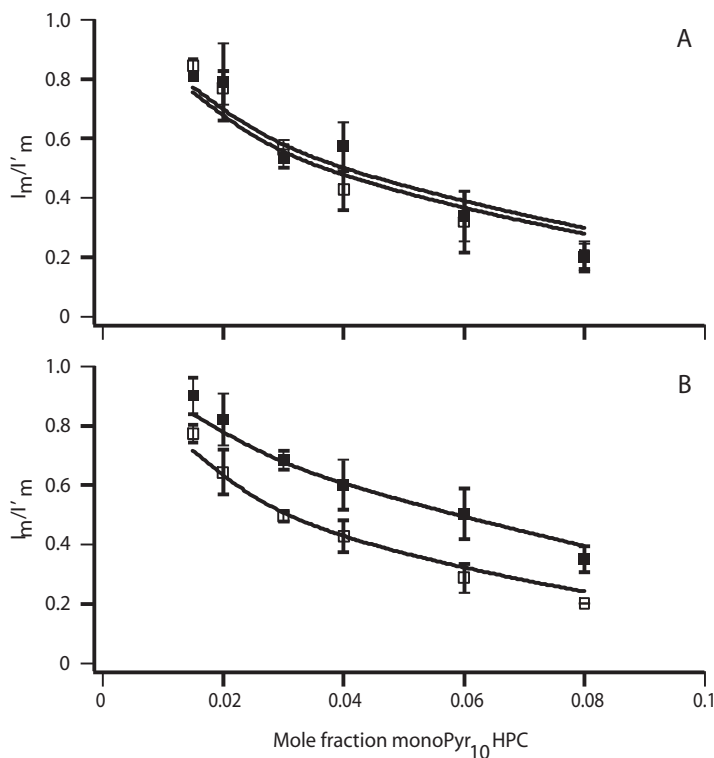


Figure 2.9: The dependence of the normalized monomeric fluorescence intensity on the mole fraction incorporated monoPyr₁₀-HPC in liposomes made from DOPC (A) and from an equal molar mixture of DOPC and SAPC (B). The error bars result from at least 3 experiments. The filled squares indicate the data points prior to oxidation; the open squares those after oxidation. The solid line through the points is the fitted curve according to equation 3.

The normalized monomer fluorescence obtained after titration of monoPyr₁₀-HPC in DOPC and DOPC:SAPC (1:1 molar ratio) is presented in figure 2.9A and 2.9B, respectively (dark symbols). The results of measurements with the same lipids after oxidation have been presented as well in figure 2.9A and 2.9B (open symbols). Also the fitted curves according to equation 3 have been included (solid lines). It can be clearly observed that any oxidation of DOPC SUV's did not result in large changes in the dependence of normalized monomeric fluorescence intensity on the mole fraction incorporated monoPyr₁₀-HPC implying that the lateral diffusion rate is comparable in oxidized and non-oxidized DOPC (see Fig. 2.9A).

Changes in lateral diffusion rates are, however, clearly observed in the oxidized and non-oxidized mixtures of DOPC:SAPC (1:1 molar ratio) (see Fig. 2.9B). If we assume that lateral diffusion of pyrene lipids is mainly dependent on the properties of the host lipid matrix, it can then be concluded that the lateral diffusion is distinctly slower in oxidized membranes. The average fluorescence lifetime τ_m for the all lipid systems have been determined separately (Table 2.3). From the fits the product $\tau_m \cdot f_{min}$ is obtained, which leads to values of D_{lat} via equation 4 (collected in Table 2.3). Inspection of the data in Table 2.3 very clearly shows that oxidation of SAPC results in much slower lateral diffusion.

Table 2.3: Fluorescence lifetimes and lateral diffusion constants of monoPyr₁₀-HPC in SUV's prepared from different DOPC/SAPC mixtures^a

Molar % SAPC	Non-oxidized		Oxidized	
	τ_m (ns)	D_{lat} ($10^{-8}\text{cm}^2\text{s}^{-1}$)	τ_m (ns)	D_{lat} ($10^{-8}\text{cm}^2\text{s}^{-1}$)
0% SAPC	129	0.14±0.02	105	0.16±0.02
50% SAPC	113	0.20±0.03	96	0.11±0.02
100% SAPC	122	0.21±0.02	90	0.13±0.01

^a See text for details

2.4 Conclusions

Fluorescence spectroscopy is a powerful tool to obtain information on details of a variety of membrane processes. We have used different fluorescent approaches: i) fluorescence correlation spectroscopy for size measurements of non-oxidized SUV's to determine vesicle sizes with large accuracy; ii) a ratiometric measurement of a specific probe, which fluorescence emission changes color upon oxidation; iii) ratiometric methods (E/M ratio and fluorescence anisotropy, respectively) and time-resolved fluorescence anisotropy measurements to obtain information on local rigidity (or fluidity) of the membrane structure before and after oxidation; iv) measurements of lateral diffusion by titrating increasing amounts of monopyrenyl-PC in membranes. Ratiometric methods have several advantages. The fluorescence probe can be administered at very low concentrations to the membrane bilayer so that the structure will be minimally perturbed. Another advantage is that the absolute concentration of the probe is not important since it does not influence the final results.

The results of these four measurements show very nice qualitative correlation. The increased membrane curvature with increasing amount of unsaturated lipids can explain

the larger oxidation rate: the oxidant can reach the target more easily. Once the unsaturation is removed by addition of peroxy or hydroxyl groups, the membrane becomes more rigid and the 2-dimensional diffusion becomes slower. It is very likely that the phase transition temperature (liquid-crystalline to gel state) becomes much higher than 0 °C, because the fluorescence anisotropy approaches the value of that in DMPC vesicles in the gel state. In order to corroborate this point it will be necessary to perform comparative fluorescence measurements on well-defined lipids with peroxy or hydroxyl groups attached to a specific site of the unsaturated fatty acyl chain of the lipid. Finally, the oxidation probe used by us lends itself very well to monitor oxidation processes in biological membranes and in living cells (Pap *et al* 1999).

Acknowledgements

This work has been supported by EC-FAIR project no. 97-3228. Olga Kouptsova was supported by NWO (The Netherlands Organisation for Scientific Research) grant 047-007-005 providing scientific cooperation between The Netherlands and the Russian Federation. We thank Mark Hink, Arie van Hoek and Anatoli Digris for assistance with fluorescence correlation spectroscopy, time-resolved fluorescence and data analysis, respectively.

Chapter 3

Imaging of Oxidative Stress in Plant Cells by Quantitative Fluorescence Microscopy and Spectroscopy

Abstract

In this chapter the application of two different fluorescent probes is described that are able to interrogate lipid peroxidation in whole plant cells and hydrogen peroxide production in plant cell suspensions.

This chapter has been published as:

J. W. Borst, M. A. Uskova, N. V. Visser and A. J. W. G. Visser. (2002). Imaging of oxidative stress in plant cells by quantitative fluorescence microscopy and spectroscopy. In: *Fluorescence Spectroscopy, Imaging and Probes, New Tools in Chemical, Physical and Life Sciences* (Kraayenhof, R., Visser, A.J.W.G., and Gerritsen, H.C., Eds.) Springer Series on Fluorescence, Methods and Applications, Vol. 2, Springer Verlag, Heidelberg, pp. 337-348

3.1 Introduction

The production of reactive oxygen species (ROS) plays an important role in the plant defense mechanism and is one of the reactions of plants to pathogen infection or elicitor production (elicitors are pathogen-produced signaling compounds) (Lamb and Dixon 1997; Ebel and Mithofer 2001). The actual involvement of oxygen radicals in plant diseases has been difficult to assess, since an array of protective enzymes as well as antioxidants are involved. In addition, lipid peroxidation may also be initiated by production of ROS in response to pathogen invasion (Rogers *et al* 1988; Adam *et al* 1989; Keppler and Baker 1989; Keppler *et al* 1989; Rusterucci C. *et al* 1996). Generally, peroxidation of unsaturated lipids plays an important role in cell membrane properties, signal transduction pathways, apoptosis and the deterioration of foods.

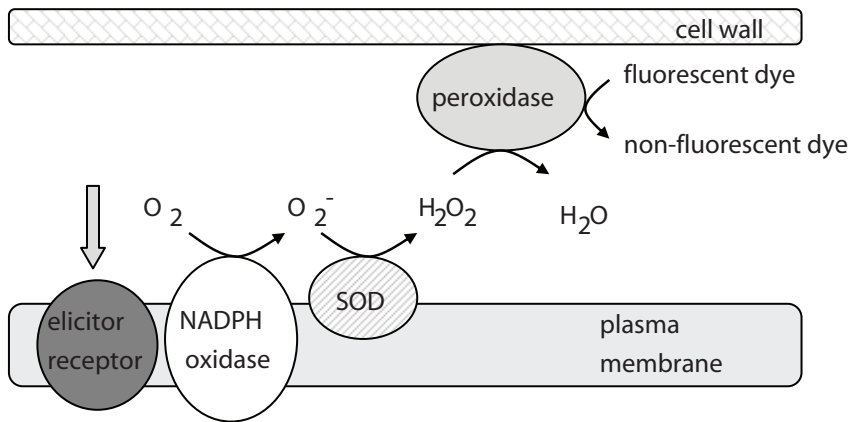


Figure 3.1: Schematic view of the enzymes involved in oxidative burst.

Two phases of responses to pathogens exist in plant tissues and suspension-cultured cells. First, there is a fast response, the so-called oxidative burst, occurring within minutes after elicitor treatment, which is followed after a few hours by a second phase of ROS production and is accompanied by specific gene activation. Several enzymatic systems have been proposed to generate ROS. (Apostol *et al* 1989; Auh and Murphy 1995; Lamb and Dixon 1997; Mithofer *et al* 1997) (see Fig. 3.1 for a schematic view). One of them involves the activation of a large protein: NADPH oxidase. This enzyme facilitates reduction of oxygen to a superoxide radical through the oxidation of cytosolic NADPH. It consists of a membrane-bound flavocytochrome b and a larger glycoprotein subunit and requires a number of cytosolic factors for enzymatic activity.

Because the oxidant O_2^- (superoxide radical) is poorly diffusible across membranes, it is most likely released at the surface of the membrane, where O_2^- is spontaneously or enzymatically (by superoxide dismutase) dismutated into H_2O_2 . Hydrogen peroxide participates in many signal transduction pathways and serves as a substrate for extracellular peroxidases located in the apoplastic region (Apostol *et al* 1989). In most plant systems H_2O_2 accumulation can be detected. Another oxidant produced includes the highly toxic $OH\cdot$.

(hydroxyl radical). The oxygen compounds may have direct antimicrobial activity and have a role in other defense mechanisms including lipid peroxidation, oxidative cross-linking of cell walls and hypersensitive response (Mithofer *et al* 1997).

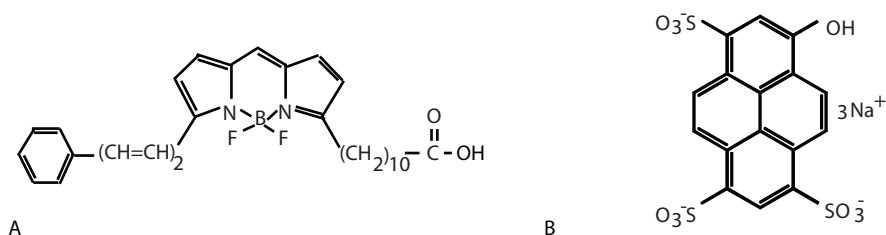


Figure 3.2. A: Chemical structures of 4,4-difluoro-5-(4-phenyl-1,3-butadienyl)-4-bora-3a,4a-diaza-s-indacene-3-undecanoic acid (BP-C11) and B: 8-hydroxypyrene-1,3,6-trisulfonic acid, trisodium salt (pyranine).

The oxidative burst includes the activation of several other enzymes such as phospholipases and lipoxygenases and is governed by the phosphorylation-dephosphorylation poise because the phosphatase 2A inhibitor cantharidin induces ROS production in several plant species while the protein-serine kinase inhibitor K252A suppresses it (Li and Casida 1992; Levine *et al* 1994; Lamb and Dixon 1997). In this chapter attention is focused on two aspects of ROS detection, namely lipid oxidation and hydrogen peroxide production. Fluorescent probes were used that report on oxidation and can look at the effect of specific inhibitors allowing interrogating the mechanism of oxidative burst in plant cells.

In order to track lipid oxidation a new fluorescent oxidation probe, abbreviated as BP-C11 (Fig. 3.2A), was used (Haugland 1996; Pap *et al* 1999; Pap *et al* 2000). BP-C11 represents a long chain fatty acid with a fluorophore composed of a boron dipyrromethene difluoride extended with a phenyl moiety by a diene bond. The probe is sensitive to the presence of ROS, which are likely to oxidize the diene bond. The BP-C11 probe has been used previously

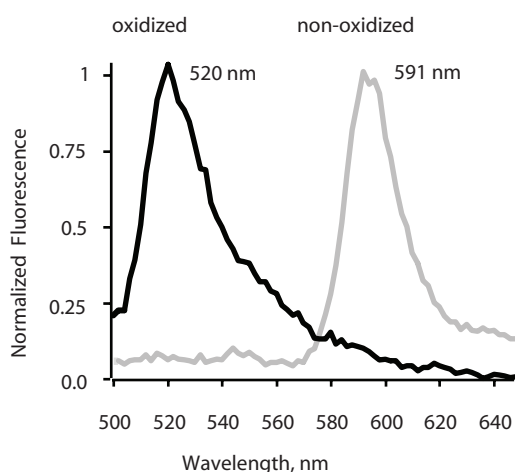


Figure 3.3: Fluorescence spectra of BP-C11 in DOPC vesicles. Oxidation was induced by adding 150 μ M cumene hydroperoxide (oxidant) and 0.5 μ M hemin (catalyst). Non-oxidized BP-C11 has a fluorescence maximum at 591 nm, while the maximum of the oxidized BP-C11 spectrum is at 520 nm.

for oxidation assays in model systems of membrane bilayers (Borst *et al* 2000) and animal cells (Pap *et al* 1999; Pap *et al* 2000). In figure 3.3 an example of the oxidation of BP-C11 in DOPC vesicles is shown. It can be clearly seen that oxidation with cumene hydroperoxide and hemin as oxidant-catalyst pair causes a shift from “red” to “green” fluorescence. The beneficial property of BP-C11 upon oxidation is allowing 2-channel tracking fluorescence imaging microscopy in live cells (Pap *et al* 1999). It was further found that the oxidation of BP-C11 proceeds at a comparable rate as arachidonic acid (Pap *et al* 2000).

Utilizing all the advantages of the BP-C11 probe we have developed a fluorescent assay for on-line localization and quantification of lipid oxidation in living tobacco plant cells. A second line of approach is followed by use of the fluorescent peroxidase substrate pyranine (Fig. 3.2B) for studying the effect of elicitors, inhibitors and ROS scavengers on H_2O_2 production in suspensions of tobacco cells. Upon oxidation the probe becomes non-fluorescent. Pyranine has been widely used as a pH-sensitive probe (Oja *et al* 1999), but has also found applications as a sensor for peroxidases (Apostol *et al* 1989). Because of its high charge pyranine will not pass the plasma membrane and is confined to the periplasmic cellular space.

3.2. Experimental procedures

3.2.1 Tobacco BY-2 cells

The tobacco cell line *Nicotiana tabacum* cv. Bright Yellow-2 (abbreviated as BY-2) possesses unique features such as very large growth rates and high homogeneity. The cells lack chlorophyll yielding therefore relatively low background fluorescence (Nagata *et al* 1992).

3.2.2 Preparation of cell suspension

BY-2 suspension culture was grown in a liquid medium containing Murashige and Skoog salts (without vitamins), supplemented with 30 g sucrose, 0.255 g KH_2PO_4 , 0.1 g myo-inositol, 1 mg thiamine-HCl and 0.2 mg 2,4-dichlorophenoxyacetic acid per liter (pH 5.8) (Linsmaier 1965). The cell culture was maintained by subculturing 1 ml of cells into 50 ml of fresh medium weekly and kept on a rotary shaker (130 rpm) in the dark at 22°C. For experiments, 3-4 days-old cells were collected by centrifugation for 5 minutes at 130 g and resuspended in fresh medium to a concentration of 0.01 packed cell volume (pcv). The cells are in the log-phase at 2-5 days after subculturing.

3.2.3 Protoplast isolation

For protoplast isolation 1 ml of BY-2 cells was transferred into 50 ml of fresh medium and grown for 2-3 days before use. The cells were collected by centrifugation to obtain a 2.5 pcv value and immersed in 10 ml of enzymatic solution (1% cellulase, 0.1% pectolyase, 0.4 M mannitol, pH 5.8), transferred to a 9-cm petri-dish and incubated for 2-3 hours at 25°C on a rotary shaker with low speed in the dark. Prior to further purification, protoplasts were checked with light microscopy to ensure that all cell walls had been removed. The protoplasts were purified over 63 μm nylon filter and transferred to 50 ml plastic tube, collected by centrifugation at 130 g, washed three times with 0.4 M mannitol solution (pH 5.8) and resuspended in protoplast culture medium (BY-2 medium with addition of 0.4 M mannitol).

The BY-2 protoplasts were used for experiments on the same day of isolation.

3.2.4 Labeling cells with BP-C11

BY-2 cells of 3 days old were diluted with fresh growth medium to 0.01 pcv and incubated with 1 μ M BP-C11, taken from an ethanol stock solution, for 1 hour in a petri-dish at room temperature on a shaker at low speed in the dark. Cells were washed twice with medium prior to use.

3.2.5 Confocal microscopy

The cells were examined under a LSM 510 confocal laser scanning microscope (Carl Zeiss). Samples (100-300 μ l) were placed into the 8-well chamber holder of the microscope and treated with the desired agents. The fluorescence of BP-C11 was acquired using 488 and 543 nm laser-line excitation and emission was collected in two channels: 505-550 nm for the oxidized form (channel 2) and 560-615 nm for the non-oxidized form (channel 1) of BP-C11. Integration of the fluorescence intensity of the desired image area was performed using LSM 510 software.

3.2.6 Steady-state fluorescence

Steady-state fluorescence spectra or intensities were obtained using a Spex Fluorolog 3.2.2 spectrofluorometer. The assay for H_2O_2 production was performed in BY-2 cells using pyranine. Basically, 1 μ l from a stock solution of 1 mg/ml pyranine in water was added directly to 1 ml of a prepared cell suspension in a quartz cuvette having a magnetic stirring bar approximately one minute prior to elicitor addition. The cells were continuously stirred at low speed to avoid mechanical disruption and cell sedimentation. The excitation wavelength was 405 nm and the emission was monitored at 512 nm.

3.3. Results and Discussion

3.3.1 Measurements and imaging of oxidative stress in tobacco BY-2 cells

The susceptibility of the probe towards reactive oxygen is comparable to that of endogenous fatty acids. Various radicals, such as for example, oxyl, peroxy or hydroxyl radicals, can initiate oxidation of BP-C11 but not superoxide, nitric oxide or hydroperoxide (Pap *et al* 2000). Because of its lipophilic character BP-C11 incorporates easily into plasma and organelle membranes. After five minutes of incubation, only the fluorescence of the non-oxidized fraction of the probe in the plasma membrane is visible (data not shown).

After one hour most of the probe was taken up by the cells staining also organellar membranes. It is remarkable, that the incorporated probe did not show toxicity towards the cells and was resistant to self-oxidation, degradation by cellular enzymes or bleaching during the course of an experiment requiring typically one hour. An incubation time of 60 minutes was chosen for further experiments.

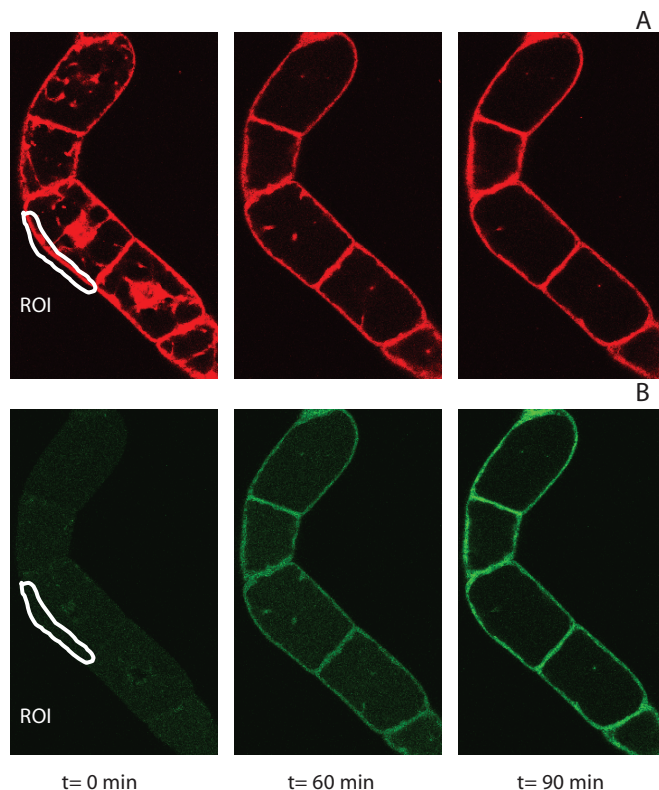


Figure 3.4: Time course of oxidation of BP-C11 in BY-2 cells induced by cumene hydroperoxide (1.5 mM) and hemin (5 μ M) by confocal laser scanning microscopy. Panel A represents channel 1 (non-oxidized), while panel B represents channel 2 (oxidized). A region of interest (ROI) has been indicated.

In order to investigate whether the incorporated probe into BY-2 cells is susceptible to oxidation, we exposed the cells to cumene hydroperoxide and hemin as an oxidant-catalyst pair (Fig. 3.4). Within one hour a significant fraction of the probe is oxidized (Fig. 3.4B). The degree of oxidation depends, among others, on the concentrations of oxidative agents used and the age of the cells (data not shown). Similar experiments were done with BY-2 protoplasts. The absence of the cell wall did not greatly affect the lipid oxidation rate, which led us to conclude that the cell wall was permeable to the chosen oxidants. The experiments were quantified in terms of average fluorescence intensity changes in a selected region of interest in the image. Examples of selected regions of interest (ROI's) are shown in figure 3.4. In figure 3.5 the average fluorescence intensity in membrane ROI's in BY-2 cells and in protoplasts is plotted against time. During the exposure to oxidative agents, the average fluorescence of the non-oxidized fraction of the probe decreases, while the fluorescence of the oxidized fraction becomes more intense. Within one hour approximately 20% of the probe underwent oxidation. The observed lipid oxidation rate in BY-2 cells is much smaller than reported previously in animal cells, in which about 70% oxidation of probe was detected within 30 minutes using a 20-fold lower concentration

of oxidative agents (Pap *et al* 1999). This difference is probably due to the strong defense response of higher plants (Lamb and Dixon 1997). Another factor to consider is that the composition and morphology of the membranes in plant cells are different from those in animal cells.

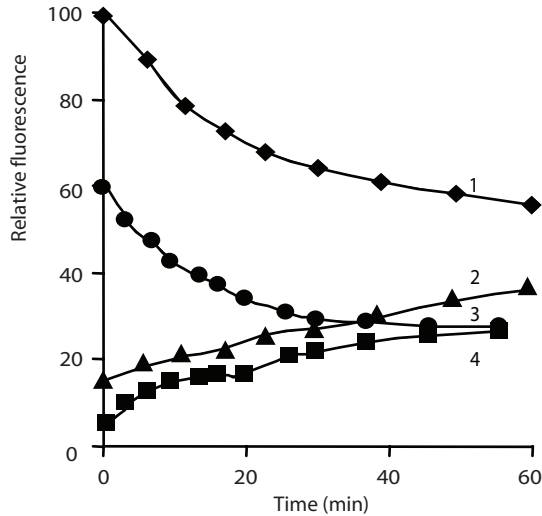


Figure 3.5: Time traces of the average fluorescence intensity of BP-C11 probe in selected regions of interests (ROI, see Figure 3.4) of BY-2 cells (curve 1 - channel 1, non-oxidized; curve 2 - channel 2, oxidized) and protoplasts (curve 3 - channel 1, non-oxidized; curve 4 - channel 2, oxidized) during incubation with 1.5 mM cumene hydroperoxide and 5 μ M hemin.

3.2 Effect of inhibitors and ROS scavengers on the hydrogen peroxide production in BY-2 cells

Oxidative burst is accompanied by the activation of several enzymes such as phospholipases and lipoxygenases. The phosphorylation-dephosphorylation balance also governs oxidative burst, because the protein phosphatase 2A inhibitor cantharidin induces ROS production in several plant species, while the protein-serine kinase inhibitor K252A suppresses it (Li and Casida 1992; Levine *et al* 1994; Lamb and Dixon 1997). The production of ROS can be measured by hydrogen peroxide production in cell suspensions induced by the elicitor cantharidin (Van Gestelen 1998). Activation of the oxidative burst also involves perturbations of cytosolic calcium levels (Lamb and Dixon 1997; Jones 1998; Takahashi 1998). Calcium serves as an activator of many enzymes, including phospholipase A_2 , and is an important second messenger in signal transduction. The nature of the enzymatic system responsible for generation of H_2O_2 in the tobacco BY-2 cell suspension was studied using pyranine, which can act as a fluorescent peroxidase substrate becoming non-fluorescent after oxidation. In figure 3.6A the effect of the relative oxidation rate versus the concentration of pyranine probe is plotted. The effect is already maximal at 2 μ M probe which has been used in the subsequent experiments.

Pyranine is located in the extracellular space and serves as a probe for cell wall peroxidases. The treatment of the BY-2 cell suspension culture with cantharidin leads to an increase of hydrogen peroxide production (see Fig. 3.6B). An oxidative burst occurred

within 30 minutes following a brief lag period. The rate of H_2O_2 production depends on the concentration of elicitor (see Fig. 3.6B) and the growth stage of the cells (logarithmic phase). For inhibition experiments a concentration of 100 μM cantharidin and 2 μM pyranine was used. The inhibitor effect was calculated based on oxidative quenching of the pyranine fluorescence.

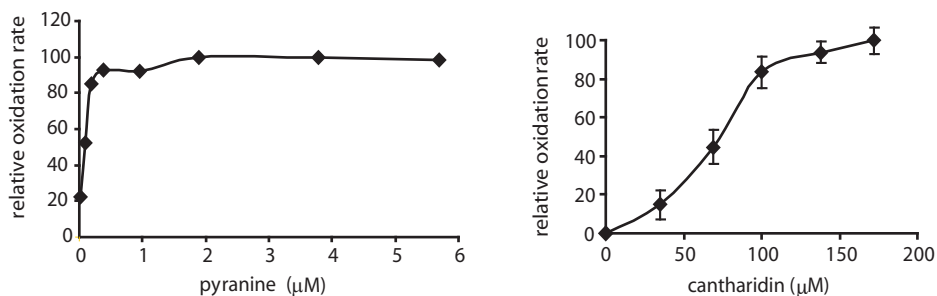


Figure 3.6: Effect of pyranine concentration (panel A) and elicitor concentration (panel B) on the relative oxidation rate of the fluorescent probe.

A few enzymatic systems have been proposed to generate active oxygen species during the elicited oxidative burst (Apostol *et al* 1989; Auh and Murphy 1995; Lamb and Dixon 1997; Mithofer *et al* 1997). One of them involves activation of NADPH oxidase (Dwyer *et al* 1996; Lamb and Dixon 1997), but also superoxide dismutase and cell wall peroxidases play a role (see Fig. 3.1). In our studies we tested a number of specific inhibitors of these enzymes for their ability to inhibit production of hydrogen peroxide in BY-2 cells induced by treatment with cantharidin. The molecular compounds, their common effects and results of inhibition studies are summarized in Table 3.1. Activators of phospholipase A_2 , calcium and mastoparan, did not stimulate hydrogen peroxide production, although mastoparan may induce an oxidative burst involving other oxidative species. We tested α -tocopherol (vitamin E) and ascorbic acid (vitamin C) in a near-physiological concentration range for their influence on the elicited response. The effect of α -tocopherol was not strong (in any tested concentration), although, because of its poor solubility, there is some doubt as to the actual concentration coming into contact with cells, whilst ascorbic acid completely abrogated the response at 10 mM. The temptation is to speculate that most reactions involved in the elicited cascade do not occur in the membrane region (vitamin E locates in hydrophobic areas), but in the apoplastic water phase where vitamin C can scavenge the produced oxygen species. Several inhibitors of NADPH oxidase and peroxidase result in almost complete inhibition and indicate participation of these enzymes in a cascade reaction. Removal of the cell walls diminishes the oxidation rate consistent with peroxidases being attached to the cell walls. The results obtained support the mechanism of cantharidin-elicited hydrogen peroxide production that has been proposed for other plant cells.

Table 3.1: Effect of inhibitors and ROS scavengers on H₂O₂ production by BY-2 cell suspension induced by cantharidin.

Addition to BY2 suspension culture	Common effects	Pyranine oxidation rate, % of 100 μ M cantharidin
none or 2%(v/v) DMSO		0
1 mM calcium	stimulates phospholipase A ₂ activity	0
200 μ M mastoparan	stimulates phospholipase A ₂ activity	0
100 μ M cantharidin (A)	inhibitor of protein phosphatase 2A	100 \pm 2
A + catalase	H ₂ O ₂ scavenger	19 \pm 4
A + superoxide dismutase	catalyst of conversion of O ₂ ⁻ into H ₂ O ₂	91 \pm 1
A + peroxidase		146 \pm 2
A + 40 μ M α -tocopherol	lipid-soluble antioxidant, reacts directly with superoxide anion-production (O ₂ ⁻), singlet oxygen	80 \pm 16
A + 10 mM ascorbic acid	water-soluble antioxidant	2 \pm 0.2
A + 25 μ M diphenylene iodonium	flavin analogue inhibitor of plant and mammalian NADPH oxidase	0.3 \pm 0.4
A + 0.1 mM p-hydroxymercurybenzoic acid	inhibitor of mammalian NADPH oxidase	0.7 \pm 0.7
A + 100 μ M iodoacetate	membrane-permeative thiol reagent	5 \pm 1
A + 100 μ M N-pyrene maleimide	membrane-permeative thiol reagent	0
A + 2 mM salicylhydroxamic acid	plant peroxidase inhibitor	5 \pm 2
A + 10 mM imidazole	inhibitor of plant NADPH oxidase	15 \pm 3
protoplasts	removed cell walls and attached peroxidases	11 \pm 4

3.4. Conclusions

The lipophilic probe BP-C11 has the advantageous property that the fluorescence changes color upon oxidation and is therefore very appropriate to be used in live cells as a probe for lipid oxidation as demonstrated here. Pyranine can be easily oxidized by hydrogen peroxide and loses its fluorescence. This probe can then be conveniently applied in suspension cells to monitor hydrogen peroxide levels for screening activation or inhibition of the pathways leading to H_2O_2 formation. In the future pyranine fluorescence can be viewed with 2-photon confocal laser scanning microscopy opening the way for *in situ* detection of H_2O_2 .

Acknowledgements

This research was supported by EU-FAIR project 97-3228. Marsha Uskova was supported by the Netherlands Organization of Scientific Research (NWO) grant 047-007-005 providing scientific cooperation between The Netherlands and the Russian Federation.

Chapter 4

Multiphoton Microspectroscopy in Living Plant Cells

Abstract

Microspectroscopic measurements in plant cells are complicated by the presence of dense cellular structures such as the cell wall that causes severe light scattering. In addition, the low penetration depth of the excitation light limits the fluorescence signal originating from deeper cell layers in thick multi-cellular plant preparations when one-photon excitation (OPE) is applied. However, two-photon excitation (TPE) can overcome these problems. We report on two-photon microscopy studies of Histone 2B-YFP, a nuclear-expressed protein involved in chromatin packaging. In contrast to OPE, TPE allows imaging throughout the whole root. Therefore by using TPE it was also possible to visualize the root quiescent centers using SCARECROW-EGFP localized in the middle of the root. The interactions between various members of the FLORAL BINDING PROTEINS (FBP) have been studied by monitoring Förster resonance energy transfer (FRET) between FBP-ECFP and FBP-EYFP fusion proteins using fluorescence lifetime imaging microscopy (FLIM) of the two-photon excited ECFP component.

This chapter has been adapted from:

J. W. Borst, M. A. Hink, A. van Hoek, A. J. W. G. Visser (2003). Multiphoton microspectroscopy in living plant cells. *Proc. Spie* 4963: 231-238

and

J. W. Borst, I. Nougalli-Tonaco, M. A. Hink, A. van Hoek, R. G. H. Immink and A. J.W.G. Visser (2006) Protein-Protein Interactions *In Vivo*: Use of Biosensors Based on FRET. Reviews in Fluorescence 2006. (in press) C. D. Geddes, and J. R. Lakowicz, editors, Kluwer Academic/Plenum Publishers. New York, pp 341-355.

4.1. Introduction

In the early 1930s two-photon excitation of molecules was predicted by Maria Göppert-Mayer in the case that high photon densities are present so that two or more low energy photons can be simultaneously absorbed in a single quantum event (Göppert-Mayer 1931). Since the energy of a photon is inversely proportional to its wavelength, the two photons should be twice the wavelength necessary for one-photon excitation (OPE). It was until the beginning of the 1990s when Denk *et al.* (Denk *et al* 1990) introduced the two-photon excitation (TPE) laser scanning microscope resulting in the first biological applications of TPE. Because excitation in two-photon microscopy occurs only at the focal point of a diffraction-limited spot, it is possible to create thin optical sections of thick biological specimens in order to obtain three-dimensional resolution.

Two-photon excitation microscopy has some major advances over OPE confocal microscopy for 3D imaging. First of all is the penetration of near-infrared light used for TPE much deeper than that of visible light used in OPE confocal microscopy. TPE of thick biological samples allows imaging to a depth of more than 200 μm whereas OPE confocal microscopy is limited to depths of approximately 50 μm (Piston 1999). In OPE confocal microscopy fluorescent light is generated throughout the sample along the optical axis but only the signal from a thin focal plane is detected by placing an aperture (the so-called pinhole) at the image plane. However, by using TPE molecules are excited at the focal plane only and therefore no pinhole is required. In addition, TPE minimizes photobleaching and photodamage in out-of-focus regions that are usually limiting factors in conventional live cell imaging (Nakamura 1999)

In this chapter the unique features of two-photon imaging in plant systems are demonstrated as compared to conventional confocal imaging. One example is the GFP-fusion protein SCARECROW-EGFP, which is involved in the embryogenesis in roots and shoots of plants (Haseloff *et al* 1997; Wysocka-Diller *et al* 2000). The proteins are expressed in specialized cells called the quiescent centers. Since these centers are localized in the middle of the root, two-photon imaging was necessary to visualize these spots within the relatively thick roots.

The same accounts for another example of a fusion protein, namely Histone 2B-EYFP that is expressed in root tips of *Arabidopsis* plants. Histones are the structural proteins in chromosomes, which are only found in eukaryotic cells. Histones are relatively small proteins, are present in very high quantities (about 6000 times more copies than normally expressed proteins) and contain a high number of positively charged amino acids. Therefore binding of histones to the negatively charged DNA is very tight and they rarely dissociate from the DNA (Alberts *et al* 2004).

A third example comprises a study of MADS box transcription factor interactions in living plant cells by using fluorescence lifetime imaging microscopy (FLIM) for reporting Förster resonance energy transfer (FRET). MADS box genes encode for transcription factors involved in many developmental processes in flowering plants (Ferrario *et al* 2004). This family of transcription factors acts in a complex network of physical protein-protein and protein-DNA interactions. We have used FLIM by combining two-photon excitation

laser-scanning microscopy with time-correlated single photon counting in detection. The interactions between various types of the FLORAL BINDING PROTEIN (FBP) from *Petunia* have been studied. FBP proteins have been fused to ECFP or EYFP and single and double transfected cowpea protoplasts were analyzed. Molecular interactions have been observed by monitoring the fluorescence lifetime of ECFP. When ECFP fusion proteins are in close proximity of EYFP fusion proteins FRET can take place from ECFP to EYFP, resulting in a decrease of the fluorescence lifetime of the donor (ECFP) (Bastiaens and Squire 1999).

4.2. Materials and Methods

4.2.1 Instrument

Multiphoton imaging was performed on a multiphoton dedicated Biorad Radiance 2100 MP system (Fig. 4.1) or a Biorad Radiance 2100 MP-VIS system, combining OPE and TPE. Each system is coupled to a Nikon TE300 inverted microscope. The excitation sources, tunable Ti-Sapphire lasers (Coherent Mira) are pumped with a 5 or 10 Watt (Coherent) Verdi laser, respectively, resulting in excitation pulses of ~ 200 fs at a repetition rate of 76 MHz. In the beam-conditioning unit (BCU) the excitation power is tuned by a Pockel cell.

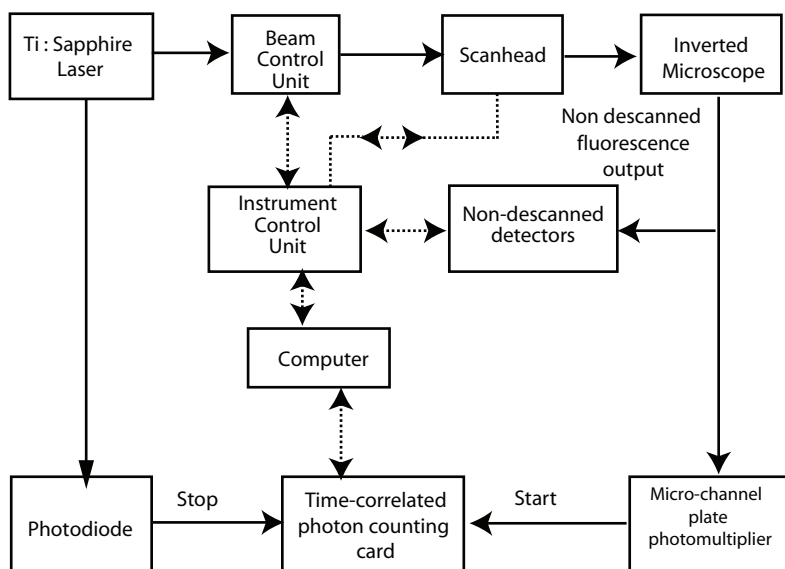


Figure 4.1: Schematic overview of the multi-photon microscopy system

The laser beam is collimated in the scanhead and focused by a Nikon 60x water immersion Apochromat objective lens (NA 1.2) into the sample. In the multiphoton dedicated microscope the fluorescence was detected by non-descanned, direct detectors (NDD), which are coupled to the sideport of the microscope. Using this type of detection the loss of fluorescence light is reduced and 3-5 times more signal is obtained as compared to internal detectors. The emission light is splitted into two channels using a dichroic mirror filter wheel. The fluorescence

in each channel was selected by bandpass filters and detected by photomultipliers (PMT) which could be set to photon counting mode, significantly enhancing the signal to noise ratio. FLIM measurements were performed by directing the fluorescence via a secondary dichroic (670UVDCLP) into a Hamamatsu R3809U photomultiplier, operated at 3.1 kV. ECFP fluorescence was selected using a 480DF30 bandpass filter. The multichannel-plate photomultiplier allows single photon detection at high time-resolution (50 ps). The output of the detector was coupled to a Becker & Hickl single photon counting module (SPC 830) (Becker and Bergmann 2002). The signal from the Hamamatsu triggers the time ramping to start the time correlated single photon counting (TCSPC) (Becker *et al* 2004). The pulses from the Ti-Sapphire laser serve as the SYNC signal in order to stop the time ramping and allow timing of the arrival of the fluorescent photons. The time window (ADC) was set to 64 channels and typically fluorescence was recorded for 2 minutes at a photon count rate of approximately 20 kHz. The signal from the PMT is combined with the pixel clock and line predivider signals from the Biorad scanhead to create 2D lifetime images.

Research in our lab is focused on visualizing molecular interactions of proteins in living plant cells. Interactions can be visualized and quantified by using the FRET approach. The most direct method to observe FRET is measuring changes in the fluorescence lifetime of the donor molecule using FLIM compared to intensity based methods. An example of FLIM will be discussed in paragraph 4.3.2.2.

4.2.2 Biological plant samples

Arabidopsis plants were mounted in medium between two cover slips. Images were acquired using the Biorad Radiance MP-VIS using the output of the Ti-Sapphire laser at 920 nm (8 mW above objective) for Histone 2B-EYFP and at 870 nm (12 mW above objective) for SCARECROW-GFP. For Histone 2B-EYFP and propidium iodide (PI) the fluorescence was splitted via a 560 nm dichroic mirror and the YFP signal was selected by a 515DF30 bandpass filter while PI was observed using a 620DF100 bandpass filters and detected by the internal PMT's. In the samples labeled with SCARECROW-EGFP and PI the same filters were used. For confocal measurements the pinholes were set at a diameter of 1 Airy unit but in case of TPE the pinholes were fully opened and the so-called "signal enhancing lens" was put in front of the pinholes to enhance the collection of scattered fluorescence light (Amos and Reichelt 2000).

The z-stack images of Histone 2B-YFP were accumulations of 5 frames, each set acquired with a step size of 500 nm. To enhance the signal-to-noise ratio the detectors were set in photon-counting mode and therefore the power of the excitation beam could be lowered. Although photobleaching in TPE will take place only at the focal spot, and not throughout a complete cell like in OPE, the level of excitation power is very critical. Destruction of the fluorophores or even the complete cell can be induced easily at higher laser powers (Cheng *et al* 2001; Feijo and Moreno 2004). As have been reported before, below a certain threshold TPE imaging is relatively harmless and no bleaching is observed allowing prolonged imaging times. The threshold excitation power seems to be different for each cell type and fluorophore. In all experiments the laser power was adjusted to be as low as possible to avoid photobleaching of the fluorescent markers.

Cowpea mesophyll protoplasts were prepared from the primary leaves of ten-days old *Vigna unguiculata*. The cells were transfected either with FBP-ECFP or doubly transfected with FBP11-ECFP and FBP24-EYFP using the PEG method (the protocol has been described in detail by Shah *et al* (2001)). The following day the protoplasts were pipetted into 8-well borosilicate bottomed holders (Naglenunc) and donor lifetimes (ECFP) were analyzed with SPCImage2.3 software (Becker & Hickl) using a two-component decay model in which the fluorescence lifetime of the donor without acceptor present was fixed.

4.3. Results

4.3.1 Imaging of plants using OPE and TPE confocal microscopy

The penetration depth of microscopic techniques is limited in multicellular and dense tissues. Therefore conventional confocal and TPE images of Histone 2B-YFP in *Arabidopsis* plants were compared. Figure 4.2A shows a TPE fluorescence image of a root expressing Histone 2B-EYFP. The plant was counterstained with propidium iodide (PI) that labels DNA and the cell wall, marking the outer borders of the individual plant cells. The black round-shaped structures within the image represent the fluorescent chromatin localized in the nuclei.

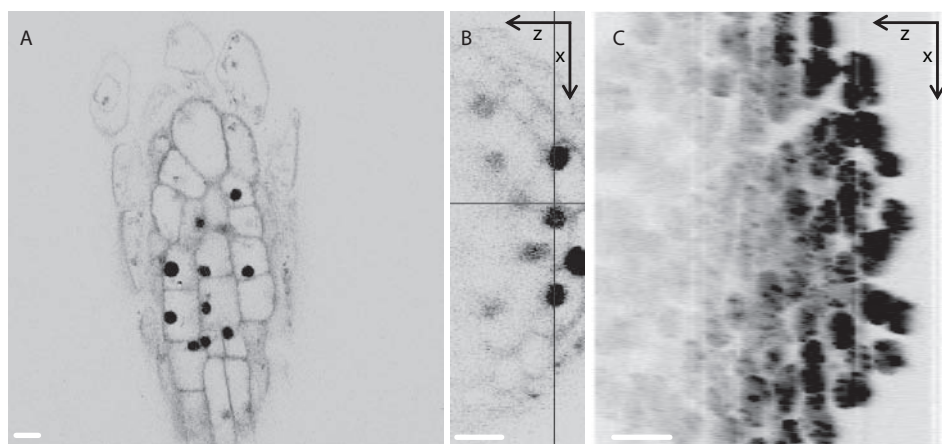


Figure 4.2: Depth images of Histone-2B-EYFP expressed in *Arabidopsis* roots counterstained with propidium iodide (PI). (A) TPE image acquired at two-cell layers depth within the root. XZ images using (B) OPE and (C) TPE. The bar denotes 10 μm .

The image was acquired by focusing the excitation beam two cell layers deep inside the root. Z-slices through the root were taken to compare the penetration depth. Figure 4.2B and 4.2C represent XZ-images acquired by OPE and TPE respectively. The fluorescent chromatin structures in figure 4.2B can be visualized up to approximately three cell layers deep corresponding to 25 μm . The fluorescence signal from cells localized deeper inside the root (at the left side of the image) is too low, as has been reported by others as well (Feijo and Moreno 2004). These data show that using TPE (920 nm) the penetration depth is at least three times deeper than for OPE. Plant cells contain dense structures that disturb the image quality. However, by using TPE, chromatin structures in the middle of the root tip become

visible now. The fluorescent DNA marker propidium iodide is co-localized with Histone 2B-EYFP confirming the proper localization of the protein. These experiments also show that both dyes can be excited with only one TPE wavelength. In conventional confocal microscopy these experiments would require expensive investments in UV lasers and optics enabling, for instance, to detect the DNA-specific dye DAPI, which absorbs light in the near-UV.

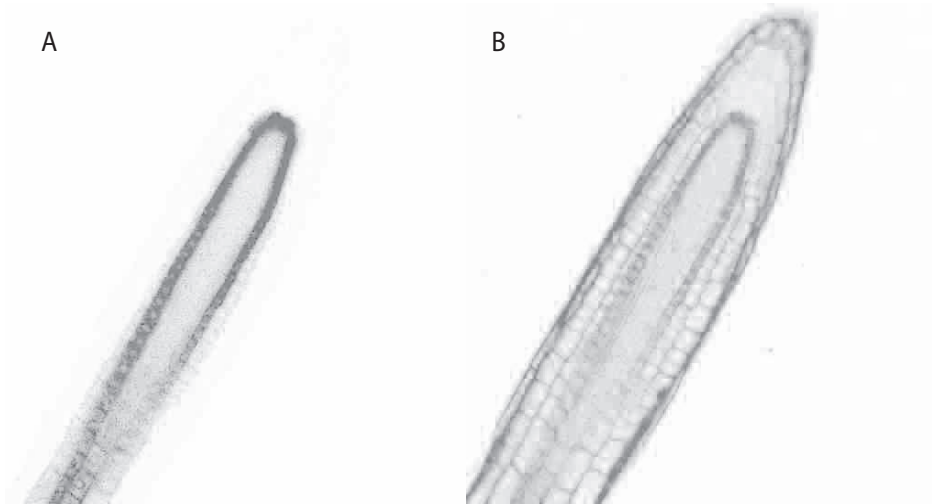


Figure 4.3: Fluorescence images of *Arabidopsis* roots labeled with SCARECROW-GFP (channel A) and PI (channel B). The image was acquired using TPE in the middle of the root.

The strength of two-photon imaging was also demonstrated in the experiments visualizing SCARECROW-EGFP in *Arabidopsis* plants. Figure 4.3A shows a TPE fluorescence image of a transformed plant root. The outline of the root is visualized by staining the cell walls by PI (Fig. 4.3B). SCARECROW-EGFP is only expressed in the endodermis, localized in the centre of the root. The quiescent centers (see arrow), which are specialized cells at the tip of the root, could be identified. In confocal images acquired with OPE, the quiescent centers could not be visualized (data not shown), since these cells are localized at a depth of $\sim 60 \mu\text{m}$.

4.3.2 Applications with plant transcription factors

4.3.2.1 Sub-cellular localization via confocal microscopy

In this paragraph an application of FRET microscopy in combination with FLIM will be described. The aim is the study of MADS box transcription factor interactions in living plant cells. MADS box genes encode for transcription factors involved in many developmental process in flowering plants, most notably in the determination of floral meristem and floral organ identity (Riechmann and Meyerowitz 1997; Ferrario *et al* 2004). This family of transcription factors acts in a complex network of physical protein-protein and protein-DNA interactions either as homo- or heterodimers and are, most likely, able to form higher order complexes (Egea-Cortines *et al* 1999; Honma and Goto 2001). To study this network of interactions, the use of the yeast two-hybrid system has become a powerful tool to get a

first impression about the ability of the MADS box proteins to form specific dimers and/or higher-order complexes. Recently, comprehensive matrix-based screens for petunia and *Arabidopsis* MADS box transcription factor interactions revealed the ability of these factors to form specific homo- and heterodimers (Immink *et al* 2003; de Folter *et al* 2005). Moreover, these interactions are conserved between different plant species (Immink *et al* 2002). Despite the fact that many studies have been done in yeast only little information is known about how these interactions occur *in planta*. In this work, different petunia MADS box proteins, the FLORAL BINDING PROTEINS (FBP's) involved in ovule development were used for the study of protein-protein interactions in living cells. First, the genetic fluorescent labels ECFP and EYFP were cloned at the C-terminal side of the different FBP's. C-terminal fusions to various *Arabidopsis* MADS box proteins appeared to give no loss in biological activity of these proteins (Angenent and Urbanus, unpublished observations). Subsequently, different combinations of the MADS box proteins were transfected in cowpea leaf protoplasts, which transfection has been described previously (Russeinova *et al* 2004).

The localization of the FBP proteins FBP11, FBP2 and FBP24 has been described by Nougalli-Tonaco and colleagues (Nougalli-Tonaco *et al* 2006). Differences in sub-cellular localization were observed among the proteins. Remarkably, the single transfected constructs FBP2 and FBP24 were localized in the nucleus, whereas FBP11 stays in the cytoplasm, probably because of its inability to homodimerize, which seems to be a prerequisite for movement into the nucleus (Immink *et al* 2002). Co-transfections of FBP2 and FBP24, as well as FBP11 and FBP24, were performed and nuclear co-localization was observed in both cases. Considering that FBP11 is expressed in the cytoplasm by its own, and taking into account the hypothesis that dimerization is essential for transport into the nucleus, the co-localization of both proteins is already a preliminary indication of the formation of dimers. Co-localization is a good indicator for interacting proteins, but, on the other hand, FRET-FLIM measurements can unambiguously prove the existence of physical interactions between the different FBP's.

4.3.2.2 Molecular interaction imaging via FRET-FLIM

Various techniques to measure FRET have been applied in animal (Bastiaens and Pepperkok 2000) and in plant cells (Russeinova *et al* 2004). We have used FLIM by combining two-photon excitation laser-scanning microscopy with time-correlated single photon counting as described above. First a fluorescence intensity image is obtained. Subsequently, the fluorescence decay of the donor molecule is determined for every pixel in the image. Depending on the fluorescent signal of the donor, an experiment typically takes 1-2 minutes. FLIM measurements of the single and double co-transfected cells, as described for the confocal imaging part, were repeated and these experiments started in a specific order. In protoplasts co-expressing the ECFP and EYFP tagged FBPs, a protoplast was selected showing EYFP fluorescence in the epi-fluorescence mode, while ECFP fluorescence is hardly visible in this configuration. If ECFP expression was observed in the 2-photon-imaging mode, this cell was chosen for a FLIM measurement. The excitation wavelength in plant cells was set to 860 nm, which mainly excites the ECFP molecules, whereas excitation of EYFP is minimal. The excitation of ECFP was also reported at 820 nm (Chen *et al* 2003) in a ECFP-EYFP pair, but

at this wavelength the auto-fluorescence detected with the ECFP band pass filter 480DF30 nm in plant protoplasts is higher than at 860 nm.

In figure 4.4A, a monochromatic image represents the fluorescence intensity of the ECFP donor molecules in the absence of EYFP acceptor molecules. This is the control experiment to obtain the fluorescence lifetime of the FBP24–ECFP donor alone. The pixel at the blue crosshair is the actual fluorescence decay shown in figure 4.4B. The fluorescence lifetime image is calculated per pixel and displayed as a pseudo color image. In figure 4.4C the fluorescence lifetime of FBP24-ECFP of 2.5 ns clearly shows up throughout the whole nucleus indicated as a blue color. The distributions of fluorescence lifetimes can be observed in figure 4.4D. The fluorescence lifetime was analyzed according to a single exponential decay model. For transcription factors in plant cells a fluorescence lifetime of typically 2.5 ns was found. After determination of the fluorescence lifetime of the FBP-ECFP donor alone, the analysis for all other combinations was performed according to a double exponential decay model, in which the value of the ECFP fluorescence lifetime (τ) was fixed to $\tau = 2.5$ ns. Upon FRET the fluorescence lifetime of the ECFP donor molecules will decrease and the amount of reduction is directly correlated with the FRET efficiency. The fluorescence lifetime images displayed in the figures represent the average lifetime values.

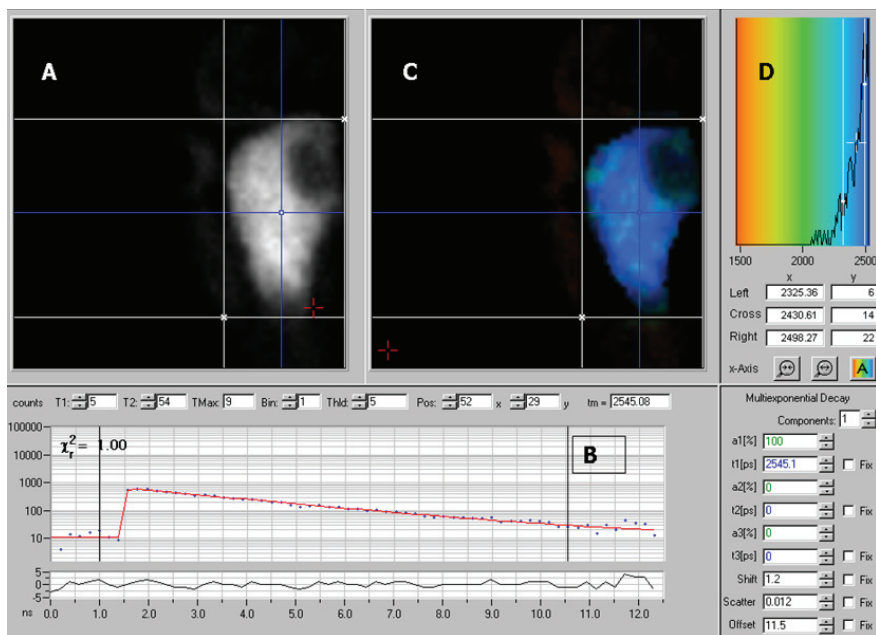


Figure 4.4: An image of a typical FLIM experiment using the Becker and Hickl analysis software. In panel A the fluorescence intensity of the nuclear localized MADS box protein, FBP24-ECFP, is shown. At the blue crosshair the fluorescence decay of the selected pixel is displayed (panel B). The fluorescence lifetimes are calculated per pixel and visualized as a pseudo color histogram image (panel D).

In figure 4.5A-B the fluorescence intensity and lifetime images are presented for the co-transfection of FBP2-ECFP and FBP24-EYFP. The fluorescence intensity image clearly shows a nuclear localization. The fluorescence lifetime image indicates a significant

reduction of the fluorescence lifetime; dark orange to green corresponds to $\tau = 1.9 - 2.0$ ns. The distribution of fluorescence lifetimes is given in the histogram in figure 4.5C. This distribution of fluorescence lifetimes in the case of the combination FBP2-ECFP and FBP24-EYFP was homogeneously spread around 2.0 ns resulting in a FRET efficiency of 20%. The localization of the co-transfection of FBP24-ECFP and FBP11-EYFP is also nuclear, but the distribution of fluorescence lifetimes in this combination is broader than that of the previous pair of proteins. The combination FBP24-ECFP and FBP11-EYFP suggests that there are sub-nuclear regions with $\tau = 1.9$ ns and without interaction $\tau = 2.5$ ns between the two FBP proteins. This effect is illustrated in figure 4.5E where green spots (interaction) are present in a ‘blue’ nucleus (no interaction). In the histogram of figure 4.5F a peak at 2.5 ns is seen that is absent in the histogram of figure 4.5C. The reciprocal combinations have been tested as well and gave the same results (data not shown).

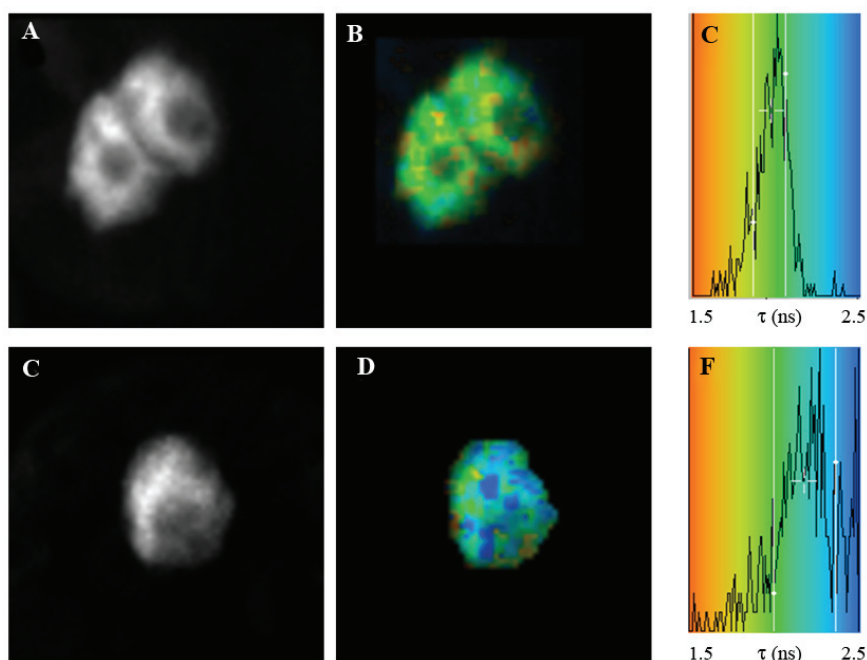


Figure 4.5: FRET-FLIM analyses using a double exponential decay model of transfected cowpea leaf protoplasts, expressing the following combinations FBP2-ECFP and FBP24-EYFP (panels A-C) and FBP24-ECFP and FBP11-EYFP (panels D-F). In panels A and D the fluorescence intensity image of the nucleus of a representative cell is shown, in panels B and E the fluorescence lifetime image of the same nucleus is shown as a pseudo color image, and in panels C and F the distribution of fluorescence lifetimes over the nucleus is presented

Several studies revealed that homo- and/or heterodimerization of transcription factors have indicated their binding to specific DNA sequences (Pellegrini *et al* 1995; Shore and Sharrocks 1995). Also higher-order complex formation of MADS box transcription factors is stabilized by specific DNA binding (Egea-Cortines *et al* 1999). It might be possible that the sub-nuclear regions represent places where the chromatin is available for transcription and to which the transcription factors are recruited, resulting in stabilization of the less stable

or “transient” interactions (Nougalli-Tonaco *et al* 2006). The FRET-FLIM data also have shown to be concentration independent. The fluorescence intensity signal over the nucleus is homogeneously distributed, but the fluorescence lifetimes showed sub-nuclear spots with reduced values indicating specific molecular interactions.

It was shown previously by yeast two-hybrid techniques, spectral imaging and FRET-FLIM that the petunia flowering gene PFG and FBP2 do not interact (Immink *et al* 2002). This combination was used as negative control and the invariant fluorescence lifetimes for different locations in the nucleus indicated no interaction (results not shown). As a positive control the combination FBP2-ECFP and FBP11-EYFP was transfected in cells and throughout the whole nucleus average fluorescence lifetimes of about 1.9 ns were measured (data not shown) (Immink *et al* 2002).

4.4 Conclusions

Imaging the dense, turbid and multilayered tissues of *Arabidopsis* plants clearly showed the advantages of confocal microscopy using two-photon excitation over that using one-photon excitation. Histone 2B-EYFP and SCARECROW-EGFP expressed deep inside plant roots could be easily visualized with our two-photon set-up whereas those structures could not be seen in images acquired with conventional confocal microscopy. A three-fold higher penetration depth could be achieved by changing from OPE to TPE. The results presented here have initiated further research to obtain more information about chromatin organisation and dynamics in plant development.

FRET applications in combination with cell biology have become a very powerful tool to obtain spatial and dynamic information of cellular processes *in vivo*. FRET can be used as a spectroscopic ruler to detect molecular interactions between proteins in living cells. We have discussed measurements of FRET by FLIM having several advantages compared to intensity-based methods. A good example of the additional valuable information is shown in the spatially resolved fluorescence lifetime images. FLIM measurements of the MADS box transcription factors showed sub-nuclear spots in the fluorescence lifetime images indicating molecular interactions between the different FBP's. The reduced fluorescence lifetimes in these regions may indicate possible transcriptional activation in the nucleus. These data could not be obtained with other FRET techniques.

Acknowledgements

Joost Willemse and Olga Kulikova (Laboratory of Molecular Biology, Wageningen University, The Netherlands) are acknowledged for making available the plant and protoplast systems. We thank Gerco Angenent and Sacco de Vries for continuing interest and fruitful collaboration. The multi-photon setup has been obtained owing to an investment grant from the Netherlands Organization for Scientific Research (NWO).

Chapter 5

Heterodimerization and Endocytosis of *Arabidopsis* Brassinosteroid Receptors BRI1 and AtSERK3 (BAK1)

Abstract

In *Arabidopsis* brassinosteroid (BR) perception is mediated by two LRR receptor-like kinases, BRI1 and AtSERK3 (BAK1). Genetic, biochemical and yeast interaction studies suggested that the BRI1-AtSERK3 receptor complex initiates BR signaling, but the role of the AtSERK3 receptor is still not clear. Transient expression of BRI1 and AtSERK3 fused to cyan and yellow fluorescent GFP variants in plant protoplasts allowed us to localize each receptor independently *in vivo*. We show that BRI1 but not AtSERK3 homodimerizes in the plasma membrane while BRI1 and AtSERK3 preferentially heterodimerize in the endosomes. Co-expression of the two proteins results in a change of the steady-state distribution of both receptors due to accelerated endocytosis. Endocytic vesicles contain either BRI1 or AtSERK3 alone or both together. We propose that the AtSERK3 protein is involved in changing the equilibrium between plasma membrane-located BRI1 homodimers and endocytosed BRI1-AtSERK3 heterodimers.

This chapter has been published in:

E. Russinova, J.W. Borst, M. Kwaaitaal, A. Caño-Delgado, Y. Yin J. Chory, and S. C. de Vries (2004) Heterodimerization and endocytosis of *Arabidopsis* brassinosteroid receptors BRI1 and AtSERK3 (BAK1). *Plant Cell* **16**: 3216-3229.

5.1 Introduction

Brassinosteroid (BR) signaling is one of the best-studied signal transduction pathways in plants. In contrast to animals where steroid hormones are perceived by nuclear receptors, plants employ plasma membrane receptors that include the BRASSINOSTEROID INSENSITIVE 1 (BRI1) protein. BRI1 belongs to the leucine-rich-repeat (LRR) receptor-like kinase (RLK) class of proteins. BRI1 was identified as a loss-of-function brassinosteroid-insensitive *Arabidopsis* mutant that cannot be rescued by exogenous application of BRs (Li and Chory 1997). The BRI1 protein consists of an extracellular domain, a single transmembrane domain and a cytoplasmic serine/threonine kinase. The extracellular domain contains 25 LRRs and a 70 amino acid (aa) island domain between the 21st and the 22nd LRR, that was found essential for BR binding (He *et al* 2000; Wang *et al* 2001). A second LRR RLK, the BRI1-ASSOCIATED RECEPTOR KINASE 1 (BAK1), was identified in an activation-tagging screen for *bril* suppressors (Li *et al* 2002) and in a yeast two-hybrid screen for BRI1 kinase domain (KD) interacting proteins (Nam and Li 2002). BAK1 has a shorter extracellular domain with only 5 LRRs and it lacks the 70 aa island domain. BAK1 is identical to the previously described *Arabidopsis thaliana* SOMATIC EMBRYOGENESIS RECEPTOR-like KINASE 3 (AtSERK3), a member of a small family of related RLKs (Hecht *et al* 2001). Genetic and molecular data support the notion that BRI1 and AtSERK3 are part of the same BR receptor complex although two other BRI1 homologues have been reported to function as BR receptors (Yin *et al* 2002). Neither of these proteins have shown to be a direct target of the BRI1/AtSERK3 heterodimer. BRI1 and AtSERK3 are localized to the plasma membrane (Friedrichsen *et al* 2000; Li *et al* 2002). How the BRI1-AtSERK3 receptor complex transmits the BR signal is not known although two recent models suggest similarities to either animal tyrosine kinase or transforming growth factor- β (TGF- β) cell surface receptor activation (reviewed by Clouse 2002; Li 2003).

Signaling events in animal cells require endocytosis and endosomes are considered to function as ‘signaling compartments’ in addition to a more general role in receptor recycling (reviewed by Gonz  les-Gait  n 2003). During endocytosis several intermediate compartments are distinguished. In the early sorting endosomes a decision is made to direct endocytosed receptors either towards late endosomes and to degradation in lysosomes or to recycle the receptors back to the plasma membrane *via* recycling endosomes (reviewed by Gruenberg 2001). In plants endocytosis is poorly understood but similar mechanisms are proposed (Ueda *et al* 2001). Recently, studies of the GDP/GTP exchange factor for small G-proteins of the ADP-ribosylation factor (ARF) class ADP-ribosylation factor G protein (ARF-GEF), GNOM (Geldner *et al* 2003) and of sterol trafficking in *Arabidopsis* (Grebe *et al* 2003) demonstrate the importance of endocytosis in plant development. Although previously demonstrated in plants (Horn *et al* 1989), virtually nothing is known about the role of endocytosis in plant receptor-mediated signaling. Previously we showed that the AtSERK1 protein internalizes into early endosomes when co-expressed with the PP2C type KINASE ASSOCIATED PROTEIN PHOSPHATASE (KAPP) in cowpea protoplasts (Shah *et al* 2002). It was proposed that the function of KAPP was tightly coupled to a mechanism of plant receptor internalization.

To study the dynamics of the BRI1/AtSERK3 interaction in living cells and to

investigate whether endocytosis of the two receptors is taking place, BRI1 and AtSERK3 proteins were coupled to the green fluorescent protein (GFP) variants exhibiting either yellow or cyan fluorescence (EYFP or ECFP respectively). This allowed us to follow both receptors simultaneously *in vivo* and to apply imaging techniques such as Fluorescence Lifetime Imaging Microscopy (FLIM) in order to determine Förster Resonance Energy Transfer (FRET), indicative of receptor heterodimerization. These techniques are essential for imaging protein-protein interactions in living plant (Shah *et al* 2001; Immink *et al* 2002; Shah *et al* 2002) and animal cells (Sorkin *et al* 2000; Haj *et al* 2002). Our results show that BRI1 and AtSERK3 are constantly recycled *via* endosomes. When the two receptors are co-expressed a sorting into different endosomal compartments takes place, containing either BRI1 or AtSERK3 alone or both together. Interestingly BRI1 and AtSERK3 do not constitutively interact as they show interaction mainly in the endosomes and in restricted areas on the plasma membrane. This resembles the endocytic pathway of internalization of animal receptors and suggests a function of the AtSERK3 protein in redistributing the BRI1 receptor.

5.2 Materials and Methods

5.2.1 Construction of the ECFP/EYFP tagged proteins

The full-length cDNA of the BRI1 was PCR amplified from an EST (Asamizu *et al* 2000) obtained from Kazusa DNA Research Institute (Japan) with primers BRI1-F, 5'-CATGCCATGGATGAAGACTTTTCAAGC-3' and BRI1-R, 5'-CATGCCATGGCTAATTTTCCTCAGGAA-3'. The BRI1 cDNA was then inserted in the NcoI site upstream of the ECFP/EYFP tags of the pMON999 (Monsanto) vectors in order to generate BRI1-ECFP and BRI1-EYFP fusions respectively. The BAK1 cDNA was PCR amplified with primers S3-F, 5'-CATGCCATGGAACGAAGATTAATGATC-3' and S3-R, 5'-CATGCCATGGCTCTTGGACCCGAGGG-3' and subcloned in the NcoI site of the vectors pMON999-CFP/YFP. All constructs were verified by sequencing. The binary constructs: *Pro*_{35S}-*BES1*-GFP and *Pro*_{35S}-*bes1*-GFP used for transient assays in protoplasts were the same as described by Yin *et al.*, (2002). The full-length AtSERK1-CFP and YFP fusions were described before (Shah *et al* 2001).

5.2.2 Transient expression in cowpea and *Arabidopsis* protoplasts

Cowpea and *Arabidopsis* mesophyll protoplasts were prepared and transfected as described previously by Shah *et al.*, (2002), Sheen (2001) (<http://genetics.mgh.harvard.edu/sheenweb>) and Birnbaum *et al* (2003). After transfection the protoplasts were incubated in protoplast medium for either overnight or 3 hours followed by addition of cycloheximide (CHX) (Sigma) in concentration 50µM from 50mM stock. The protoplasts were used for observations until 5 hours after adding the CHX.

5.2.3 Fluorescence microscopy

The ECFP and EYFP fluorescence in protoplasts and in *Arabidopsis* seedlings were analyzed by Confocal Laser Scanning Microscope 510 (Carl-Zeiss, Germany) as described before by Shah *et al.*, (2002). A 40x oil immersion objective (numerical aperture 1.3) was used for scanning. The pinhole setting was 60 µm, which yielded a theoretical thickness (full width

at half-maximum) of 1 μm . Images and data captures were analyzed with Zeiss LSM510 software (V3.2).

5.2.4 Fluorescence Lifetime Imaging Microscopy (FLIM)

FLIM was performed using a Biorad Radiance 2100 MP system in combination with a Nikon TE 300 inverted microscope. Two photon excitation pulses were generated by a Ti: Sapphire laser (Coherent Mira) that was pumped by a 5 W Coherent Verdi laser. Pulse trains of 76 MHz (150 fs pulse duration, 860 nm center wavelength) were produced. The excitation light was directly coupled into the microscope and focused into the sample using a CFI Plan Apochromat 60x water immersion objective lens (numerical aperture 1.2). Fluorescent light was detected using the non-descanned single photon counting detection, which is the most sensitive solution for two-photon imaging. For the FLIM experiment the Hamamatsu R3809U MCP PMT was used, which has a typical time resolution of 50 ps. ECFP fluorescence was selected using a 480DF30 nm band-pass filter. Images with a frame size of 64x64 pixels were acquired and the average count rate was 2.10^4 photons / s, for an acquisition time of 1-2 minutes (Borst *et al* 2003; Chen *et al* 2003; Becker *et al* 2004; Chen and Periasamy 2004). From the intensity images, complete fluorescence lifetime decays were calculated per pixel and fitted using a double exponential decay model. The fluorescence lifetime of one component was fixed to the value found for AtSERK1-ECFP (2.5 ns) (Table 5.1). The FRET efficiency (E) was determined by $E=1-\tau_{DA}/\tau_D$, where τ_D is the fluorescence lifetime of the donor in the absence of acceptor and τ_{DA} that of the donor in the presence of acceptor at a distance R . The distance between the donor and the acceptor was determined from the relation $\tau_{DA}=\tau_D/(1+(R_0/R)^6)$, where R_0 is the Förster radius, the distance between the donor and acceptor at which 50% energy transfer takes place (Elangovan *et al* 2002)

5.3 Results

5.3.1 AtSERK3 accelerates BRI1 endocytosis in protoplasts

In order to determine the subcellular localization of BRI1 and AtSERK3 proteins in plant cells, we performed *in vivo* targeting experiments in cowpea and *Arabidopsis* protoplasts derived from leaf tissue. BRI1 and AtSERK3 proteins were tagged at the C-terminus with either cyan or yellow fluorescent proteins (ECFP; EYFP). Transient expression of these proteins in protoplasts was under control of the constitutive cauliflower mosaic virus (CaMV) 35S promoter. The localization of each fusion protein was examined using confocal laser scanning microscopy (CLSM). In order to investigate the subcellular localization of the fluorescent proteins in the protoplasts, the ECFP, EYFP and chlorophyll fluorescence are displayed in separate channels (cyan and yellow, chlorophyll respectively) followed by a merged image for each confocal optical section of a cell.

The transient protein expression system in protoplasts has been successfully used to study gene regulation, signal transduction (reviewed by Sheen 2001), protein targeting and trafficking in plant cells (Jin *et al* 2001; Kim *et al* 2001; Ueda *et al* 2001; Jin *et al* 2003; Sohn *et al* 2003; Park *et al* 2004). Despite the many advantages of expressing proteins in plant protoplasts this system also has limitations. First, localization of the transiently expressed

proteins may not always reflect that of the endogenous proteins in intact plant cells. This can be due to overexpression of the proteins. Second, protoplasts are devoid of cell walls, plasmodesmata, and lack normal cell-cell communication and polarity cues so the transiently expressed proteins may behave different from the endogenous proteins in intact plant cells.

Thus, the results obtained using transient expression in protoplasts should be considered with those limitations in mind. In single transfections BRI1-ECFP and AtSERK3-ECFP fusion proteins are localized in the plasma membrane as early as 3 hours after transfection and this pattern was unchanged up to 16 hours (overnight) incubation of the protoplasts. In figure 5.1A-D representative images are shown after 8 hours of incubation. Residual AtSERK3-ECFP fluorescence was also seen in the cytoplasm (indicated by an arrow in Fig. 5.1C), similar to what was observed for AtSERK1, the previously described close homologue of AtSERK3 (Shah *et al* 2002).

When protoplasts were optically cross-sectioned close to the periphery of the cell, multiple fluorescently labeled vesicle-like compartments were observed (examples are shown in Fig. 5.1E-F for BRI1-EYFP and in Fig. 5.1G-H for AtSERK3-EYFP). Often those organelles appeared to be at a site near the plasma membrane (indicated by arrows in Fig. 5.1E and Fig. 5.1G). The protein synthesis inhibitor cycloheximide (CHX) was added to protoplasts expressing either BRI1-ECFP or AtSERK3-EYFP 3 hours after transfection and the protoplasts were examined up to 5 hours after the treatment (Fig. 5.1I-J and Fig 5.1K-L, respectively). In CHX-treated protoplasts no change in the distribution of either BRI1-ECFP or AtSERK3-EYFP fluorescence between the plasma membrane and the vesicle-like compartments were seen compared to untreated protoplasts (data not shown) or to protoplasts expressing BRI1-EYFP or AtSERK3-EYFP overnight. In general, the expression was higher when the longer incubation time was used (compare Fig. 5.1I and 5.1K with Fig. 5.1E and 5.1G, respectively). The constant level of membrane localized receptors in the absence of protein synthesis suggests that neither undergoes rapid internalization when expressed alone.

When BRI1 and AtSERK3 were co-expressed for 3 hours as ECFP and EYFP fusions respectively, followed by 5 hours of CHX treatment there was almost complete depletion of both BRI1 and AtSERK3 fluorescent proteins from the plasma membrane (compare Fig. 5.1M-P with Fig. 5.1Q-T, respectively). This suggested that the presence of AtSERK3 altered the membrane location of BRI1. This could be due to accelerated endocytosis and/or inefficient recycling back to the plasma membrane. An interesting observation in the BRI1/AtSERK3 co-expression experiments was the lack of complete co-localization between the two fluorescently tagged proteins in the endosomes (Fig. 5.1U-W). Surprisingly, we distinguished three different types of vesicle-like compartments, compartments that contained BRI1 and AtSERK3 together (indicated by an arrow in Fig. 5.1W) and compartments that contained either AtSERK3 (a cyan arrow in Fig. 5.1U) or BRI1 alone (a yellow arrow in Fig. 5.1V). The ratio between the numbers of each type of compartments differed between different protoplasts. Similar observations were seen when *Arabidopsis* protoplasts were co-transfected with BRI1 and AtSERK3 fluorescent proteins (Fig. 5.1Z). Because an endocytic compartment will contain more than a single molecule of the fluorescently labeled receptor this excludes the possibility of a random event. Thus, we conclude that the endosomal sorting mechanism in plant cells can distinguish between different plasma membrane receptors.

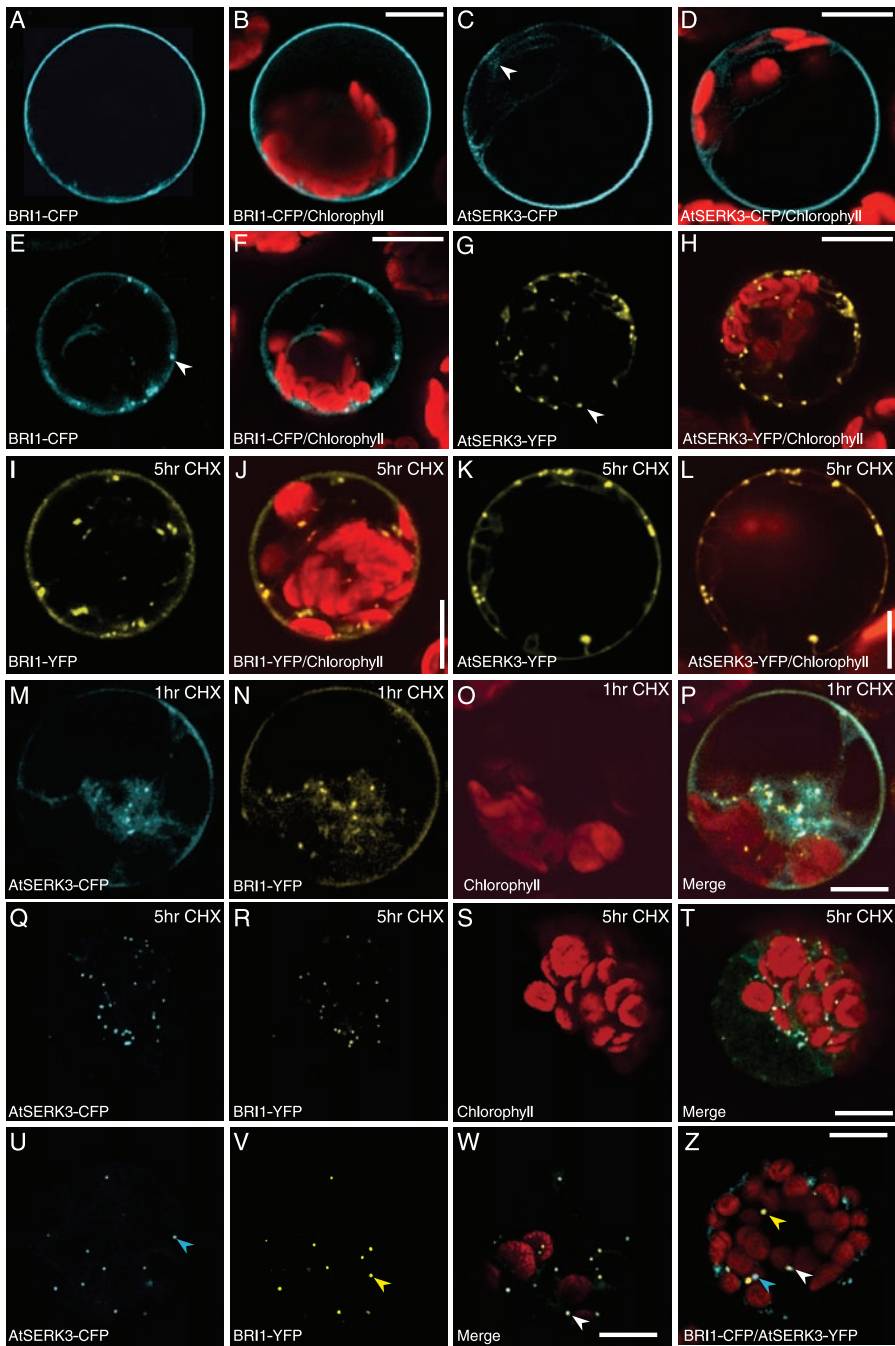


Figure 5.1

5.3.2 BRI1 and AtSERK3 heterodimerize in the plasma membrane and in endocytic compartments

BRI1 and AtSERK3 receptor homo- or heterodimerization was investigated using Förster Resonance Energy Transfer (FRET)-Fluorescence Lifetime Imaging Microscopy (FLIM) methodology. FRET can be determined between donor (ECFP) and an acceptor (EYFP) molecule when both are in close proximity (< 10 nm). This distance is regarded to be indicative of direct protein-protein interaction (Bastiaens and Pepperkok 2000; Hink *et al* 2002). A two-photon laser-scanning microscope is combined with a time correlated single photon counting (TCSPC) acquisition card to determine spatially resolved fluorescence lifetimes. First, a fluorescence intensity image of the tagged receptors is obtained and subsequently the fluorescence lifetime (τ) of the ECFP donor molecule for every pixel of the image is calculated. The fluorescence lifetime of the donor is analyzed according to a double exponential fit model. Upon FRET the τ of the ECFP donor molecules will decrease and is visualized as a false color-coded image superimposed over the visible light image. The mean fluorescence lifetime ranges from dark blue ($\tau = 2.5$ ns; no interaction) to dark orange or red ($\tau = 1.9$ ns; interaction) (Fig. 5.2). FLIM measurements carried out with all receptor combinations used in this analysis are summarized in Table 5.1.

We first investigated whether AtSERK3 or BRI1 were able to form homodimers using FRET-FLIM (Fig. 5.2A-B and Fig. 5.2C-D). First the fluorescence lifetime of the donor was determined and a value of $\tau = 2.49$ ns was found for AtSERK3-ECFP at the plasma membrane (displayed as a homogeneous dark blue colored membrane in Fig. 5.4B and corresponding τ values in Table 5.1). A transfection of the combination AtSERK3-ECFP/AtSERK3-EYFP showed no interaction along the plasma membrane. However, occasionally a reduction of the fluorescence lifetime was found in very small areas in the plasma membrane but only in few protoplasts (Table 5.1). In contrast, in BRI1-ECFP/BRI1-EYFP expressing protoplasts a significant reduction in the fluorescence lifetime of the donor molecules (τ from 2.5 to 1.9 ns) was detected suggesting that BRI1 was able to form homodimers in the plasma membrane

Figure 5.1: Localization of BRI1 and AtSERK3 proteins in cowpea and in *Arabidopsis* protoplasts. (A-H) Confocal images of cowpea protoplast transfected with single constructs: BRI1-ECFP (A and E), AtSERK3-ECFP and AtSERK3-EYFP in (C) and (G) respectively and incubated in protoplast medium for 8 hours. Because no differences in the localization and the expression levels between the ECFP and the EYFP tagged versions of the proteins were observed, we present the data with either the ECFP or the EYFP construct. BRI1 and AtSERK3 localized to the plasma membrane as shown in (A) for BRI1-ECFP and in (C) for AtSERK3-ECFP (cyan). An arrow in (C) indicates some residual AtSERK3-ECFP fluorescence in the cytoplasm. BRI1 and BAK1 also localized to the multiple vesicles when protoplast transiently expressing BRI1-ECFP (E) (cyan) and AtSERK3-EYFP (G) (yellow) were optically cross-sectioned through the periphery of the cell. Note the arrows pointing to vesicles budding from the plasma membrane. The combined images of (A), (C), (E) and (G) with the chlorophyll autofluorescence (red) are shown in (B), (D), (F) and (H) respectively. (I-L) Confocal images of cowpea protoplasts transfected with BRI1-EYFP (I and J) and AtSERK3-EYFP (K and L), incubated for 3 hours in protoplast medium and then for 5 hours in the presence of 50 μ M CHX. The combined with the chlorophyll autofluorescence (red) images are shown in (J) and (L) respectively. (M-T) Confocal images of cowpea protoplast co-transfected with AtSERK3-ECFP and BRI1-EYFP, incubated for 3 hours in protoplast medium and then for 1 hour (M-P) and for 5 hours (Q-T) in the presence of 50 μ M CHX. The AtSERK3-ECFP fluorescence is shown in (M) and (Q). The BRI1-EYFP fluorescence is shown in (N) and (R). The chlorophyll autofluorescence is shown in (O) and (S) and the combined images in (P) and (T) respectively. (U-W) Confocal images of cowpea protoplast cotransfected with AtSERK3-ECFP and BRI1-EYFP recorded 3 hours after transfection. The AtSERK3-ECFP and the BRI1-EYFP fluorescence localized in the endosomes is shown in (U) and (V) respectively and the combined image in (W). Note the arrows pointing to the three different types of endosomes present in the cell. (Z) A confocal image of *Arabidopsis* protoplast cotransfected with BRI1-ECFP and AtSERK3-EYFP recorded 16 hours after transfection. Scale bars, 10 μ m.

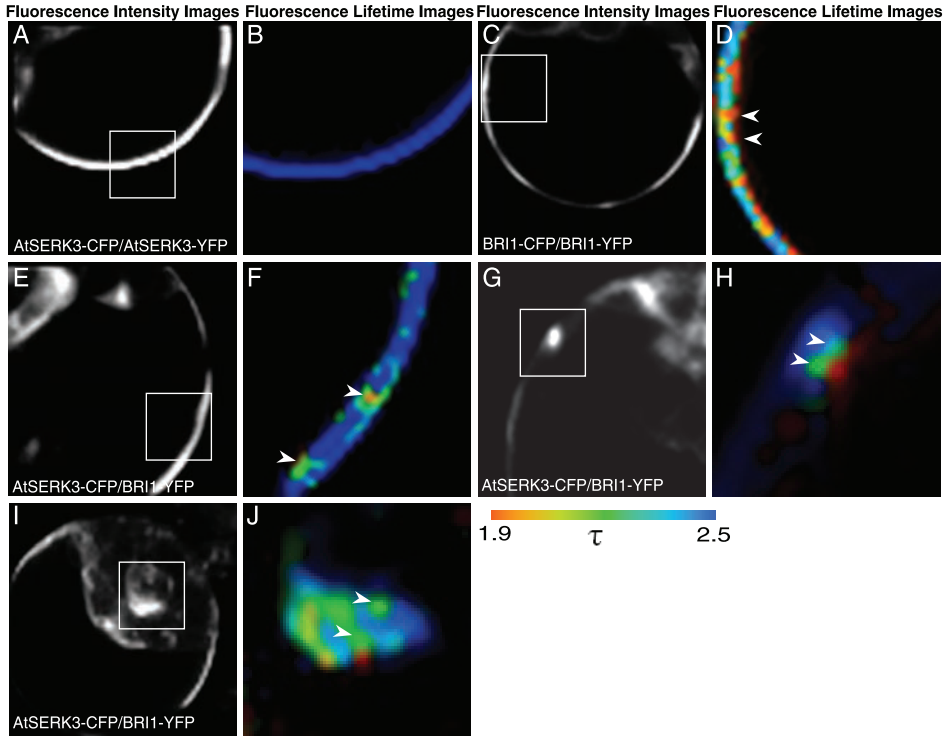


Figure 5.2: FRET between BRI1 and AtSERK3 imaged by FLIM. (A-D) FLIM on cowpea protoplast transiently expressing AtSERK3-ECFP/AtSERK3-EYFP (A-B) and BRI1-ECFP/BRI1-EYFP (C-D) for 16 hours. This time point was selected because a sufficient amount of fluorescence is required in order to measure FRET. Intensity images representing a steady state of the donor ECFP fluorescence are presented in (A) for AtSERK3-ECFP and in (C) for BRI1-ECFP respectively. The mean fluorescence lifetime values (τ) were calculated as described in the Experimental Procedures, and the lifetime distribution of the outlined regions in (A) and (C) are presented as enlarged pseudocolor images in (B) and (D). Arrows point to the areas with a significant reduction of the lifetime (dark orange to green color, τ 1.9 ns to 2.0 ns). Note the color bar where dark blue color is used to display τ = 2.5 ns (no interaction) and the red to dark orange color to display τ = 1.9 ns (interaction). (E-J) FLIM on cowpea protoplast transiently coexpressing AtSERK3-ECFP and BRI1-EYFP proteins for 16 hours. The intensity images of the donor ECFP fluorescence are presented in (E), (G), and (I). Enlargements of the outlined regions in (E), (G) and (I) are presented as pseudocolor images in (F), (H) and (J) respectively. The arrows point to the areas with short lifetime, indicative for FRET.

(FRET efficiency 23%). The reduction in the fluorescence lifetime of BRI1-ECFP in the presence of BRI1-EYFP was comparable to the reduction of the fluorescence lifetime of AtSERK1-ECFP in the presence of AtSERK1-EYFP (Table 5.1), which was previously shown to form homodimers in the plasma membrane (Shah *et al* 2001) (M.A. Hink and A.J. Visser unpublished results). The areas where BRI1/BRI1 homodimers in the plasma membrane occur do not appear to be organized, but fairly frequent (note the dark orange areas indicated by arrows in Fig. 5.2D). From these data we conclude that the BRI1 receptor exists as a homodimer in the plasma membrane of living plant cells. We cannot exclude the possibility that in some cases the lack of FRET is due to a competitive interaction between endogenous and transiently expressed BR receptors. This depends on the abundance of the endogenous receptors in the respective tissues. Although the BRI1 receptor is expressed relatively high in

mesophyll cells (Friedrichsen *et al* 2000), FRET was always observed between transiently co-expressed BRI1-ECFP and BRI1-EYFP receptors. The abundance of AtSERK3 transcripts in mesophyll cells was low as predicted by a semi-quantitative reverse transcriptase- polymerize chain reaction (RT-PCR) (C. Albrecht and S.C. de Vries., unpublished results).

Table 5.1: Fluorescence lifetime analysis and FRET characterization in cowpea protoplasts

Proteins	Cellular localization	Lifetime τ (ns) \pm SD	FRET Efficiency E (%)	N FRET + FRET -	n	
CFP	Cytoplasm	2.57 \pm 0.03	-	3	1	
BRI1-CFP	PM	2.47 \pm 0.03	-	5	3	
AtSERK3-CFP	PM	2.53 \pm 0.04	-	6	3	
AtSERK1-CFP	PM	2.51 \pm 0.02	-	6	3	
BRI1-CFP/AtSERK3-YFP&	PM &	2.00 \pm 0.11	20	9	6	3
BRI1-YFP/AtSERK3-CFP	Endosomes	2.00 \pm 0.09	20	6	0	1
BRI1-CFP/AtSERK3-YFP+BL&	PM	2.01 \pm 0.10	20	3	1	1
BRI1-YFP/AtSERK3-CFP+BL						
BRI1-CFP/BRI1-YFP	PM	1.90 \pm 0.11	23	7	0	2
AtSERK3-CFP/AtSERK3-YFP	PM	2.49 \pm 0.02	-	2	12	2
AtSERK1-CFP/AtSERK1-YFP	PM	1.96 \pm 0.11	23	7	0	1

\pm SD, Standard deviation; FRET efficiency (E) is determined as described in the Experimental procedures; N, Total number of protoplasts analysed; FRET +, Number of protoplasts showing FRET; FRET -, Number of protoplasts not showing FRET; *n*, Number of independent transfection experiments; PM, Plasma membrane

These results suggest that the lack of interaction between transiently co-expressed AtSERK3-ECFP and AtSERK3-EYFP receptors is unlikely to be caused by interaction with its native counterpart and most likely reflects the monomeric state of AtSERK3. Those values corresponded to the values of the fluorescence lifetimes determined for protoplasts transfected with either BRI1-ECFP (τ = 2.47 ns) or AtSERK3-ECFP (τ = 2.53 ns) constructs alone (Table 5.1) and indicated no interaction occurring between AtSERK3 and BRI1 in those areas. In addition, multiple small patches that showed a significant reduction in τ from 2.5 to 2.0 ns (Table 5.1) of the donor (BRI1-ECFP) molecules (visible as green to orange patches in Fig. 5.2F and indicated by arrows) were observed. The FRET efficiency in these areas was approximately 20% (Table 5.1). The size and the frequency of these discrete areas varied between different protoplasts.

To determine whether BRI1/ AtSERK3 heterodimerize *in vivo*, protoplasts were transfected with either BRI1-ECFP and AtSERK3-EYFP or AtSERK3-ECFP and BRI1-EYFP constructs. Because the plasma membrane of co-transfected cells with BRI1 and AtSERK3 is rapidly depleted of the receptors we first analyzed those parts where the fluorescent proteins were still present (Fig. 5.2E and 5.2F). In such areas the fluorescence intensity image of a protoplast co-transfected with e.g. AtSERK3-ECFP and BRI1-EYFP showed a uniform distribution of the ECFP fluorescence (see the boxed plasma membrane area in Fig. 5.2E). In most parts of the plasma membrane no (τ = 2.5 ns) or very little reduction in the fluorescence

lifetime ($\tau = 2.47$ ns) was observed (visualized by the dark blue color in Fig. 5.2F). The fluorescence lifetime of the AtSERK3-ECFP donor molecules was determined in the presence of BRI1-EYFP in the endocytic compartments at a site near the plasma membrane (Fig. 5.2G and 5.2H) or located in the cytoplasm (Fig. 5.2I and 5.2J). ‘Twins-like’ organelles next to the plasma membrane showed a reduction in τ of the AtSERK3-ECFP from 2.5 to 2.0 ns (arrows in Fig. 5.2H, FRET efficiency 20%). Comparable reductions in the fluorescence lifetime of the AtSERK3-ECFP were observed in most of the BRI1 and AtSERK3 containing endocytic compartments located in the cytoplasm (see Fig. 5.2J where spotted areas with different fluorescence lifetimes are visualized in green and orange color and indicated by arrows). We conclude that BRI1-AtSERK3 heterodimerization is non-uniformly distributed in the plasma membrane and appears to coincide with developing endocytic compartments that contain both receptors.

5.4 Discussion

5.4.1 BRI1 and BAK1 dynamics in protoplasts

When BRI1 and AtSERK3 coupled to either ECFP or EYFP are transiently expressed in cowpea protoplasts our results indicate that both fluorescently labeled proteins are localized to the plasma membrane, similar to what was observed in *Arabidopsis* roots for BRI1 (Friedrichsen *et al* 2000) and AtSERK3 (Li *et al* 2002; Nam and Li 2002). We also detected both proteins in small vesicle-like compartments in the cytoplasm close to the plasma membrane. Results of several experiments led to the conclusion that these vesicles represent endosomes.

The turnover of BRI1 and AtSERK3 proteins in protoplasts expressing either BRI1 or AtSERK3 alone was relatively slow, but when co-expressed in protoplasts, BRI1 and AtSERK3 first co-localized at the plasma membrane and then are rapidly internalized into endosomes. Most of the internalized BRI1 and AtSERK3 proteins were not recycled back to the membrane and were possibly targeted for degradation, resulting in a nearly complete depletion of BRI1 and AtSERK3 fluorescent proteins from the plasma membrane. We believe that the rapid internalization of the co-expressed BRI1 and AtSERK3 proteins is not a result of overexpression or heterodimerization with cowpea orthologs because neither BRI1-ECFP/EYFP nor AtSERK3-ECFP/EYFP co-expression resulted in increased rate of protein internalization. As no differences between cowpea and *Arabidopsis* expression systems were observed we conclude that receptor internalization *via* endocytosis generally occurs in plant cells. Receptor recycling is well documented in animal cells. For instance all members of the epidermal growth factor receptor (EGFR) family are predominantly localized in the plasma membrane and even in the absence of ligands are slowly internalized yet quickly recycled back to the membrane through endosomes. EGF ligand binding and activation of the EGF receptor resulted in accelerated endocytosis eventually leading to receptor down-regulation in the lysosomes (reviewed by Wiley 2003).

When BRI1 and AtSERK3 were co-expressed together three different endosomal compartments were observed. Surprisingly, endosomes could contain either BRI1 or AtSERK3 alone or BRI1 and AtSERK3 together. This intriguing observation suggests that BRI1 and AtSERK3 might undergo receptor-specific sorting. It is not known whether this occurs before

or after heterodimerization or how the observed proportions between endosomes containing individual monomeric, homodimeric or heterodimeric receptors were accomplished. It seems likely that the three different endosomes arise directly from the plasma membrane. Studies of endocytosis in plants are fairly limited but the analysis of *Arabidopsis* genome point to conservation in most of the endocytic machinery (reviewed by Jurgens and Geldner 2002). In our protoplast system we observed that the interaction between BRI1 and AtSERK3 was restricted to only a few small parts of the plasma membrane. This was surprising because BRI1 and AtSERK3 were co-localized in the entire plasma membrane. BRI1-AtSERK3 heterodimerization was also consistently observed in vesicles that were at the site near the plasma membrane and vesicles that were internalized and located in the cytoplasm. We therefore propose that heterodimerization between both receptors mainly occurs upon the onset of endocytosis. Whether this can be equated with transphosphorylation events between BRI1 and AtSERK3 is at present not known. For instance for the EGF receptor ErbB1 it has been shown that intermolecular phosphorylation can occur between individual receptor molecules in the absence of a ligand (Verveer *et al* 2000).

We observed that in protoplasts exogenous brassinosteroids were not required for BRI1 and AtSERK3 interaction. This could mean that the observed endocytosis is a ligand-independent process. In that case it apparently does not require brassinolide dependent BRI1 activation *via* phosphorylation (He *et al* 2000; Wang *et al* 2001). In protoplasts a part of the BRI1 receptor molecules are in the homodimeric state. AtSERK1, a close homologue of AtSERK3, is able to homodimerize similarly when expressed in protoplasts (Shah *et al* 2001). In contrast, AtSERK3 was completely unable to homodimerize in protoplasts. AtSERK3 lacks the second cysteine pair flanking the LRR in the extracellular domain, and this pair might be essential for intermolecular interactions and receptor homodimerization (Dievart and Clark 2003). Although not excluded BRI1 homodimerization has so far not been demonstrated in plants and *bri1* mutant analysis suggested that BRI1 might function in a heterodimer (Li *et al* 2002; Nam and Li 2002). If a situation such as observed in our protoplasts reflects the situation in plants, a mosaic of homo- and heterodimeric BRI receptors could be envisaged. In that scenario, BRI1 can transduce a signal through either BRI1/BRI1 homodimers or through heterodimers with AtSERK3. We can propose that one of the roles of the AtSERK3 would be to fine tune BR signaling by shifting the equilibrium of the membrane localized BRI1 receptors towards the endosomes.

Acknowledgments

We thank Joan Wellink and Jeroen Pouwels for providing us with the STtmd-YFP Golgi marker, for growing the cowpea plants and for protoplasts transfections; Antonie Visser and Mark Hink for help with FRET measurements and during data analysis; Niko Geldner and Jiří Friml for helpful discussions and the critical reading of the manuscript. J.C. is an investigator of the Howard Hughes Medical Institute. This work was supported by a grant ERBIO4-CT96-0689 from the EU Biotechnology program, a grant QLG2-2000-00602 from the EU Quality of Life and Management of Living Recourses program and Wageningen University, Department of Agrotechnology and Food Sciences to E.R. M.K. and S.deV., by Human Frontier Science Program Organization long-term fellowship to A.C-D. and grants from the USDA and HESP to J.C.

Chapter 6

Effects of Refractive Index and Viscosity on Fluorescence and Anisotropy Decays of Enhanced Cyan and Yellow Fluorescent Proteins

Abstract

The fluorescence lifetime strongly depends on the immediate environment of the fluorophore. Time-resolved fluorescence measurements of the enhanced forms of ECFP and EYFP in water-glycerol mixtures were performed to quantify the effects of the refractive index and viscosity on the fluorescence lifetimes of these proteins. The experimental data show for ECFP and EYFP two fluorescence lifetime components: one short lifetime of about 1 ns and a longer lifetime of about 3.7 ns of ECFP and for EYFP 3.4. The fluorescence of ECFP is very heterogeneous, which can be explained by the presence of two populations: a conformation (67% present) where the fluorophore is less quenched than in the other conformation (33% present). The fluorescence decay of EYFP is much more homogeneous and the amplitude of the short fluorescence lifetime is about 5%. The fluorescence anisotropy decays show that the rotational correlation time of both proteins scales with increasing viscosity of the solvent similarly as shown earlier for GFP. The rotational correlation times are identical for ECFP and EYFP, which can be expected since both proteins have the same shape and size. The only difference observed is the slightly lower initial anisotropy for ECFP as compared to the one of EYFP.

This chapter has been published as:

J.W. Borst, M.A. Hink, A. van Hoek, A.J.W.G. Visser (2005) Effects of refractive index and viscosity on fluorescence and anisotropy decays of enhanced cyan and yellow fluorescent proteins. *J. Fluoresc.* **15**:153-160.

6.1 Introduction

The green fluorescent protein (GFP) isolated from the pacific jellyfish *Aequorea victoria*, its many colored variants and new fluorescent proteins from coral species are abundantly applied as genetically encoded markers in cell biology (Tsien 1998; Miyawaki *et al* 2003). GFP and its variants are also widely used in various undergraduate and graduate courses organized in our universities (for an example see Hink *et al* 2003b). In this context we have paid attention to one aspect of GFP-imaging that was published recently (Suhling *et al* 2002a). Briefly, it was demonstrated by fluorescence lifetime imaging microscopy (FLIM) of GFP that the fluorescence lifetime depends on the local refractive index. The main cause for this effect is that the radiative lifetime and the absorption and emission spectra of a fluorophore are dependent on the refractive index due to the polarizability of the medium surrounding the fluorophore. The Strickler-Berg formula describes the relationship between the radiative lifetime, the absorption spectrum of the fluorophore, the third moment of the fluorescence spectrum and the square of the refractive index (Strickler 1962). Toptygin *et al* (2002) performed a detailed study of the refractive index effect on the radiative decay rate of a single tryptophan in a protein and showed that the theoretical prediction agrees with the experimental data. These authors derived a more complex model than the Strickler-Berg equation with a dependence of the inverse radiative lifetime on the power of the refractive index in excess of 2 (Toptygin *et al* 2002). Suhling *et al* (2002a) studied the fluorescence decay of GFP in different solvents and in glycerol-water mixtures (0-90%) and found that the inverse of the average lifetime scales linearly with the square of the refractive index. Alternatively, by using FLIM experiments these authors could then also image the refractive index of the environment of GFP. The observations may have implications for FLIM measurements of fluorescent proteins in cells. In cells the refractive index can adopt a range of values varying from 1.45-1.6 in membrane environments to 1.35 in the cytoplasm.

The cyan fluorescent protein (CFP, donor) and the yellow fluorescent protein (YFP, acceptor) are frequently used as donor-acceptor pairs in Förster resonance energy transfer (FRET) studies for the investigation of protein-protein interactions in cells. Especially for FLIM measurements reporting on FRET we need to know the fluorescence lifetime of the donor in the absence of acceptor. This would imply that these reference lifetimes depend on the local refractive index and will be different in either membrane- or cytosolic environments of the cell. This prompted us to study the time-resolved fluorescence properties of the enhanced forms of CFP and YFP (ECFP and EYFP, respectively) in water-glycerol mixtures. Since glycerol is much more viscous than water we also study the fluorescence anisotropy decays of the same samples. From these experiments we determine the rotational correlation time of both proteins and show that the rotational correlation time scales with increasing viscosity of the solvent similarly as shown earlier for GFP (Suhling *et al* 2002b).

6.2 Theoretical background

6.2.1 Time-Resolved Fluorescence

The fluorescence lifetime τ is the time a fluorophore remains in its excited state after excitation and is related to the radiative (k_r) and nonradiative (k_{nr}) rate constants:

$$\tau = \frac{1}{k_r + k_{nr}} \quad (1)$$

The fluorescence lifetime strongly depends on the immediate environment of the fluorophore and can therefore be used as a sensor for environment. There exists a fundamental relationship between the fluorescence lifetime τ and the fluorescence quantum yield Q :

$$Q = \frac{\tau}{\tau_r} = \frac{k_r}{k_r + k_{nr}} \quad (2)$$

in which $\tau_r (= 1/k_r)$ is the radiative lifetime of the fluorescent molecule. The radiative lifetime can be visualized as that lifetime of the excited state when the only deactivation process consists of photon emission. One of the empirical relationships between τ_r and the optical spectra is that derived by Strickler and Berg (1962):

$$\frac{1}{\tau_r} = 2.88 \times 10^{-9} n^2 \frac{\int I(\sigma) d\sigma}{\int I(\sigma) \sigma^{-3} d\sigma} \int \frac{\varepsilon(\sigma)}{\sigma} d\sigma \quad (3)$$

in which n is the refractive index, I is the fluorescence emission, ε is the molar extinction coefficient connected with the first (lowest) electronic transition and σ is the wavenumber. The Strickler-Berg equation strictly applies to the natural fluorescence lifetime (τ_r). However, Suhling *et al* (2002a) found no distinct effect of the quantum yield of GFP fluorescence on the refractive index, whereas a clear dependence of the inverse actual lifetime on the quadratic refractive index is observed.

6.2.3 Time-Resolved Fluorescence Anisotropy

The experimental observable in a time-resolved fluorescence anisotropy experiment defined as:

$$r(t) = \frac{I_{\parallel}(t) - I_{\perp}(t)}{I_{\parallel}(t) + 2I_{\perp}(t)} \quad (4)$$

where $I_{\parallel}(t)$ and $I_{\perp}(t)$ are the observed time-dependent parallel and perpendicular polarized components relative to the polarization direction of the exciting beam.

The general expression relating the experimental anisotropy $r(t)$ with the time-dependent correlation function of the transition moments has the form of a second order Legendre polynomial $P_2(x)$ (Szabo 1984):

$$r(t) = \langle P_2 [\mu_a(0) \cdot \mu_e(t)] \rangle \quad (5)$$

where $\mu_a(0)$ and $\mu_e(t)$ are unit vectors along the absorption transition moment at time zero (note that light absorption is a femtosecond process) and emission at time t after excitation, respectively. The brackets $\langle \rangle$ denote an ensemble average. In proteins there are several contributions to the loss of anisotropy (Lakowicz 1999). In case of GFP the main sources of depolarization are an intrinsic one leading to the fundamental anisotropy (the anisotropy at time zero) and protein tumbling, since the fluorophore is rigidly embedded within the protein matrix (Uskova *et al* 2000; Volkmer *et al* 2000; Suhling *et al* 2002b). The fundamental anisotropy contains information about the angle θ between absorption and emission transition moments:

$$r(0) = \frac{2}{5} \left(\frac{3 \cos^2 \theta - 1}{2} \right) \quad (6)$$

Note that $r(0) = 0.4$ corresponds with parallel absorption and emission dipoles ($\theta = 0^\circ$). For an spherically shaped protein with firmly attached fluorophore the anisotropy decays mono-exponentially with a characteristic rotational correlation time ϕ :

$$r(t) = r(0) e^{-t/\phi} \quad (7)$$

The rotational correlation time ϕ is proportional to the viscosity η and the molecule volume V according to the Stokes-Einstein relationship:

$$\phi = \frac{\eta V}{kT} \quad (8)$$

where k is the Boltzmann constant and T the absolute temperature.

6.3 Materials and Methods

The enhanced forms of CFP and YFP were isolated as described in (Visser *et al* 2002). The glycerol mixtures (0, 10, 30, 50, 70 and 90% v/v) were prepared by mixing glycerol, (Merck: spectroscopic grade) with phosphate buffered saline pH 7.4 (PBS). The purified proteins ECFP and EYFP were diluted to a final concentration of 200 nM.

Time-resolved fluorescence measurements were carried out using mode-locked continuous wave lasers for excitation and time-correlated photon counting as detection technique. The pump laser was a CW diode-pumped, frequency-doubled Nd:YVO₄ laser (Coherent Inc., Santa Clara, CA, model Verdi V10). The mode-locked laser was a titanium:sapphire laser (Coherent Inc., Santa Clara, CA, model Mira 900-D in fs mode), tuned to 860

nm for CFP and 960 nm for EYFP. At the output of the titanium:sapphire laser a pulse picker was placed (APE GmbH, Berlin, Germany, model Pulse Select), decreasing the repetition rate of excitation pulses to $3.8 \cdot 10^6$ pulses per second. The output of the pulse picker was directed towards a frequency doubler (Inrad Inc, Northvale, NJ, model 5-050 Ultrafast Harmonic Generation System). For excitation maximum pulse energy of sub-pJ was used, the wavelength was 430 nm for CFP and 480 for EYFP and the pulse duration about 0.2 ps.

The samples were in 1.5 ml and 10 mm light path fused silica cuvettes (Hellma GmbH, Müllheim, Germany, model 111-QS), placed in a sample holder, temperature controlled (20°C) by applying thermo-electric (Peltier) elements and a controller (Marlow Industries Inc., Dallas, TX, model SE 5020). The sample holder was placed in a housing also containing the main detection optics. Extreme care was taken to avoid artifacts from depolarization effects. At the front of the sample housing a Glan-laser polarizer was mounted, optimizing the already vertical polarization of the input light beam. The fluorescence was collected at an angle of 90° with respect to the direction of the exciting light beam. Between the sample and the photomultiplier detector were placed: a single fast lens (uncoated fused silica, F/3.0), cut-off filters KV470 for ECFP and OG515 for EYFP (both filters are from Schott, Mainz, Germany), a rotatable sheet type polarizer and a second single fast lens (uncoated fused silica, f/3.0), focusing the fluorescence on the photomultiplier cathode. The polarizer sheet was in a dc motor driven ball-bearing holder with mechanical stops, allowing computer-controlled rotation (0.2 s) to parallel and perpendicular polarized detection of emission. The sheet polarizer was Polaroid type HNP'B. The polarizers were carefully aligned and the performance of the set-up finally checked by measuring reference samples.

Detection electronics were time-correlated single photon counting modules. With a small portion of the mode-locked light at 860 nm (or 960 nm) wavelength, left from the harmonics conversion, a fast PIN-photodiode (Hewlett Packard Inc., Palo Alto, CA, model 5082-4204 at 45 V reverse bias) was excited. The output pulses of this photodiode were fed to one channel of a quad constant fraction discriminator (CFD, Tennelec Inc., Oak Ridge, TS, modified model TC 454), and then used as stop signal for a time-to-amplitude converter (TAC, Tennelec Inc., Oak Ridge, TS, model TC 864). A microchannel plate photomultiplier (Hamamatsu, Hamamatsu, Japan, model R3809U-50 at 3100 V, cooled down by a water bath to a few degrees centigrade) was used for the detection of the fluorescence photons. The single photon responses of this PMT were amplified by a wide-band amplifier (Becker & Hickl GmbH, Berlin, Germany, model ACA-2; 21 dB, 1.8 GHz), analyzed in another channel of the CFD and then used as a start signal for the TAC. The output pulses of the TAC were analyzed by an analogue-to-digital converter (ADC, Nuclear Data Inc., Schaumburg, IL, model 8715, 800 ns fixed dead-time), used in Coincidence and Sampled Voltage Analysis mode, gated by the Valid Conversion Output of the TAC. The output of the ADC was gathered in 4096 channels of a multichannel analyzer (MCA board from Nuclear Data Inc., Schaumburg, IL, model AccuspecB, in a personal computer). The channel time spacing was 5.0 ps.

By reducing the energy of the excitation pulses with neutral density filters, the rate of fluorescence photons was decreased to less than 30,000 per second ($\approx 1\%$ of 3,8 MHz, (Vos *et al* 1987)), to prevent pile-up distortion. Also other instrumental sources for distortion of data were minimized (Van Hoek and Visser 1985) to below the noise level of normal photon

statistics. Measurements consisted of repeated sequences of measuring during 10 s parallel and 10 s perpendicular polarized emissions. After measuring the fluorescence of the sample, the background emission of the buffer solution was measured and used for background subtraction.

For obtaining a dynamic instrumental response of the experimental setup the single exponential fluorescence decay of erythrosine B in water (90 ps) was recorded. One complete experiment for a fluorescence decay measurement consisted of the recording of data sets of the reference compound, the unknown sample, the background (buffer) fluorescence and again the reference compound. Data analysis was performed using a model of discrete exponential terms. Global fitting of the experimental data was performed using the ‘TRFA Data Processing Package’ of the Scientific Software Technologies Center (Belarusian State University, Minsk, Belarus) (Digris *et al* 1999).

The total fluorescence intensity decay $I(t)$ and anisotropy decay $r(t)$ are obtained from the measured parallel $I_{\parallel}(t)$ and perpendicular $I_{\perp}(t)$ fluorescence intensity components through the relations:

$$I(t) = I_{\parallel}(t) + 2gI_{\perp}(t) \quad (9)$$

$$r(t) = \frac{I_{\parallel}(t) - gI_{\perp}(t)}{I_{\parallel}(t) + 2gI_{\perp}(t)} \quad (10)$$

in which the g -factor describes the sensitivity of the detection system for the perpendicular component with respect to the parallel one. For the setup used the g -factor equals unity (Van Hoek *et al* 1987) leading to the same expression as equation 4. The fluorescence lifetime profile consisting of a sum of discrete exponentials with lifetime τ_i and amplitude α_i can be retrieved from the total fluorescence $I(t)$ through the convolution product with the instrumental response function $E(t)$:

$$I(t) = E(t) \otimes \sum_{i=1}^N \alpha_i e^{-t/\tau_i} \quad (11)$$

Fluorescence lifetime analysis of the enhanced forms of CFP and YFP required a two-component model ($N=2$) for optimal fitting. In fluorescence anisotropy analysis, after deconvolution the time-dependent fluorescence anisotropy $r(t)$ is calculated from the parallel and perpendicular intensity components through the relations (Lakowicz 1999):

$$I_{\parallel}(t) = \frac{1}{3} \sum_{i=1}^N \alpha_i e^{-t/\tau_i} [1 + 2r(0)e^{-t/\phi}] \quad (12)$$

$$I_{\perp}(t) = \frac{1}{3} \sum_{i=1}^N \alpha_i e^{-t/\tau_i} [1 - r(0)e^{-t/\phi}] \quad (13)$$

Global analysis (Beechem *et al* 1991), in which data sets were fitted simultaneously with a sum of discrete exponentials, were performed through linking the fluorescence lifetimes for multiple data sets. In addition, a rigorous error analysis at the 67% confidence level was applied to the optimized fluorescence lifetimes and rotational correlation times.

6.4 Results and discussion

6.4.1 Excitation and fluorescence spectra on wavenumber scale

The corrected, normalized excitation and emission spectra of ECFP and EYFP in water on wavenumber scale are presented in figure 6.1. In case of ECFP the fine structure of excitation and emission bands can be clearly distinguished. This fine structure originates from vibrational transitions superimposed on the single electronic transition (Tsien 1998; Visser *et al* 2002). The spectra and the maximum extinction coefficients are taken as described previously (Hink *et al* 2003b). The radiative lifetimes of the fluorescence of ECFP and EYFP are calculated as 5.0 ns and 7.2 ns, respectively. Since the absorption and emission spectra of both proteins do not change upon a change of refractive index (data not shown), the use of equation 3 allows calculating the radiative lifetime as function of refractive index.

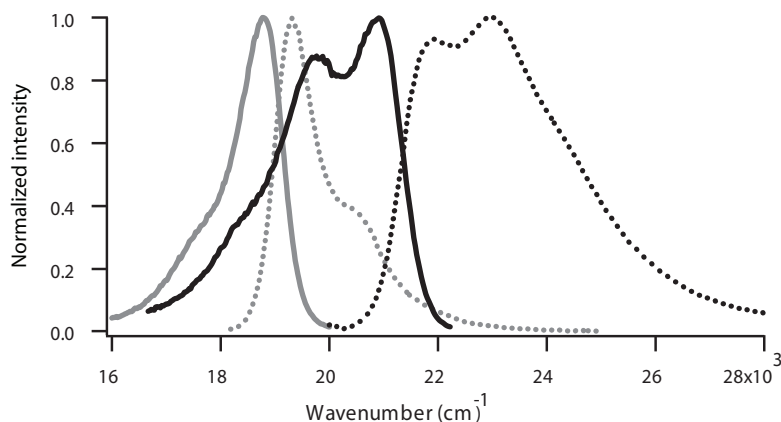


Figure 6.1: Fluorescence excitation (dotted) and emission (solid) spectra of ECFP (black) and EYFP (gray) in PBS (pH 7.4) on wavenumber scale.

6.4.2 Fluorescence decays in different water-glycerol mixtures

The total fluorescence decay of ECFP in aqueous solution is shown in figure 6.2. These experimental data could not be fitted with a single exponential component, but needed (at least) two lifetime components for an optimal fit. One shorter lifetime of 1.1 ns contributing for 33% and one longer lifetime of 3.7 ns contributing for 67% could be recovered. The departure of single-exponential fluorescence decay is also observed by others (Habuchi *et al* 2002; Tramier *et al* 2002; Rizzo *et al* 2004). The presence of multiple fluorescent states is most probably due to two different conformations of ECFP in the crystal structure in which two amino acids, Tyr145 and His148, are positioned differently with respect to the fluorophore (Hyun Bae *et al* 2003). The heterogeneity of ECFP fluorescence can be explained by the presence of two populations: a conformation (67% present)

where the fluorophore is less quenched than in the other conformation (33% present). The interconversion between both conformations is slow on the fluorescence time scale. From site-directed mutagenesis studies His148 has been found to be the major quencher of the fluorophore (Rizzo *et al* 2004).

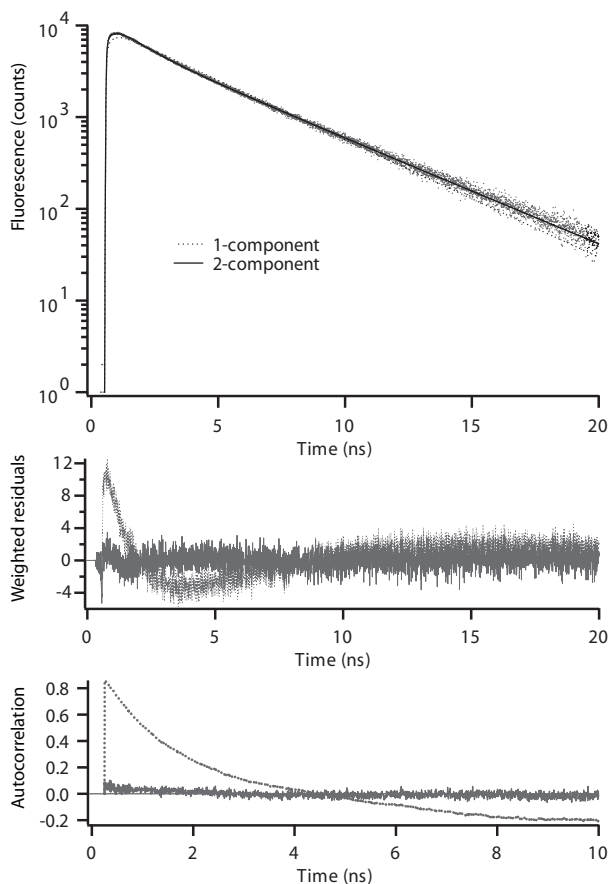


Figure 6.2: Fluorescence decay analysis of ECFP in PBS (pH 7.4) using one lifetime component (dotted) or two lifetime components (solid). The weighted residuals between experimental and calculated points and the autocorrelation of the residuals clearly illustrate the superior fit with two lifetimes. One-exponential fit: $\tau = 3.34$ ns, $\chi^2 = 6.8$. Two-exponential fit: $\alpha_1 = 0.335$, $\tau_1 = 1.14$, $\alpha_2 = 0.665$, $\tau_2 = 3.72$, $\chi^2 = 1.12$. A three-exponential fit gave a slight improvement with a sub-nanosecond lifetime of small amplitude and $\chi^2 = 1.07$ (results not shown).

Addition of increasing amounts of glycerol did not change the heterogeneous fluorescence decay pattern. The short lifetime does not change, whereas the long lifetime becomes progressively shorter at higher glycerol concentration (or higher refractive index of the solvent). Since the short lifetime is hardly influenced, we have performed a global analysis of six decay curves linking the short lifetime and leaving the fluorescence lifetime of the longer component as an adjustable parameter. The fitted curves are presented in figure 6.3. The plots of weighted residuals and autocorrelation of the residuals are similar compared to the ones presented for the two-component fit in figure 6.2.

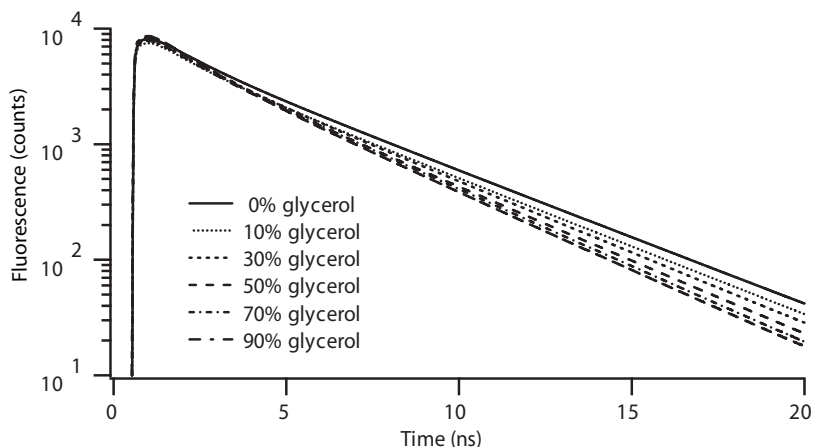


Figure 6.3: Calculated fluorescence decays of ECFP in different water-glycerol mixtures obtained after global analysis linking the shorter lifetime. Analysis results are collected in Table 6.1.

All parameters (amplitudes and lifetimes), confidence limits of the lifetimes and the average lifetimes ($\langle\tau\rangle$) are collected in Table 6.1. The long decay time, the average fluorescence lifetime and calculated radiative lifetime are plotted against the inverse quadratic refractive index (n^{-2}) in figure 6.4. Both experimental lifetimes show a linear relationship similarly as found for GFP (Suhling *et al* 2002a). Therefore, also ECFP shows a fluorescence decay that is sensitive for its immediate environment. In addition, it is verified that the fluorescence quantum yield (see equation 2) of ECFP is indeed independent of refractive index as has been experimentally shown for GFP (Suhling *et al* 2002a).

Table 6.1: Effect of refractive index changes on the fluorescence decay parameters of ECFP

ECFP in:	Refractive index n	α_1 (-)	τ_1 (ns)	α_2 (-)	τ_2 (ns)	$\langle\tau\rangle$ (ns)
0% glycerol	1.33	0.335	1.14 (1.07-1.20)	0.665	3.72 (3.65-3.77)	2.86
10% glycerol	1.34	0.35	1.14 (1.07-1.20)	0.65	3.65 (3.58-3.69)	2.77
30% glycerol	1.37	0.35	1.14 (1.07-1.20)	0.65	3.50 (3.46-3.54)	2.67
50% glycerol	1.40	0.35	1.14 (1.07-1.20)	0.65	3.34 (3.32-3.42)	2.57
70% glycerol	1.43	0.36	1.14 (1.07-1.20)	0.64	3.22 (3.19-3.28)	2.48
90% glycerol	1.46	0.40	1.14 (1.07-1.20)	0.60	3.19 (3.15-3.24)	2.37

Values in parentheses are the 67% confidence limits. The average lifetime is calculated as $\langle\tau\rangle = \alpha_1\tau_1 + \alpha_2\tau_2$

Similar fluorescence decay experiments in different glycerol-water mixtures were performed for EYFP. For EYFP in PBS a one-component fit yielded a lifetime of 3.34 ns ($\chi^2 = 1.20$).

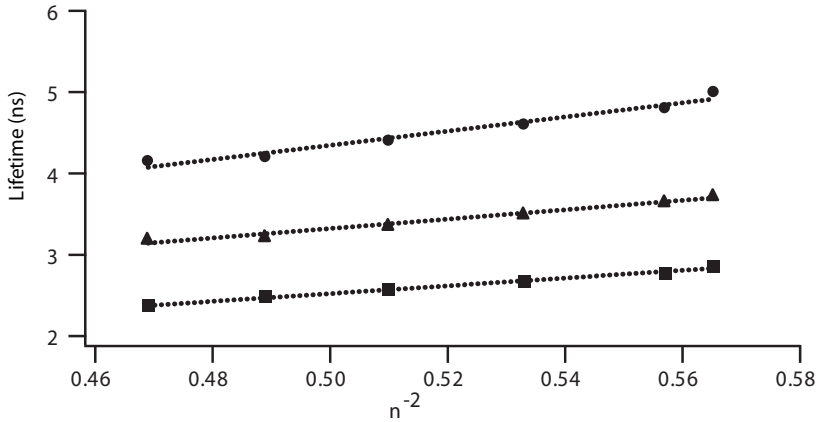


Figure 6.4: Fluorescence lifetimes of ECFP in different water-glycerol mixtures as a function of the inverse of the squared refractive index. Radiative lifetime: ●; long lifetime: ▲; average lifetime: ■

A slightly better fit ($\chi^2 = 1.13$) to the experimental data is obtained with two fluorescence lifetime components: one short lifetime of 0.85 ns and a longer lifetime of 3.37 ns of EYFP in aqueous solution. However, the amplitude of the short lifetime is much smaller (4 %) than the one of the long lifetime (96 %) making the fluorescence decay of EYFP much more homogeneous.

Table 6.2: Effect of refractive index changes on the fluorescence decay parameters of EYFP

EYFP in:	Refractive index n	α_1 (-)	τ_1 (ns)	α_2 (-)	τ_2 (ns)	$\langle\tau\rangle$ (ns)
0% glycerol	1.33	0.043	1.06 (0.71-1.54)	0.957	3.37 (3.31-3.41)	3.27
10% glycerol	1.34	0.030	1.06 (0.71-1.54)	0.970	3.25 (3.19-3.29)	3.18
30% glycerol	1.37	0.057	1.06 (0.71-1.54)	0.943	3.15 (3.09-3.19)	3.03
50% glycerol	1.40	0.032	1.06 (0.71-1.54)	0.968	3.01 (2.95-3.05)	2.95
70% glycerol	1.43	0.053	1.06 (0.71-1.54)	0.947	2.89 (2.86-2.96)	2.79
90% glycerol	1.46	0.152	1.06 (0.71-1.54)	0.848	2.74 (2.66-2.83)	2.48

Values in parentheses are the 67% confidence limits. The average lifetime is calculated as $\langle\tau\rangle = \alpha_1\tau_1 + \alpha_2\tau_2$

6.4.3 Fluorescence anisotropy decays in different water-glycerol mixtures

Experimental and fitted fluorescence anisotropies of ECFP in water and 30% glycerol-water mixtures are shown in figure 6.6. The weighted residuals and autocorrelation plots are randomly distributed around zero illustrating the good quality of the fits (results not shown). Only within this range of viscosity values the rotational correlation times can be accurately determined. When the relative viscosity becomes too high (> 6), the anisotropy is decaying

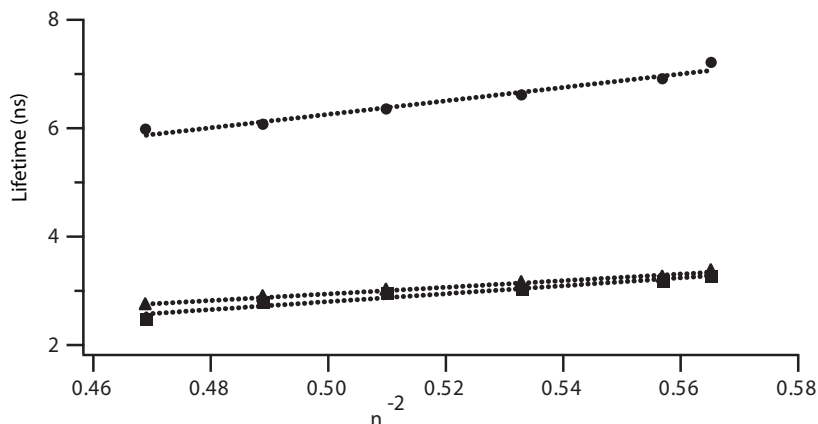


Figure 6.5: Fluorescence lifetimes of EYFP in different water-glycerol mixtures as a function of the inverse of the squared refractive index. Radiative lifetime: ●; long lifetime: ▲; average lifetime: ■

too slowly in the available time window of the experiments (20 ns) leading to inaccurate rotational correlation times with undefined confidence limits.

The recovered rotational correlation times are plotted against the relative viscosity in figure 6.7. It can be clearly seen that there is a linear relationship as predicted by the Stokes-Einstein equation (equation 8). In addition, the confidence limits become larger at longer correlation times in agreement with the abovementioned explanation. The fluorescence anisotropy data of EYFP show the same tendencies as observed for those of ECFP. The rotational correlation times, the confidence limits and initial amplitudes determined from the analysis of time-dependent anisotropies of ECFP and EYFP at four relative viscosities are collected in Table 6.3. The rotational correlation times are identical for ECFP and EYFP, which can be expected since both proteins are the same. The only difference arises from a different fundamental anisotropy that is slightly lower for ECFP ($\beta = 0.356 \pm 0.004$) as compared to EYFP ($\beta = 0.382 \pm 0.002$). This is probably caused by a different angle between absorption and emission moments in both chromophores. By using equation 6 these angles are $\theta = 16^\circ$ for ECFP and $\theta = 10^\circ$ for EYFP.

Table 6.3: Anisotropy decay parameters of ECFP and EYFP in different water- glycerol mixtures

Solution	Relative viscosity	ECFP β (-)	ECFP ϕ (ns)	EYFP β (-)	EYFP ϕ (ns)
0% glycerol	1.00	0.353	14.8 (13.5-16.2)	0.381	15.6 (14.2-17.1)
10% glycerol	1.29	0.359	21.8 (19.6-24.7)	0.383	22.5 (19.8-25.7)
30% glycerol	2.45	0.351	47.4 (38.4-60.3)	0.382	47.7 (39.5-60.5)
50% glycerol	6.0	0.362	78 (56-123)	0.384	120 (75-n.f.)

Values in parentheses are the 67% confidence limits. n.f. upper confidence limit could not be found

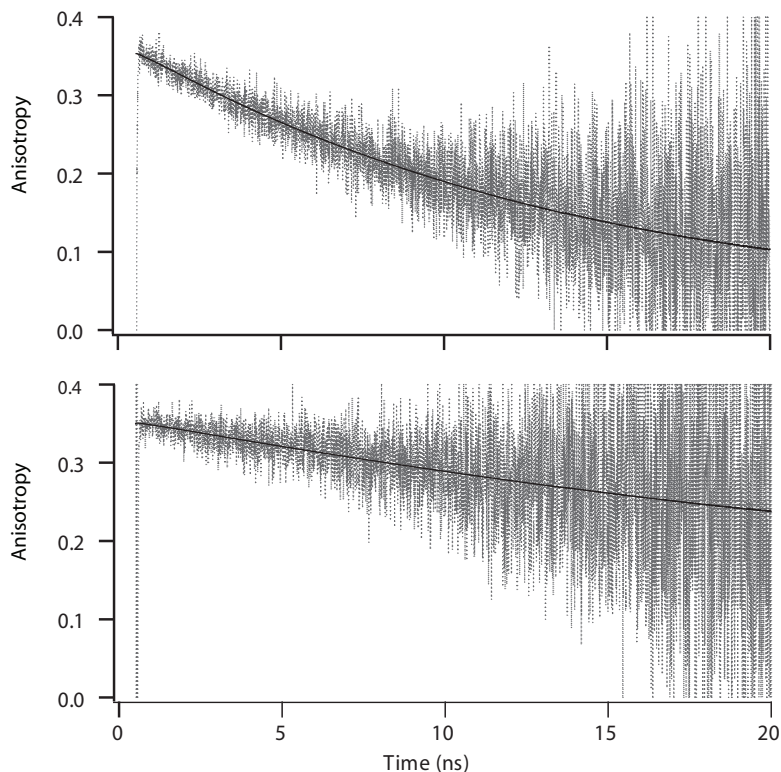


Figure 6.6: Experimental and fitted fluorescence anisotropy decays of ECFP in water (PBS, pH 7.4) (top panel) and in a mixture of 70% water and 30% glycerol (lower panel). The recovered anisotropy parameters are listed in Table 6.3.

6.5 Concluding remarks

We have shown that the fluorescence lifetimes of ECFP and EYFP are dependent on the refractive index of the medium. In the range of refractive index values 1.33-1.46 the average lifetimes decrease from 2.9 to 2.4 ns for ECFP and from 3.3 to 2.5 ns for EYFP. Provided that the accuracy of FLIM measurements is sufficiently high, these lifetime changes should be measurable in living cells allowing imaging of relative refractive index changes. EYFP should then be preferably used, since the relative change in lifetime is larger and the fluorescence decay is largely single exponential.

Some caution is necessary for FLIM measurements reporting on FRET when ECFP is the donor, since the fluorescence decay is clearly non-exponential having a relatively long lifetime of 3.7 ns (67% present) and a relatively short lifetime of 1.1 ns (33% present). In FLIM experiments using single-photon timing, fluorescence decays are usually obtained with much less photons collected in the peak than for the cuvette-experiment shown in figure 6.2. The ECFP-lifetime values obtained in the absence of acceptor are usually in the range of the average lifetimes 2.5-2.7 ns corresponding to refractive indices characteristic for cellular

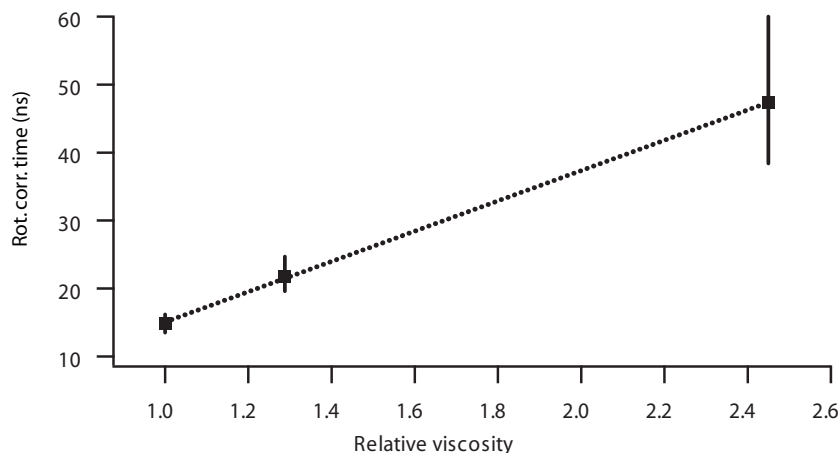


Figure 6.7: Plot of rotational correlation time ϕ of ECFP against relative viscosity for three water-glycerol mixtures (0%, 10% and 30% glycerol, respectively). The confidence limits are also plotted in the same graph.

environments (Borst *et al* 2003). When one uses the average lifetime in case of FRET to calculate the transfer efficiency, one important assumption is that both lifetimes must equally reflect the rate of energy transfer. For example, when the transfer efficiency is 50%, then the short lifetime must be reduced from 1.14 ns to 0.57 ns and the longer one from 3.5 ns to 1.75 ns yielding an average fluorescence lifetime of 1.34 ns as compared to 2.67 ns in the absence of FRET (see Table 6.1). In order to eliminate the environment-sensitive lifetime of ECFP in FLIM experiments reporting on FRET, acceptor photobleaching should then be applied yielding a reference donor fluorescence lifetime (Wouters *et al* 2001). Again, because of its mono-exponential fluorescence decay, EYFP would be a much better donor in FLIM experiments reporting on FRET.

The anisotropy decays of ECFP and EYFP accurately reports on the protein rotational motion when the macroscopic viscosity is up to 2.5 larger than that of water. The average fluorescence lifetime is too short to report on slower rotations higher-viscosity media. The initial anisotropy of ECFP is significantly lower than that of EGFP and EYFP.

Acknowledgments

This work was supported by an investment grant from the Council for Earth and Life Sciences of the Netherlands Organization for Scientific Research.

Chapter 7

Polarized Resonance Energy Transfer Spectroscopy Reveals Structural Changes in the Calcium Sensor YC3.60

Abstract

Polarized fluorescence experiments at picosecond time resolution of the calcium sensor yellow cameleon 3.60 (YC3.60) in aqueous solution have been performed. Upon donor (ECFP) excitation, fast resonance energy transfer is manifested by a distinct growing-in of acceptor (Venus) fluorescence intensity at a rate characteristic for this process. In addition, time-resolved fluorescence anisotropy measurements under the same excitation and emission conditions showed a rapid decay with a correlation time that is similar to the time constant of the resonance energy transfer process. From the parameters retrieved after associative fitting of the time-resolved fluorescence and anisotropy data the change in the relative orientation of donor and acceptor transition dipoles was determined. This allowed us to make comparative structural models of this FRET sensor in the open ($-Ca^{2+}$) and closed ($+Ca^{2+}$) conformation.

This chapter has been submitted for publication.

J.W. Borst, S. Laptanok, N.V. Visser, A.H. Westphal, J. Aker, M.A. Hink, A. van Hoek, A.J.W.G. Visser.

7.1 Introduction

Calcium is one of the most important second messengers in cell biology. For *in vivo* fluorescence imaging fluorescent calcium indicators ('cameleons') have been developed and continuously improved (Miyawaki *et al* 1997; Miyawaki *et al* 1999; Nagai *et al* 2002; Nagai *et al* 2004). Cameleons are genetically encoded protein constructs without any cofactors, which can be targeted to specific intracellular locations. They are designed on basis of the Förster Resonance Energy Transfer (FRET) principle, in which a donor (ECFP) can transfer the excited-state energy non-radiatively to an acceptor (EYFP) molecule positioned at short distance. Currently, the enhanced forms of CFP and YFP are the most frequently used FRET pairs in cell biology. Cameleons consist of a fusion of ECFP and EYFP linked by calmodulin and a calmodulin binding peptide M13. The determination of enhanced intramolecular FRET is sensed by the binding of calcium ions to calmodulin. The dynamic range and the mono- or bi-phasic response to calcium are dependent on the version of the yellow cameleon (YC) used. Binding of calcium makes the calmodulin wrap around the M13 domain leading to an enhanced FRET signal (Truong *et al* 2001).

An additional advantage is the possibility of ratio imaging in fluorescence microscopy, since both donor and acceptor fluorescence intensities can be simultaneously measured after donor excitation. Since the introduction of the fluorescent indicators their sensitivity of calcium binding has continuously been improved by optimization of the FRET pair (Griesbeck 2004; Heim and Griesbeck 2004; Mank *et al* 2006). FRET can occur when there is sufficient spectral overlap between donor emission and acceptor absorption and when the distance and orientation criteria are satisfied. The efficiency of energy transfer varies inversely with the sixth power of the distance between donor and acceptor molecules limiting FRET-related distances between 1 and 10 nm (Lakowicz 1999; Wouters and Bastiaens 1999; Hink *et al* 2002). To increase the spectral overlap (and thus the critical distance) the molar extinction coefficient of the acceptor should be as high as possible. Therefore the EYFP moiety has been modified continuously for the optimization of the ECFP-EYFP FRET pair. It has been shown that the enhanced form of YFP (EYFP) is sensitive to pH and has poor photo-stability (Griesbeck *et al* 2001). This resulted in the development of newer versions of EYFP, such as Citrine, which is very bright relative to EYFP and is much more resistant to photobleaching, acidic pH, and other environmental effects. Another derivative, named Venus, is the fastest maturing one and among the brightest yellow variants developed to date and has been used in several cameleon versions (Evanko and Haydon 2005).

Next to distance, the dipole orientation factor of the donor emission dipole moment and acceptor absorption dipole moment is also important for the energy transfer efficiency (Dale *et al* 1979; van der Meer 2002). Nagai and co-workers (2004) have optimized the dynamic range of the YC by changing the position of the N-terminus via circular permutation of the Venus molecule (Nagai *et al* 2004). In this way the relative orientation, position and distance between ECFP and Venus were modified. Several mutants were tested and the Asp173 mutation resulted into the most sensitive Ca^{2+} sensor, called YC3.60. Compared to the latest improved version of YC (YC3.12), YC3.60 is equally bright but shows a 5- to 6-fold larger response (Nagai *et al* 2004). Furthermore, YC3.60 exhibits an unusual spectroscopic feature

in steady-state fluorescence anisotropy measurements when ECFP is excited and the emission of Venus is detected. The steady-state anisotropy values changed from 0.12 in the absence of Ca^{2+} to an extreme value of -0.05 in the presence of Ca^{2+} . This effect was only observed for the YC3.60 and not for the other mutants.

Steady-state fluorescence spectroscopy of the calcium-sensing YC3.60 provides only information on average fluorescence properties of donor and acceptor molecules. The advantage of time-resolved fluorescence spectroscopy over steady-state fluorescence spectroscopy is that more detailed information on protein dynamics can be obtained (Lakowicz 1999). The time that a molecule spends in the excited state, the fluorescence lifetime, gives information about the local environment of the chromophore, for instance the effect of pH, the presence of quenching groups, change in refractive index or the occurrence of FRET. An additional advantage of fluorescence lifetime measurements over intensity-based measurements is the insensitivity of lifetimes to molecular concentration. To gain more detailed insight in changes in conformational dynamics of the protein upon calcium addition to YC3.60, time-resolved fluorescence and fluorescence anisotropy measurements were performed. Fluorescence anisotropy provides information on the motion or reorientation of transition dipole moments of fluorescent macromolecules. Dynamical processes such as overall rotation, internal motion or energy transfer between different fluorescent probes inside the macromolecule can be observed. In this contribution it is shown that by using time-resolved polarized fluorescence spectroscopy quantitative information on geometry changes between both visible fluorescent proteins upon calcium binding can be obtained. According to the best of our knowledge this is the first time that this quantitative approach is applied to observe structural changes in biological macromolecules consisting of VFP FRET pairs.

7.2 Materials and Methods

7.2.1 Protein material, sample preparation.

cDNA of YC3.60 was kindly provided by Dr. Atsitsu Miyawaki (RIKEN Brain Science Institute, Japan). The full length sensor was cloned into the GST fusion vector (pGEX5x2 vector). The YC3.60 was isolated and purified as described in Smith and Johnson (1988). YC3.60 was diluted in 100 mM Hepes buffer at pH 7.9 containing either 50 μM EGTA or 50 μM EGTA and 100 μM Ca^{2+} to a final concentration of 200 nM for time-resolved fluorescence experiments and to 20 nM for FCS experiments. The experiments were performed in Hepes buffer pH 7.9, because this buffer lacks chloride ions as chloride ions are known quenchers of the YFP fluorescence (Jayaraman *et al* 2000). In this buffer the maximal change in ratio of fluorescence intensity induced by calcium binding amounts to 5, while in PBS buffer (containing chloride ions) this ratio change was only a factor of 3. Experiments were performed in either quartz cuvettes of 1.0×0.4 cm for time-resolved fluorescence or 8-chambered coverslips for FCS measurements. All measurements were performed at room temperature.

7.2.2 Steady-state fluorescence measurements.

Steady-state fluorescence experiments using an excitation wavelength of 420 nm were performed on a Fluorolog 3.2.2 (Horiba Jobin Yvon Ltd.) spectrofluorimeter equipped with a thermostatically controlled cuvette holder (details in Visser *et al* (2005)).

7.2.3 Time resolved polarized fluorescence experiments and data analysis.

Time-resolved fluorescence measurements were carried out using a mode-locked continuous wave laser for excitation and time-correlated photon counting as detection technique as described previously (Borst *et al* 2005). The samples were excited with vertically polarized light pulses (0.2 ps FWHM) at an excitation frequency of 3.8 MHz and both parallel- and perpendicular-polarized fluorescence intensities were detected. At 420-nm excitation ECFP fluorescence was detected with a 480-nm interference filter (Schott, Mainz, Germany, half-bandwidth of 5.4 nm). The sensitized emission of Venus fluorescence was detected with an OG 530 cut-off filter (Schott) and a Schott 557.6 nm interference filter (half-bandwidth 5.9 nm). The dynamic instrumental response function of the setup was approximately 40–50 ps FWHM, and was obtained at the ECFP or Venus emission wavelengths by using a solution of xanthione in ethanol as reference compound having an ultrashort fluorescence lifetime of 14 ps. Global analysis of the experimental data using multi-exponential model functions was performed using the ‘TRFA Data Processing Package’ of the Scientific Software Technologies Center (Belarusian State University, Minsk, Belarus; <http://www.sstcenter.com>) as described in detail previously (Digris *et al* 1999; van den Berg *et al* 2004; Borst *et al* 2005; Visser *et al* 2005). To obtain an optimal fit of the time-resolved fluorescence anisotropy data of YC3.60 an associative fitting protocol was used, in which short fluorescence lifetimes are grouped with short correlation times and longer fluorescence lifetimes with longer correlation times.

7.2.4 Fluorescence correlation spectroscopy

FCS experiments were performed with a Zeiss LSM510-ConfoCor-2 system. The details of the setup have been described previously (Hink *et al* 2003a). Samples were excited with a wavelength of 514 nm from an argon-ion laser and fluorescence photons were collected through a BP527-562 filter and a size-adjustable pinhole and fibre-coupled to an avalanche photodiode (SPCM-AQ Perkin-Elmer, USA). Measurements of 60 s were repeated at least ten times. The autocorrelation traces were globally analyzed as detailed in Skakun *et al* (2005). The model function that appropriately fit the experimental data was the one for three-dimensional diffusion with triplet kinetics. The obtained translational diffusion coefficient D is related to the thermal bath kT and to the friction $6\pi\eta R_h$ experienced by the (spherical) particle through the Stokes-Einstein relationship $D = kT/(6\pi\eta R_h)$ where k is Boltzmann constant, T is temperature, η is viscosity and R_h is the hydrodynamic radius of a spherical particle. This hydrodynamic radius is used in the calculation of the Stokes’ hydrodynamic expression for rotational friction $8\pi\eta R_h^3$. The rotational correlation time τ_{rot} of the protein complex can then be obtained through the Stokes-Einstein relation for rotational diffusion $\tau_{rot} = 4\pi\eta R_h^3/(3kT)$.

7.2.5 Modeling

Three-dimensional models of the open ($-Ca^{2+}$) and closed ($+Ca^{2+}$) conformation of YC3.60 were constructed. For the closed conformation the crystal structure files 2BBM.pdb (calmodulin with light chain myosin kinase helix; M13) and 1C4F.pdb (GFP) were used. For the open conformation the calmodulin part of 1XFU.pdb and 1C4F.pdb (GFP) were used. The transition dipole moments (Rosell and Boxer 2003) and the relative angle between these

vectors of the two chromophores within the two fluorescent protein units were used to orient the individual parts of the YC3.60 molecule using the program PyMOL (<http://www.pymol.org>) (DeLano 2002). We have assumed that the absorption and emission dipole moments of the two chromophores are identical.

7.3 Results

7.3.1 Steady state fluorescence spectroscopy

The complete fluorescence spectrum of YC3.60 is shown in figure 7.1. The first peak originates from the ECFP (λ_{max} 475nm) fluorescence and the second peak mainly arises from sensitized emission of the acceptor (Venus λ_{max} 539nm). The Venus/ECFP fluorescence intensity ratio changes from 1.6 in the absence of Ca^{2+} (50 μM EGTA) to 8.3 in the presence of 100 μM Ca^{2+} . A similar enhanced FRET signal was also found by Nagai and co-workers (Nagai *et al* 2004).

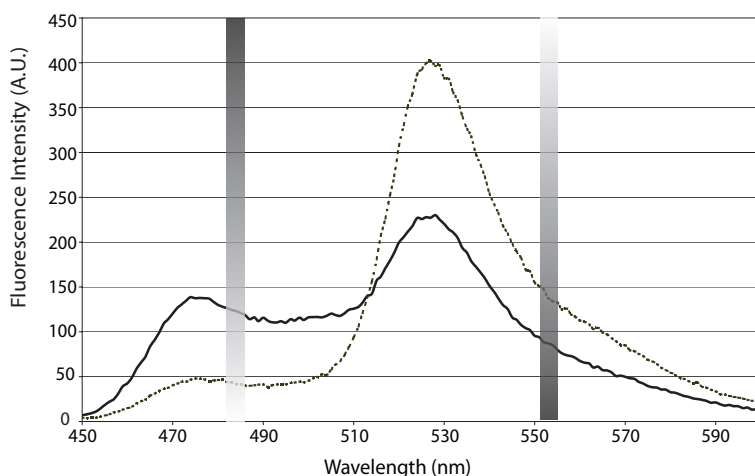


Figure 7.1: Corrected fluorescence emission spectra of YC3.60 in the absence (black line) and presence (dashed line) of Ca^{2+} . The spectra were obtained upon excitation at 420 nm. The fluorescence spectra originate from the donor ECFP (λ_{max} 480nm) fluorescence and from sensitized emission of the acceptor Venus (λ_{max} 539nm). In the figure the bandpass filters used for the time-resolved spectroscopy experiments are indicated.

7.3.2 Time resolved fluorescence spectroscopy

In time-resolved fluorescence experiments YC3.60 was excited at 420 nm (ECFP moiety) and the fluorescence of either ECFP (480 nm) or Venus (557 nm) was detected. The fluorescence decay in the ECFP channel requires a three-component exponential model to obtain a satisfactory fit. Analysis of the fluorescence decays resulted in fluorescence lifetimes of 0.29 ns (26%), 1.27 ns (36%) and 3.3 ns (34%) (Table 7.1) yielding an average fluorescence lifetime $\langle \tau \rangle = 1.7$ ns. In the presence of Ca^{2+} the fluorescence lifetimes were 0.055 ns (65%), 0.93 ns (18%) and 3.5 ns (17%) resulting in reduction of the average lifetime to 0.81 ns (Table 7.1). The quenching of the ECFP fluorescence within the calcium sensor results in significantly shorter average lifetime compared to the unquenched average fluorescence lifetime of purified ECFP alone (Fig. 7.2 curve 1; $\tau = 2.85$ ns Borst *et al* (2005)).

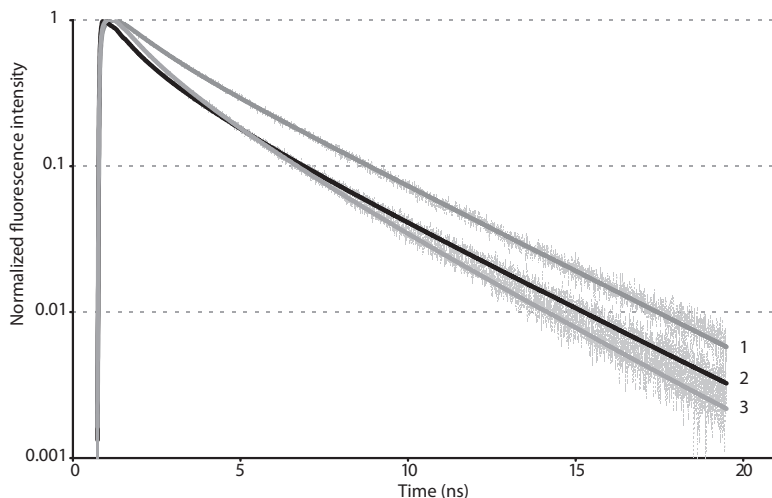


Figure 7.2: Experimental and fitted fluorescence decay curves of ECFP (1), YC3.60 in presence of Ca^{2+} (2), YC3.60 in absence of Ca^{2+} (3). The excitation wavelength was 420 nm and the detection wavelength of ECFP emission was 480 nm.

The time-dependent rise in fluorescence intensity of the Venus following pulse excitation of the donor is a direct consequence of energy transfer (Visser *et al* 2005) (Fig. 7.3). The data were analyzed using a two-component model with both positive and negative pre-exponential factors (Table 7.1). The short lifetime with negative amplitude reflects the energy transfer process. The actual transfer rate is determined by the reciprocal lifetime. The part of the decay with positive amplitude corresponds to the fluorescence of the acceptor. In the absence of Ca^{2+} a fluorescence lifetime of 1.17 ns with negative amplitude was found. A strong effect was observed upon addition of Ca^{2+} resulting in a decrease of the short lifetime component to 0.026 ns. A long fluorescence lifetime of 3.1-3.2 ns of Venus with positive amplitude was found independent of the presence of calcium.

Table 7.1: Fluorescence decay (rise) parameters of YC3.60 (-/+ Ca^{2+}) upon excitation at 420 nm and either donor (480 nm) or acceptor (557 nm) detection.

Sample	λ_{em} (nm)	α_i (%)	τ_i (ns)	α_{2+} (%)	τ_{2+} (ns)	α_3 (%)	τ_3 (ns)	$\langle\tau\rangle$ (ns)
YC3.60	480	26	0.29 (0.25-0.33)	36	1.27 (1.21-1.34)	34	3.30 (3.27-3.32)	1.70
YC3.60 + Ca^{2+}	480	65	0.055 (0.050-0.059)	18	0.93 (0.89-0.95)	17	3.52 (3.50-3.53)	0.81
YC3.60	558	-15	1.17 (1.10-1.31)	85	3.23 (3.21-3.24)			
YC3.60 + Ca^{2+}	558	-24	0.026 (0.025-0.038)	76	3.11 (3.10-3.12)			

Note that the absolute values of the amplitudes (α) are normalized to one. A negative α indicates a rise of fluorescence intensity. Values in parentheses are the confidence limits obtained after rigorous error analysis at the 67% confidence level.

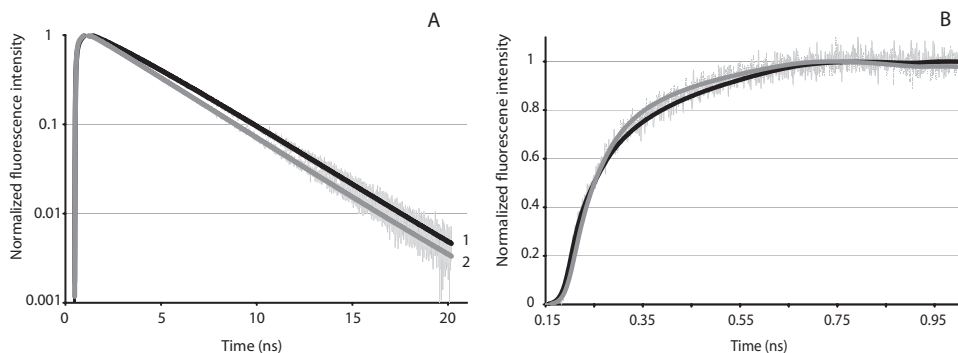


Figure 7.3: Experimental and fitted fluorescence rise and decay curves of the acceptor in YC 3.60. Acceptor fluorescence (557 nm) was monitored upon donor excitation at 420 nm. The growing in fluorescence of acceptor is faster in presence of Ca^{2+} (2) compared to the curve without Ca^{2+} (1). Figure 7.3 B is an expanded view of the first nanosecond of figure 7.3 A. The recovered parameters (α , τ) are collected in Table 7.1.

7.3.3 Time resolved fluorescence anisotropy

The time-dependent fluorescence anisotropy exhibits a peculiar pattern under conditions of donor excitation and acceptor fluorescence detection (Fig. 7.4). The fluorescence anisotropy exhibits an initial decay with correlation time that is compatible to the time needed for the acceptor fluorescence to reach maximum intensity. This correlation time becomes much shorter when calcium is present. In the latter case the anisotropy becomes even negative and is slowly increasing to zero. All time-resolved fluorescence anisotropy curves were globally analyzed using a two-component model, in which the different fluorescence lifetimes were associated with different correlation times ϕ_1 and ϕ_2 with their corresponding amplitudes β_1 and β_2 (Table 7.2) (see details in Visser *et al* (2005) and Borst *et al* (2005))

Table 7.2: Anisotropy ($\beta_1/\phi_1, \beta_2/\phi_2$) decay parameters of YC3.60 (-/+ Ca^{2+}) upon excitation at 420 nm and detection at 557 nm obtained after associative analysis.

Sample	$\lambda_{\text{em}}, \text{nm}$	β_1	$\phi_1 \text{ (ns)}$	β_2	$\phi_2 \text{ (ns)}$
YC3.60	558	0.166 (0.161-0.170)	1.09 (1.02-1.17)	0.068 (0.065-0.070)	34.38 fixed
YC3.60 + Ca^{2+}	558	0.112 (0.090-0.116)	0.025 (0.012-0.05)	-0.055 (-0.059- -0.054)	34.38 fixed

Values in parentheses are the confidence limits obtained after a rigorous error analysis at the 67% confidence level. ϕ_2 was determined from direct excitation of Venus in YC3.60 (see Fig. 7.4) and fixed.

The long correlation time (ϕ_2) of 34 ns can be attributed to overall protein rotation. Its value was obtained after fitting the fluorescence anisotropy decay of YC3.60 upon excitation and fluorescence detection of the Venus moiety (Fig. 7.4, curve 3). The overall rotational correlation time, unaffected by calcium, was fixed during further analysis. The short correlation time (ϕ_1) in the presence of Ca^{2+} appears to be due to energy transfer, and changes in presence of Ca^{2+} (from 1.09 to 0.025 ns).

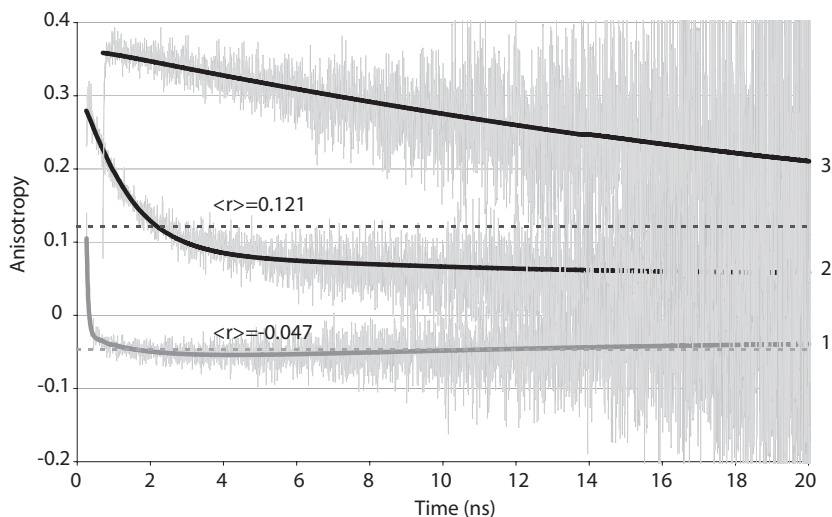


Figure 7.4: Experimental (dotted line) and fitted (solid line) fluorescence anisotropy decays of YC3.60 with (1) and without (2) Ca^{2+} . Excitation was set at 420 nm and acceptor fluorescence was detected at 557 nm. Direct excitation (500 nm) and detection (557 nm) of the Venus moiety of the YC3.60 ($-\text{Ca}^{2+}$) is represented by curve 3. The horizontal lines (dashed) represent steady-state anisotropy. The data were analyzed using associative model and yielded correlation times (ϕ) and amplitudes (β) that are collected in Table 7.2.

From the time-resolved fluorescence and fluorescence anisotropy results one can calculate the steady-state anisotropy $\langle r \rangle$. The calculated values are $\langle r \rangle = 0.121$ ($-\text{Ca}^{2+}$) and $\langle r \rangle = -0.047$ ($+\text{Ca}^{2+}$). These values, incorporated in figure 7.4 are in excellent agreement with experimental values reported previously (Nagai *et al* 2004).

7.3.4 Fluorescence correlation spectroscopy

As described in paragraph 7.3.2 upon excitation of ECFP and detection of the Venus fluorescence the data were fitted with a two-component model. A short lifetime with negative amplitude was found reflecting the energy transfer process. The other component with a positive amplitude corresponds to the intrinsic lifetime ($\tau = 3.2$ ns) of the Venus moiety. The rotational correlation time of YC3.60 having a molecular mass of 80 kDa is expected to be at least tenfold longer and is therefore be less precisely determined on the fluorescence timescale. In order to verify the results of time-resolved fluorescence anisotropy experiments we performed complementary experiments of fluorescence correlation spectroscopy (FCS). Using FCS the translational diffusion coefficient of YC3.60 was determined by excitation and fluorescence detection of the Venus moiety (see Fig. 7.5).

The diffusion coefficient of YC3.60 was determined as $63\text{--}65 \times 10^{-12} \text{ m}^2/\text{s}$ in the absence and presence of Ca^{2+} . This value is in accordance with the molecular mass of YC3.60 (80 kD). For free YFP in solution a diffusion coefficient of $90 \times 10^{-12} \text{ m}^2/\text{s}$ was found (Hink (2002)). From the diffusion coefficient a rotational correlation time of 38–42 ns was calculated. This result is in good agreement with the rotational correlation time retrieved from fluorescence anisotropy decay experiments.

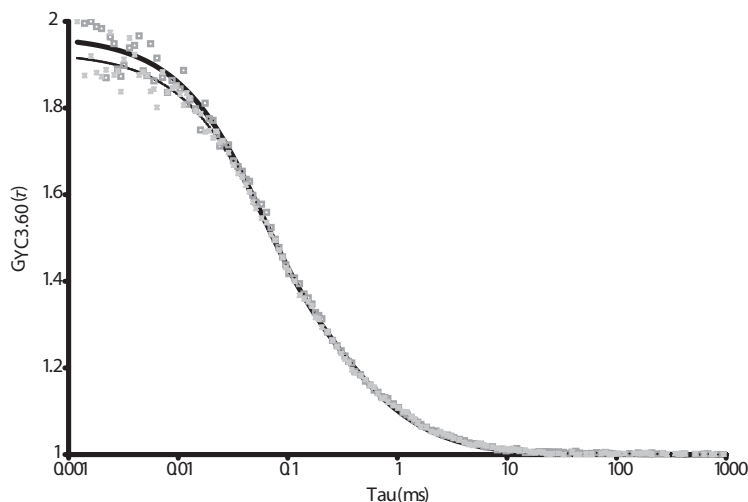


Figure 7.5: Representative autocorrelation curves of YC3.60 in absence (□) or presence (x) of Ca^{2+} . Experimental curves (symbols) and theoretical fits (black line) are shown in the graph.

7.4 Discussion

The genetically encoded yellow cameleons (YC's) Ca^{2+} sensors (Miyawaki *et al* 1997; Miyawaki *et al* 1999) have been modified for optimal detection of Ca^{2+} in specific organelles of living systems (Hara *et al* 2004; Filippin *et al* 2005). Nagai and co-workers have developed a new Ca^{2+} sensor with a large dynamic FRET range leading to improvement in both temporal and spatial resolution of Ca^{2+} imaging (Nagai *et al* 2004). The new calcium sensor YC3.60 was created via the circular permutation method (Baird *et al* 1999) in which the orientation and position of the donor and acceptor was changed resulting in significantly higher change in FRET efficiency upon the addition of Ca^{2+} . This method also has proven to be valuable using other calcium linkers (Mank *et al* 2006). In the absence of Ca^{2+} , a FRET signal was already observed because the acceptor is located near (or within) the Förster radius to the donor. As expected addition of Ca^{2+} leads to an increased FRET signal because binding of Ca^{2+} changes the conformation making the distance between donor and acceptor smaller.

In time-resolved FRET studies, the fluorescence lifetime of the donor molecule is usually measured. Quenching of the donor by an acceptor molecule leads to a shorter fluorescence lifetime of the donor resulting in an increased FRET efficiency. The experimental data of the donor fluorescence decay had to be fitted with three fluorescence lifetime components because the fluorescence decay of ECFP alone is already heterogeneous and had to be analyzed with at least two components to obtain a satisfying fit (Habuchi *et al* 2002; Borst *et al* 2005). The decrease in average lifetime from 1.70 ns ($-\text{Ca}^{2+}$) to 0.81 ns ($+\text{Ca}^{2+}$) is caused by a more efficient relaxation pathway of energy transfer. The FRET efficiency changed upon Ca^{2+} addition from 40 % to 71.5 %. Close examination of Table 7.1, however, learns that there are still long lifetime components > 3 ns present in the donor fluorescence decay at 480 nm (34% and 17%, Table 7.1). These lifetime components must arise from a population

of YC3.60 molecules in which energy transfer is abolished. One possibility is that a small population of Venus molecules within YC3.60 exists in a molecular conformation that is not suitable for accepting energy from donor ECFP, for instance, because of the presence of a small fraction of protonated acceptor (Nagai *et al* 2002). The long lifetime components of the donor fluorescence make the average lifetime apparently too long. As discussed previously (Borst *et al* 2005) the ECFP fluorescence decay is clearly double exponential having a longer lifetime of 3.7 ns (fraction 67%) and a shorter lifetime of 1.1 ns (fraction 33%). The origin of the two lifetimes has been attributed to the presence of two conformers of the chromophore in ECFP, which are in slow equilibrium (Seifert *et al* 2002; Hyun Bae *et al* 2003). It has been recently shown by molecular dynamics simulations that both conformers exhibit similar spectra (Demachy *et al* 2005). Then, in principle, both lifetimes must become shorter in case of FRET. That would imply that the fluorescence decay profile of ECFP in YC3.60 would even consist of four lifetimes: two unquenched donor lifetimes and two quenched donor lifetimes. The four-component fit might be of the same quality as a three-component fit because of possible overlapping values of two middle lifetimes of ~ 1 ns (one quenched and one unquenched).

In view of this complexity in donor lifetime properties we have applied an alternative FRET method by detecting the growing in of acceptor fluorescence upon donor excitation (Fig. 7.3). In this way one can selectively observe the pure FRET process between donor and acceptor molecules, since the transfer rate constant (k_T) can be directly determined from the rise time of the acceptor fluorescence, which is equivalent to the donor fluorescence lifetime in the presence of acceptor (τ_{DA}). Assuming an average donor fluorescence lifetime without acceptor (τ_D) of 2.86 ns, k_T ($= 1/\tau_{DA} - 1/\tau_D$) can be calculated from the data in Table 7.1 and amounts to 0.50 ns^{-1} for YC3.60 (without calcium) and 38 ns^{-1} for the calcium-bound YC3.60 conformation. On the other hand the transfer rate constant can be related to the distance through $k_T = \tau_D^{-1} (R_0/R)^6$, in which R_0 is the critical transfer distance and R the actual distance. From the ECFP-EYFP emission and absorption spectra a R_0 of 4.90 nm can be calculated using an orientation factor $\kappa^2 = 1$ (Hink *et al* 2003b). According to our data, the average distance between the ECFP and Venus within YC3.60 decreases from 4.60 nm ($-\text{Ca}^{2+}$) to 2.24 nm for the Ca^{2+} -bound conformation. A distance of 4.60 nm is in the same order of magnitude as the critical transfer distance R_0 and is therefore accurately determined, whereas a distance of 2.24 nm is so short that it corresponds to an energy transfer efficiency of 99%, making this distance undetermined.

With fluorescence anisotropy one measures the change in direction of transition dipole moments. The time-resolved fluorescence anisotropy of YC3.60 upon donor excitation and observation of the acceptor first shows a rapid decay followed by a much slower decay. In case of the calcium-bound form of YC3.60 this decay is more rapid and even reaches a negative anisotropy value before slowly decaying to zero. The short correlation time can be considered as the characteristic time needed to change the transition dipole direction of the initially photoselected donor molecules into the transition dipole direction of the acceptor molecules. This time must be equivalent to the reciprocal transfer rate constant. A two-component analysis could be used to fit the experimental time-resolved anisotropy data. The short correlation time arising from energy transfer changes from 1.09 ns ($-\text{Ca}^{2+}$) to 0.025 ns ($+\text{Ca}^{2+}$).

The long correlation time of YC3.60 was obtained by direct excitation and emission detection of the Venus part, without interference of ECFP. Only a single rotational correlation time (34 ns) was obtained confirming Venus is rigidly bound within the complete YC3.60 complex. On the other hand, similar rotational correlation times (40 ns) were also indirectly retrieved by translational diffusion measurements in FCS experiments. FCS is then a good alternative method to determine rotational correlation times of larger complexes with molecular mass > 80 kDa.

The pre-exponential factors (β_i) of the fluorescence anisotropy decay (Table 7.2) can be related to geometrical parameters describing the relative change in transition dipole moment orientations of ECFP and Venus in the YC3.60 complex: $\beta_2 - \beta_1 = 0.6\cos^2\theta - 0.2$ (Visser *et al* 2005), where θ is the angle between the transition dipole moments of the chromophores in ECFP and Venus of YC3.60. In the absence of Ca^{2+} we determined an angle $\theta = 65^\circ$. Binding of Ca^{2+} changed the angle to $\theta = 77^\circ$. Besides that this angle between ECFP and Venus becomes larger we calculated that the distance between the chromophores becomes smaller (R changed from 4.60 nm to 2.24 nm, calculation with the assumption of $\kappa^2 = 1$).

The orientation factor κ^2 for a donor-acceptor pair depends on three orientation angles (Dale *et al.*, 1979): the angle (θ_D) between the emission transition dipole moment of the donor (μ_D) and the line connecting the centers of the donor and acceptor chromophores, the separation vector \mathbf{R} , the angle (θ_A) between the absorption transition dipole moment of the acceptor (μ_A) and the separation vector and the angle (θ_T) between transition dipole moments μ_D and μ_A . Two planes are formed by μ_D and \mathbf{R} and by μ_A and \mathbf{R} , intersecting at \mathbf{R} and under an angle φ . The orientation factor can be expressed in two ways in terms of the various angles: $\kappa^2 = (\cos \theta_T - 3\cos \theta_D \cos \theta_A)^2 = (\sin \theta_D \sin \theta_A \cos \varphi - 2\cos \theta_D \cos \theta_A)^2$. The ‘experimental’ angle θ is equivalent to θ_T .

We were able to design a structural model from three parts (two fluorescent protein moieties and the calmodulin-M13 complex) of YC3.60 (-/+ Ca^{2+}). In the closed conformation the distance between the chromophores was set at 2.3 nm and a relative angle between the transition dipole moments of 77° was used for construction. For the open conformation values of 4.6 nm and 66° , respectively, were applied. The proposed structure is a realistic model because all parameters like the angle between the transition dipole moments, distances between the chromophores and the conformation of the calmodulin-M13 unit were taken into account for the design. In the closed conformation (Fig. 7.6A) the two fluorescent proteins are positioned adjacent of each other and the calmodulin is wrapped around the M13 helix. It is clear from the structure shown in figure 7.6B that in the open position the fluorescent proteins remain close to the calmodulin but that the M13 helix is released from the calmodulin. From these data we have obtained a good insight in the orientation and distances of the donor and acceptor molecules in the YC3.60. The experiments only yield the angle between the transition dipole moments of ECFP and Venus (θ_T), but not the angles θ_D , θ_A , and φ . For that reason the exact value of κ^2 can not be evaluated.

The structural models depicted in figure 7.6 indicate that the FRET process in YC3.60 is mainly distance dependent. For a more precise description of the FRET process the exact spatial coordinates of the chromophores are necessary to determine the influence of κ^2 on this system. Therefore a crystal structure of YC3.60 could supply the missing structural information.

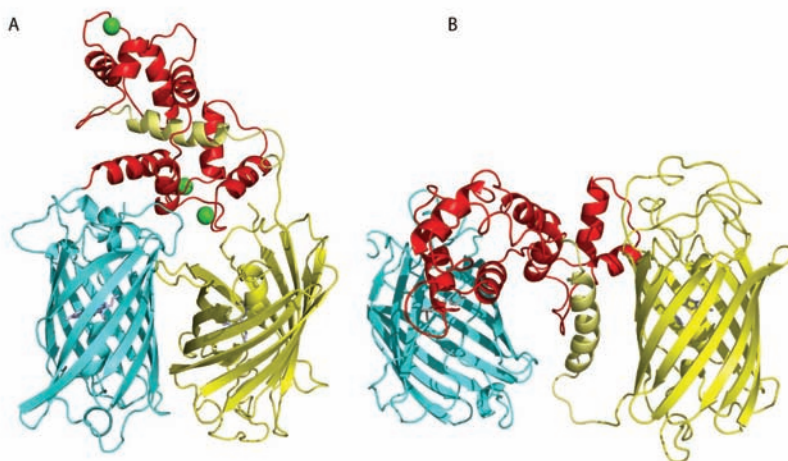


Figure 7.6: Structural model of YC3.60 in the closed (A) and open (B) conformation. The left barrel (ECFP) is connected at the N-terminus of the calmodulin part (A, top; B, middle). The C-terminus of the M13 helix finally connects to the right barrel (Venus).

Chapter 8

Summarizing Discussion

This thesis focuses on the study of cellular biochemistry with the use of fluorescence microspectroscopy techniques. Fluorescence microspectroscopy of living cells has the advantage that not only proteins of interest can be localized, but also their interactions can be spatially resolved. Therefore the combination of cell biology with biophysical techniques is an important step forward to identify and quantify biological processes in their natural environment. Several imaging techniques are available to obtain high resolution images to identify cellular components or structures. Using electron microscopy one can obtain images with spatial resolutions down to 1.0 nm (Joy and Pawley 1992). These images have far better resolution as compared to that of light microscopy, which resolution is diffraction-limited to a few hundred nanometers. However, electron microscopy requires fixation of molecules in the specimen making it impossible to study dynamic processes in cells. Therefore light microscopy, particularly fluorescence-based microscopy, is the most used method to obtain molecular and dynamical information from living cells. On the other hand, the resolution limits of fluorescence microscopy can be reduced by combining microscopy with FRET spectroscopy. FRET microscopy provides quantitative, temporal and spatial (1-10 nm) information about binding and interaction of proteins *in vivo* (Herman 1998; Wallrabe *et al* 2003).

This thesis describes several microspectroscopic applications to obtain quantitative information on the dynamic properties of bio-molecules in well defined molecular model systems as well as in living plant cells.

8.1. Lipid oxidation *in vitro* and *in vivo* (Chapters 2 and 3)

Lipid (per)oxidation of unsaturated lipids plays an important role in cell membrane properties, which have an impact on a wide variety of processes such as cell signaling, apoptosis and deterioration of foods. Oxidation of these lipids leads to dynamical and structural changes of membrane bilayers. The oxidation process can be monitored by incorporating a special fluorescent lipid-like probe, BP-C11, in the membrane. This probe changes its fluorescence color from red to green upon oxidation. Mass spectrometry analysis of oxidized BP-C11 showed the loss of the entire phenyl moiety, which explains the shift in fluorescence of the probe from red to green upon oxidation because the fluorescence originates from a smaller conjugated system (Drummen *et al* 2004). Studies on artificial bilayer membranes using increasing amounts of unsaturated phospholipids showed an increase of the oxidation rate, which could be related to a larger curvature of the outer leaflet of the bilayer. As a result of this, the lipid-lipid spacing is larger and the unsaturated fatty acyl chains are better accessible for the oxidant. Furthermore, several specific fluorescent probes have revealed the dependence

of microfluidity and lateral lipid mobility on i) vesicle composition, ii) the extent of oxidation and iii) the position of the fluorescent group relative to the phospholipid headgroup. The composition of natural eukaryotic membranes consists of many more other components than that of artificial lipids used in this study. Components like membrane proteins and cholesterol are not taken into account. Especially cholesterol (mammalian cells) and sterols (plant cells) might play a crucial role in membrane integrity. It is known that cholesterol can have a drastic effect on the membrane fluidity and lateral diffusion (Filippov *et al* 2003). The next natural step in this line of research is to include cholesterol in the lipid bilayers. One should realize, however, that inclusion of a third lipid component would require knowledge of the phase diagram of the lipid mixture.

The research on oxidation processes was extended to living plant systems (Chapter 3). In plant cells the production of reactive oxygen species (ROS) is one of the reactions in the plant defense mechanisms to pathogen infection or elicitor production (Lamb and Dixon 1997; Ebel and Mithofer 2001). On-line visualization of lipid per-oxidation in tobacco BY-2 cells was demonstrated using the BP-C11 probe, which is easily incorporated in the plasma membrane. The observed lipid oxidation rate in plant cells is much smaller than reported previously for these rates in animal cells (Pap *et al* 1999). This difference is probably due to the defense response of higher plants (Lamb and Dixon 1997) and to the particular composition and morphology of plant cell membranes. Oxidative bursts in plant cells are accompanied by the activation of several enzymes such as phospholipases and lipoxygenases. Pyranine is a fluorescent probe to monitor hydrogen peroxide produced during oxidation. Steady-state fluorescence measurements of pyranine in BY2 suspension cells were performed to screen for the activation or inhibition pathways leading to H_2O_2 formation. Currently, two-photon excitation (TPE) confocal microscopy is available to excite pyranine enabling *in situ* detection of ROS formation. Very recently a genetically encoded fluorescent indicator for detecting intracellular hydrogenperoxide has been developed (Belousov *et al* 2006). This sensor consists of circularly permuted yellow fluorescent protein inserted in a prokaryotic H_2O_2 sensing protein.

8.2 Applications using two-photon excitation microscopy(Chapters 4 and 5)

To get new insight in signal transduction cascades in living plant tissue through imaging of fluorescent key proteins, one has to overcome the barrier of dense structures, which limits light penetration. Plant cells consist of cell walls leading to severe scattering and low penetration depth using one-photon excitation (OPE). However, imaging of thick multi-cellular preparations is much improved by using lower-energy infrared laser light. The localization of Histon 2B-YFP, for instance, a nuclear protein involved in chromatin packaging, could be visualized at much higher detail in *Arabidopsis* plants with two-photon excitation (TPE). By using TPE the penetration depth is at least three times better than for OPE. In addition, the direct detection method in this microscope configuration showed improved signal to noise ratio enabling the observation of specific cells in the middle of the root tip which was not feasible using OPE. Furthermore, TPE confocal microscopy allows measuring spatially resolved fluorescence lifetimes. This technique is called fluorescence lifetime imaging microscopy (FLIM). The occurrence of Förster resonance energy transfer (FRET) can be

established with FLIM. Two applications are described. It was shown previously by yeast two-hybrid experiments that different members of the FLORAL BINDING PROTEINS (FBP) transcription factors were identified in a complex, which was not true for all variants. FRET-FLIM was used to detect the interaction of fluorescently tagged FBP's in plant protoplasts. The fluorescence lifetime images revealed sub-nuclear spots indicating that two different FBP members were forming a dimer or higher order complex. Although no interaction was observed in the rest of the nucleus the observation of those specific spots was only possible by FLIM measurements. The two FBP's did not show interaction by yeast two-hybrid analysis. Therefore FRET-FLIM proves to be advantageous for *in vivo* interaction studies, which can not be detected by classical *in vitro* techniques.

Another example of a FRET-FLIM application is the signal transduction pathway in plant cells of Brassinosteroid (BR) signaling. In *Arabidopsis* brassinosteroid (BR) perception is mediated by BRI1 and AtSERK3 (BAK1). Genetic, biochemical and yeast interaction studies suggested that the BRI1-AtSERK3 receptor complex initiates BR signaling, but the role of the AtSERK3 receptor was still not clear. Transient expression studies in protoplasts of fluorescently labeled BRI1 and AtSERK3 allowed us to localize each receptor independently *in vivo*. In addition, FRET-FLIM showed that homodimerization of BRI1 receptors only takes place in the plasma membrane. On the other hand BRI1 and AtSERK3 preferentially heterodimerize in endosomes.

The results of interactions between transcription factors and receptor oligomerization could not be obtained with other FRET detection methods like acceptor photobleaching (APB), because this approach lacks the spatial resolution. APB is a good, first indicator for the presence of interacting molecules but the technique has some disadvantages. For instance, the strong bleaching pulse needed for destruction of the EYFP molecule can also photoconvert the emission wavelengths to higher energy (Valentin *et al* 2005). It will then be detected as an added ECFP signal, which leads to FRET efficiencies biased to too low values. In addition, APB experiments are often restricted to fixed samples, because of the rapid redistribution of donor and acceptor molecules in living cells. This fast recovery of EYFP fluorescence may interfere with quantitative determination of FRET efficiencies. Sometimes APB experiments are combined with FLIM measurements to verify the donor fluorescence quenching. Interaction between donor and acceptor molecules will result in a faster fluorescence decay of the donor molecule, but photo-destruction of the acceptor molecule will abolish the FRET effect yielding the initial fluorescence lifetime of the donor in the absence of acceptor (Bastiaens and Squire 1999).

8.3 Environmental effects on the fluorescence lifetime of VFP's (Chapter 6)

Fluorescence lifetimes strongly depend on the immediate environment of the fluorophore. The local refractive index can change the fluorescence lifetime of the fluorescent proteins significantly (Toptygin *et al* 2002; Suhling *et al* 2002a; Toptygin 2003). The range over which the fluorescence lifetime is sensing refractive index can amount to one micrometer. We therefore have purified the fluorescent proteins ECFP and EYFP to perform a time-resolved fluorescence study. The local environment of the purified ECFP and EYFP was changed by diluting the proteins in different amounts of glycerol/water mixtures. A clear effect on

the fluorescence lifetimes upon differences in refractive index was observed. A relatively low refractive index around the fluorescent protein in aqueous solution leads to the longest lifetime, whereas an increase in refractive index induced causes a progressive shortening. When FLIM experiments are performed, the localization of visible fluorescent proteins in specific regions of living cells can already yield different fluorescence lifetimes even in the absence of FRET. The higher refractive index at the plasma membrane as compared to that in cytoplasm or nucleus can result in shorter fluorescence lifetimes. These observations confirm that time-resolved fluorescence analysis of purified fluorescent proteins is needed. A proper choice of donor-acceptor pair should also be considered in the design of an experiment. The combination ECFP (donor) and EYFP (acceptor) is widely used in FRET-FLIM studies. However, the fluorescence decay of ECFP is heterogeneous with at least two lifetime components (33% of 1.1 ns and 67% of 3.7 ns), which is attributed to the presence of two chromophore conformations already visible in the crystal structure (Hyun Bae *et al* 2003) and slowly interconverting on NMR time scale (Seifert *et al* 2002). This intrinsic heterogeneity of fluorescence decay of ECFP as donor would complicate a quantitative FRET analysis from FLIM data. EGFP and EYFP would be much better donor candidates in FRET-FLIM experiments, since time-resolved fluorescence experiments have shown that the fluorescence decays of EGFP and EYFP are almost mono-exponential showing a long lifetime of around 3 ns. Therefore donor lifetime determinations in FRET-FLIM studies would be less complex, although refractive index effects of the fluorophore's environment still must be taken into account. With the design of new (monomeric) versions of the red fluorescent proteins (Shaner *et al* 2004) suitable acceptor molecules have become available for interaction studies. Also the engineered 'dark YFP' which is a non-fluorescent protein, but with retaining light absorption properties, is a potential, alternative acceptor molecule in FRET-FLIM experiments (Ganesan *et al* 2006). The advantage of using this protein in combination with EGFP as donor is the increased sensitivity, because the complete spectral detection window of EGFP can be used for photon collection (Ganesan *et al* 2006).

8.4 Yellow cameleons (Chapter 7)

Quite a number of fluorescent dyes have been developed, that are used, for instance, as indicators for cell viability, nuclear staining, calcium measurements or as markers for the localization of mitochondria and Golgi (Haugland 1996). Cellular imaging of calcium concentrations has also been performed by so-called cameleons (Miyawaki *et al* 1997; Miyawaki *et al* 1999; Nagai *et al* 2004). Cameleons are genetically encoded protein constructs without any cofactors, which can be targeted to specific intracellular locations. In this study YC3.60 is used (Nagai *et al* 2004). YC3.60 is composed of a calmodulin domain and the M13 peptide, which are flanked by the fluorescent proteins ECFP and Venus. Their action is based on intra-molecular FRET, which efficiency becomes larger when calcium is bound. Time-resolved fluorescence experiments of purified YC3.60 have yielded a detailed insight into FRET kinetics both in the presence and in the absence of calcium. This was achieved by exciting the donor (ECFP) and the detection of growing-in fluorescence of the acceptor (Venus). Time-resolved fluorescence anisotropy measurements under the same excitation and emission conditions showed a rapid decay with a correlation time that is similar to the

time constant of the resonance energy transfer process. Both growing-in lifetime and rapid correlation time were shorter when calcium was bound to YC3.60. The YC3.60 sensor has a compact and rigid structure, which is concluded from time-resolved anisotropy experiments with selective excitation and fluorescence detection of Venus. From the parameters retrieved after fitting of time-resolved fluorescence anisotropy data the change in the relative orientation of donor emission and acceptor transition dipoles was determined. This is, according to the best of our knowledge, the first time that this angle of a VFP-FRET system has been obtained. From the data a structural model of YC3.60 has been built. The very high FRET efficiencies and negative steady-state fluorescence anisotropy value in the calcium bound form was achieved by changing the relative orientation between ECFP and Venus by circular permutation of the acceptor molecule (Nagai *et al* 2004). These observations clearly show that specific mutagenesis of fluorescent proteins is extremely helpful for the design of brighter VFP's or more efficient FRET pairs.

In very recent years, several fluorescent (FRET-based) sensors have been developed to track signal transduction processes in living cells. These sensors require high specificity and the ability to report rapidly on dynamic signaling processes. FRET sensors have been developed for the detection of caspase activity (Xu *et al* 1998), the visualization of second messengers like cyclic AMP, cyclic GMP, (DiPilato *et al* 2004; Jalink 2006; Nikolaev *et al* 2006) and phosphoinositides (Cicchetti *et al* 2004). Phosphatase activity in *E. coli* cells (Vaknin and Berg 2004) or EGFR phosphorylation in mammalian cells (Offterdinger *et al* 2004) can be detected with FRET imaging. Most FRET sensors are built like the cameleons where a tandem of cyan and yellow fluorescent proteins is coupled via a linker of 12 and 20 amino acids. The composition of this linker determines the specificity of the FRET sensor. A large advantage is the possibility of ratio-imaging of the intensities of yellow and cyan fluorescent proteins when the donor is selectively excited. Enhancement or reduction of the FRET signal measured in this way is then a direct measure of a specific activity.

8.5 General conclusions and future developments

The spatial resolution of optical microscopy is of invaluable importance in many applications in life sciences. Confocal microscopy was one of the earliest methods developed for improved spatial resolution (see for a recent survey of advances in high-resolution optical microscopy (Garini *et al* 2005)). It enables to resolve particular cellular structures in living cells and to visualize (co)localization of differently colored proteins. An alternative optical method with improved axial resolution is total internal reflection microscopy (TIRF). TIRF makes use of an evanescent electromagnetic field that is created when light is totally reflected at a planar interface between two materials of different refractive indices, for instance glass and water (Thompson and Lagerholm 1997). The evanescent field is created in the medium of lower refractive index (water) and penetrates up to 100 nm. The evanescent field will excite fluorescent molecules nearby the interface. Fast detection of endosome trafficking or visualization of membrane compartments in living cells are applicable targets to study. Other non-linear microscopy approaches to achieve higher spatial resolution have been pioneered by Stefan Hell and co-workers. Combination of two-photon excitation with a confocal microscope using two high numerical-aperture objectives and special deconvolution software

resulted in images with spatial resolution of about 100 nm (Hell *et al* 1997). Combination of 4-Pi microscopy with stimulated fluorescence emission depletion (STED) can probably result in images up to 10 nm resolution (Gugel *et al* 2004).

Although these non-linear optical microscopy techniques have improved spatial resolution, the instrumentation is still too complex to be routinely used in protein interaction studies. Therefore, FRET-FLIM still remains the method of choice for measuring protein-protein interactions in cells. However, some aspects of VFP technology must be also discussed. Fluorescence (lifetime) imaging of biochemical processes in living cells using genetically encoded proteins often requires the use of strong constitutive promoters. High expression levels of these proteins can be reached, but as a result of this over-expression the localization of these proteins can be altered. Furthermore, fluorescent proteins have the tendency to form dimers at high expression levels, although the proteins of interest are not necessarily related. It has been demonstrated that the main amino acid responsible for this “sticky” behaviour of the visible fluorescent proteins from *Aequoria* is alanine 206. Replacement of this amino acid for a lysine residue resulted in truly monomeric fluorescent proteins (Zacharias *et al* 2002).

As discussed in this thesis FRET can be determined with different methods such as acceptor photobleaching and FLIM. There is also an intensity-based method like spectral imaging, which directly measures spatially resolved fluorescence spectra from the specimen. Spectral imaging microscopy allows measuring the ratio between donor and acceptor intensities upon donor excitation and analyzing FRET efficiencies quantitatively. However, precise quantification of FRET parameters is very difficult, when cells express constructs with overlapping fluorescence spectra (like ECFP and EYFP) and when the expression level of the fluorescent proteins varies. For this reason special algorithms were developed for quantifying spectrally based FRET measurements. As the profile of the individual donor and acceptor spectra is known, their individual contribution to the measured spectrum can be resolved in a process called spectral unmixing (Bunt and Wouters 2004). Such spectral unmixing algorithms have been described recently for accurate determination of donor and acceptor concentrations in a FRET system (Thaler *et al* 2005).

In this thesis much emphasis has been put on single-photon timing FLIM to measure FRET. Although single-photon timing FLIM has advantages compared to intensity-based methods, the limiting step is the relatively long time needed for determination of a fluorescence lifetime image. The experiments often require about half a minute for cells with highly expressed proteins, but in case of lower expression levels measurement times of three minutes or more are needed. In FRET experiments on fast moving objects like endosome trafficking much faster FLIM imaging is required. Developments in novel photon-counting detector technology and associated electronics are under way, so that real-time imaging of protein-protein interactions can be anticipated in the next decade.

References

- Adam, A., Farkas, T., Somlyá, G., Hevesi, M., Kiraly, Z. (1989). Consequence of O_2^- generation during a bacterially induced hypersensitive reaction in tobacco - deterioration of membrane-lipids. *Physiol. Mol. Plant Pathol.* **34**: 13-26.
- Alberts, B. (1998). The cell as a collection of protein machines: Preparing the next generation of molecular biologists. *Cell* **92**: 291-294.
- Alberts, B. A., Johnson, J. L., Raff, M., Roberts, K., Walter, P. (2004). Molecular Biology of the Cell. 4th edition. New York, Garland Science Publishing.
- Ameloot, M., Hendricks, H., Herreman, W., Pottel, H., van Cauwelaert, F., van der Meer, W. (1984). Effect of orientational order on the decay of the fluorescence anisotropy in membrane suspensions. Experimental verification on unilamellar vesicles and lipid/ α -lactalbumin complexes. *Biophys. J.* **46**: 525-539.
- Amos, W. B., Reichelt, S. (2000). Bio-Rad signal enhancing lens system (SELS) - turbo mode for confocal. *Bio-Rad Technical Note*
- Ando, R., Mizuno, H., Miyawaki, A. (2004). Regulated fast nucleocytoplasmic shuttling observed by reversible protein highlighting. *Science* **306**: 1370-1373.
- Apostol, I., Heinsteins, P.F., Low, P. S. (1989). Rapid stimulation of an oxidative burst during elicitation of cultured plant cells. *Plant Physiol.* **90**: 109-116.
- Asamizu, E., Nakamura, Y., Sato, S., Tabata, S. (2000). A large scale analysis of cDNA in *Arabidopsis thaliana*: generation of 12,028 non-redundant expressed sequence tags from normalized and size-selected cDNA libraries. *DNA Res.* **7**: 175-180.
- Auh, C. K., Murphy, T. M. (1995). Plasma-membrane redox enzyme is involved in the synthesis of O_2^- and H_2O_2 by *Phytophthora* elicitor-stimulated rose cells. *Plant Physiol.* **107**: 1241-1247.
- Baird, G. S., Zacharias, D. A., Tsien, R. Y. (1999). Circular permutation and receptor insertion within green fluorescent proteins. *Proc. Natl. Acad. Sci. USA* **96**: 11241-11246.
- Baird, G. S., Zacharias, D. A., Tsien, R. Y. (2000). Biochemistry, mutagenesis, and oligomerization of DsRed, a red fluorescent protein from coral. *Proc. Natl. Acad. Sci. USA* **97**: 11984-9.
- Bastiaens, P. I. H., Squire, A. (1999). Fluorescence lifetime imaging microscopy: spatial resolution of biochemical processes in the cell. *Trends Cell Biol.* **9**: 48-52.
- Bastiaens, P. I., Pepperkok, R. (2000). Observing proteins in their natural habitat: the living cell. *Trends Biochem. Sci.* **25**: 631-7.
- Batzri, S., Korn, E. D. (1973). Single bilayer liposomes prepared without sonication. *Biochim. Biophys. Acta.* **298**: 1015-1019.
- Becker, W., Bergmann, A. (2002). Lifetime imaging techniques for optical microscopy. Becker & Hickl GmbH, Berlin.
- Becker, W., Bergmann, A., Hink, M. A., König, K., Benndorf, K., Biskup, C. (2004). Fluorescence lifetime imaging by time-correlated single-photon counting. *Microsc. Res. Tech.* **63**: 58-66.
- Becker, W. (2005). Advanced Time-Correlated Single Photon Counting Techniques. Berlin, Springer
- Beechem, J. M., Gratton, E., Ameloot, M., Knutson, J. R., Brand, L. (1991). The global analysis of fluorescence intensity and anisotropy decay data: second generation theory and programs. In: Lakowicz J. R., editor. Topics in Fluorescence Spectroscopy. New York, Plenum Press, pp.241-305.
- Belousov, V. V., Fradkov, A. F., Lukyanov, K. A., Staroverov, D. B., Shakhbazov, K. S., Tersikh, A. V., Lukyanov, S. (2006). Genetically encoded fluorescent indicator for intracellular hydrogen peroxide. *Nat. Methods* **3**: 281-286.
- Birnbaum, K., Shasha, D. E., Wang, J. Y., Jung, J. W., Lambert, G. M., Galbraith, D. W., Benfey, P. N. (2003). A gene expression map of the Arabidopsis root. *Science* **302**: 1956-1960.
- Bligh, E. G., Dyer, W. J. (1959). A rapid method of total lipid extraction and purification. *Can. J. Biochem. Physiol.* **37**: 911-917.

-
- Booth, M. J., Wilson, T. (2001). Refractive-index-mismatch induced aberrations in single-photon and two-photon microscopy and the use of aberration correction. *J. Biomed. Opt.* **6**: 266-272.
- Borst, J. W., Visser, N. V., Kouptsova, O., Visser, A. J. W. G. (2000). Oxidation of unsaturated phospholipids in membrane bilayer mixtures is accompanied by membrane fluidity changes. *Biochim. Biophys. Acta.* **1487**: 61-73.
- Borst, J. W., Hink, M. A., van Hoek, A., Visser, A. J. W. G. (2003). Multiphoton microspectroscopy in living plant cells. *Proc. SPIE* **4963**: 231-238.
- Borst, J. W., Hink, M. A., van Hoek, A., Visser, A. J. W. G. (2005). Effects of refractive index and viscosity on fluorescence and anisotropy decays of enhanced cyan and yellow fluorescent proteins. *J. Fluoresc.* **15**: 153-160.
- Bunt, G., Wouters, F. S. (2004). Visualization of molecular activities inside living cells with fluorescent labels. *Int. Rev. Cytol.* **237**: 205-277.
- Burch, L. R., Scott, M., Pohler, E., Meek, D., Hupp, T. (2004). Phage-peptide display identifies the interferon-responsive, death-activated protein kinase family as a novel modifier of MDM2 and p21WAF1. *J. Mol. Biol.* **337**: 115-128.
- Campbell, R. E., Tour, O., Palmer, A. E., Steinbach, P. A., Baird, G. S., Zacharias, D. A., Tsien, R. Y. (2002). A monomeric red fluorescent protein. *Proc. Natl. Acad. Sci. USA* **99**: 7877-7882.
- Causier, B., Davies, B. (2002). Analysing protein-protein interactions with the yeast two-hybrid system. *Plant Mol. Biol.* **50**: 855-870.
- Chapman, S., Oparka, K. J., Roberts, A. G. (2005). New tools for *in vivo* fluorescence tagging. *Curr. Opin. Plant Biol.* **8**: 565-573.
- Chen, Y., MacDonald, P. J., Skinner, J. P., Patterson, G. H., Müller, J. D. (2006). Probing nucleocytoplasmic transport by two-photon activation of PA-GFP. *Microsc. Res. Tech.* **69**: 220-226.
- Chen, Y. E., Mills, J. D., Periasamy, A. (2003). Protein localization in living cells and tissues using FRET and FLIM. *Differentiation* **71**: 528-541.
- Chen, Y. E., Periasamy, A. (2004). Characterization of two-photon excitation fluorescence lifetime imaging microscopy for protein localization. *Microsc. Res. Tech.* **63**: 72-80.
- Cheng, P. C., Lin, B. L., Kao, F. J., Gu, M., Xu, M. G., Gan, X. S., Huang, M. K., Wang, Y. S. (2001). Multi-photon fluorescence microscopy - the response of plant cells to high intensity illumination. *Micron* **32**: 661-669.
- Cicchetti, G., Biernacki, M., Farquharson, J., Allen, P. G. (2004). A ratiometric expressible FRET sensor for phosphoinositides displays a signal change in highly dynamic membrane structures in fibroblasts. *Biochemistry* **43**: 1939-1949.
- Clouse, S. D. (2002). Brassinosteroid signal transduction: clarifying the pathway from ligand perception to gene expression. *Mol. Cell.* **10**: 973-82.
- Cox, G., Sheppard, C. J. R. (2004). Practical limits of resolution in confocal and non-linear microscopy. *Microsc. Res. Tech.* **63**: 18-22.
- Dale, R. E., Eisinger, J., Blumberg, W. E. (1979). The orientational freedom of molecular probes. The orientation factor in intramolecular energy transfer. *Biophys. J.* **26**: 161-193.
- de Folter, S., Immink, R. G., Kieffer, M., Parenicova, L., Henz, S. R., Weigel, D., Busscher, M., Kooiker, M., Colombo, L., Kater, M. M., Davies, B., Angenent, G. C. (2005). Comprehensive interaction map of the *Arabidopsis* MADS Box transcription factors. *Plant Cell* **17**: 1424-1433.
- DeLano, W. L. (2002). The PyMOL Molecular Graphics System *DeLano Scientific* San Carlos CA, USA.
- Demachy, I., Ridard, J., Laguitton-Pasquier, H., Durnerin, E., Vallverdu, G., Archirel, P., Levy, B. (2005). Cyan fluorescent protein: Molecular dynamics, simulations, and electronic absorption spectrum. *J. Phys. Chem. B* **109**: 24121-24133.
- Denk, W., Strickler, J. H., Webb, W. W. (1990). Two-photon laser scanning fluorescence microscopy. *Science* **248**: 73-76.

- Dievart, A., Clark, S. E. (2003). Using mutant alleles to determine the structure and function of leucine-rich repeat receptor-like kinases. *Curr. Opin. Plant Biol.* **6**: 507-516.
- Digris, A. V., Skakoun, V. V., Novikov, E. G., van Hoek, A., Claiborne, A., Visser, A. J. W. G. (1999). Thermal stability of a flavoprotein assessed from associative analysis of polarized time-resolved fluorescence spectroscopy. *Eur. Biophys. J.* **28**: 526-531.
- DiPilato, L. M., Cheng, X., Zhang, J. (2004). Fluorescent indicators of cAMP and Epac activation reveal differential dynamics of cAMP signaling within discrete subcellular compartments. *Proc. Natl. Acad. Sci. USA* **101**: 16513-16518.
- Dobretsov, G. E., Borschevskaya, T. A., Petrov, V. A., Vladimirov, Y. A. (1977). The increase of phospholipid bilayer rigidity after lipid peroxidation. *FEBS lett.* **84**: 125-128.
- Dowhan, W. (1997). Molecular basis for membrane phospholipid diversity: why are there so many lipids? *Ann. Rev. Biochem.* **66**: 199-232.
- Drummen, G. P., Gadella, B. M., Post, J. A., Brouwers, J. F. (2004). Mass spectrometric characterization of the oxidation of the fluorescent lipid peroxidation reporter molecule C11-BODIPY(581/591). *Free Rad. Biol. Med.* **36**: 1635-1644.
- Dwyer, S. C., Legendre, L., Low, P. S., Leto, T. L. (1996). Plant and human neutrophil oxidative burst complexes contain immunologically related proteins. *Biochim. Biophys. Acta.* **1289**: 231-237.
- Ebel, J., Mithofer, A. (2001). Early events in the elicitation of plant defence. *Planta* **206**: 335-348.
- Egea-Cortines, M., Saedler, H., Sommer, H. (1999). Ternary complex formation between the MADS-box proteins SQUAMOSA, DEFICIENS and GLOBOSA is involved in the control of floral architecture in *Antirrhinum majus*. *EMBO J.* **18**: 5370-5379.
- Eisinger, J., Flores, J., Petersen, W. P. (1986). A milling crowd model for local and long-range obstructed lateral diffusion. Mobility of excimeric probes in the membrane of intact erythrocytes. *Biophys. J.* **49**: 987-1001.
- Elangovan, M., Day, R. N., Periasamy, A. (2002). Nanosecond fluorescence resonance energy transfer-fluorescence lifetime imaging microscopy to localize the protein interactions in a single living cell. *J. Microsc.* **205**: 3-14.
- Engel, R. (2005). *Dictyostelium* chemotaxis studied with fluorescence fluctuation spectroscopy. Ph.D. Thesis: Wageningen University.
- Evanko, D. S., Haydon, P. G. (2005). Elimination of environmental sensitivity in a cameleon FRET-based calcium sensor via replacement of the acceptor with Venus. *Cell Calcium* **37**: 341-348.
- Feijo, J. A., Moreno, N. (2004). Imaging plant cells by two-photon excitation. *Protoplasma* **223**: 1-32.
- Ferrario, S., Busscher, J., Franken, J., Gerats, T., Vandenbussche, M., Angenent, G. C., Immink, R. G. (2004). Ectopic expression of the petunia MADS box gene UNSHAVEN accelerates flowering and confers leaf-like characteristics to floral organs in a dominant-negative manner. *Plant Cell* **16**: 1490-1505.
- Filippin, L., Abad, M. C., Gastaldello, S., Magalhaes, P. J., Sandona, D., Pozzan, T. (2005). Improved strategies for the delivery of GFP-based Ca^{2+} sensors into the mitochondrial matrix. *Cell Calcium* **37**: 129-136.
- Filippov, A., Oradd, G., Lindblom, G. (2003). The effect of cholesterol on the lateral diffusion of phospholipids in oriented bilayers. *Biophys. J.* **84**: 3079-3086.
- Förster, T. (1948). Zwischenmolekulare Energiewanderung und Fluoreszenz. *Ann. Phys.* **2**: 55-75.
- Förster, T., Kasper, K. (1955). Ein Konzentrationsumschlag der Fluoreszenz. *Z. Electrochem.* **59**: 976-980.
- Friedrichsen, D. M., Joazeiro, C. A. P., Li, J. M., Hunter, T., Chory, J. (2000). Brassinosteroid-insensitive-1 is a ubiquitously expressed leucine-rich repeat receptor serine/threonine kinase. *Plant Physiol.* **123**: 1247-1255.
- Galla, H. J., Sackmann, E. (1974). Lateral diffusion in the hydrophobic region of membranes: use of pyrene excimers as optical probes. *Biochim. Biophys. Acta.* **339**: 103-105.
- Ganesan, S., Ameer-Beg, S. M., Ng, T. T., Vojnovic, B., Wouters, F. S. (2006). A dark

-
- yellow fluorescent protein (YFP)-based resonance energy-accepting chromoprotein (REACH) for Förster resonance energy transfer with GFP. *Proc. Natl. Acad. Sci. USA* **103**: 4089-4094.
- Garini, Y., Vermolen, B. J., Young, I. T. (2005). From micro to nano: recent advances in high-resolution microscopy. *Curr. Opin. Biotechnol.* **16**: 3-12.
- Geldner, N., Anders, N., Wolters, H., Keicher, J., Kornberger, W., Muller, P., Delbarre, A., Ueda, T., Nakano, A., Jurgens, G. (2003). The *Arabidopsis* GNOM ARF-GEF mediates endosomal recycling, auxin transport, and auxin-dependent plant growth. *Cell* **112**: 219-230.
- Gerritsen, H. C., De Grauw, C. J. (1999). Imaging of optically thick specimen using two-photon excitation microscopy. *Microsc. Res. Tech.* **47**: 206-209.
- González-Gaitán, M. (2003). Signal dispersal and transduction through the endocytic pathway. *Nat. Rev. Mol. Cell Biol.* **4**: 213-224.
- Göppert-Mayer, M. (1931). Über Elementarakte mit zwei Quantensprungen. *Ann. Phys.* **9**: 273-295.
- Gordon, G. W., Berry, G., Liang, X. H., Levine, B., Herman, B. (1998). Quantitative fluorescence resonance energy transfer measurements using fluorescence microscopy. *Biophys. J.* **74**: 2702-13.
- Grebe, M., Xu, J., Mobius, W., Ueda, T., Nakano, A., Geuze, H. J., Rook, M. B., Scheres, B. (2003). *Arabidopsis* sterol endocytosis involves actin-mediated trafficking via ARA6-positive early endosomes. *Curr. Biol.* **13**: 1378-1387.
- Griesbeck, O., Baird, G. S., Campbell, R. E., Zacharias, D. A., Tsien, R. Y. (2001). Reducing the environmental sensitivity of yellow fluorescent protein. Mechanism and applications. *J. Biol. Chem.* **276**: 29188-29194.
- Griesbeck, O. (2004). Fluorescent proteins as sensors for cellular functions. *Curr. Opin. Neurobiol.* **14**: 636-641.
- Griffin, B. A., Adams, S. R., Tsien, R. Y. (1998). Specific covalent labeling of recombinant protein molecules inside live cells. *Science* **281**: 269-272.
- Gruenberg, J. (2001). The endocytic pathway: a mosaic of domains. *Nat. Rev. Mol. Cell Biol.* **2**: 721-730.
- Gugel, H., Bewersdorf, J., Jakobs, S., Engelhardt, J., Storz, R., Hell, S. W. (2004). Cooperative 4Pi excitation and detection yields sevenfold sharper optical sections in live-cell microscopy. *Biophys. J.* **87**: 4146-52.
- Habuchi, S., Cotlet, M., Hofkens, J., Dirix, G., Michiels, J., Vanderleyden, J., Subramaniam, V., De Schryver, F. C. (2002). Resonance energy transfer in a calcium concentration-dependentameleon protein. *Biophys. J.* **83**: 3499-3506.
- Habuchi, S., Ando, R., Dedecker, P., Verheijen, W., Mizuno, H., Miyawaki, A., Hofkens, J. (2005). Reversible single-molecule photoswitching in the GFP-like fluorescent protein Dronpa. *Proc. Natl. Acad. Sci. USA* **102**: 9511-9516.
- Haj, F. G., Verveer, P. J., Squire, A., Neel, B. G., Bastiaens, P. I. (2002). Imaging sites of receptor dephosphorylation by PTP1B on the surface of the endoplasmic reticulum. *Science* **295**: 1708-1711.
- Hara, M., Bindokas, V., Lopez, J. P., Kaihara, K., Landa, L. R., Jr., Harbeck, M., Roe, M. W. (2004). Imaging endoplasmic reticulum calcium with a fluorescent biosensor in transgenic mice. *Am. J. Physiol. Cell Physiol.* **287**: C932-938.
- Haseloff, J., Siemering, K. R., Prasher, D. C., Hodge, S. (1997). Removal of a cryptic intron and subcellular localization of green fluorescent protein are required to mark transgenic *Arabidopsis* plants brightly. *Proc. Natl. Acad. Sci. USA* **94**: 2122-2127.
- Haugland, R. P. (1996). Handbook of Fluorescent Probes and Research Chemicals. 6th edition Molecular Probes, Inc.
- He, Z., Wang, Z. Y., Li, J., Zhu, Q., Lamb, C., Ronald, P., Chory, J. (2000). Perception of brassinosteroids by the extracellular domain of the receptor kinase BRI1. *Science* **288**: 2360-2363.
- Hecht, V., Vielle Calzada, J. P., Hartog, M. V., Schmidt, E. D. L., Boutilier, K., Grossniklaus, U., de Vries, S. C. (2001). The *Arabidopsis* SOMATIC EMBRYOGENESIS

- RECEPTOR KINASE 1 gene is expressed in developing ovules and embryos and enhances embryogenic competence in culture. *Plant Physiol.* **127**: 803-816.
- Heim, N., Griesbeck, O. (2004). Genetically encoded indicators of cellular calcium dynamics based on troponin C and green fluorescent protein. *J. Biol. Chem.* **279**: 14280-14286.
- Hell, S. W., Schrader, M., van der Voort, H. T. M. (1997). Far-field fluorescence microscopy with three-dimensional resolution in the 100-nm range. *J. Microsc.* **187**: 1-7.
- Herman, B. (1998). *Fluorescence Microscopy*. 2nd edition. New York, Springer.
- Hess, S. T., Huang, S. H., Heikal, A. A., Webb, W. W. (2002). Biological and chemical applications of fluorescence correlation spectroscopy: A review. *Biochemistry* **41**: 697-705.
- Hink, M. A., Visser, A. J. W. G. (1998). Characterization of membrane mimetic systems with fluorescence correlation spectroscopy. In: Rettig W., Strehmel B., Schrader S., editors. *Applied fluorescence in chemistry, biology and medicine*. Berlin: Springer Verlag. pp. 101-118.
- Hink, M. A., van Hoek, A., Visser, A. J. W. G. (1999). Dynamics of phospholipid molecules in micelles: Characterization with fluorescence correlation spectroscopy and time-resolved fluorescence anisotropy. *Langmuir* **15**: 992-997.
- Hink, M. A., Griep, R. A., Borst, J. W., van Hoek, A., Eppink, M. H. M., Schots, A., Visser, A. J. W. G. (2000). Structural dynamics of green fluorescent protein alone and fused with a single chain Fv protein. *J. Biol. Chem.* **275**: 17556-17560.
- Hink, M. A. (2002). *Fluorescence fluctuation spectroscopy applied to living plant cells*. Ph.D. Thesis: Wageningen University.
- Hink, M. A., Bisseling, T., Visser, A. J. (2002). Imaging protein-protein interactions in living cells. *Plant Mol. Biol.* **50**: 871-883.
- Hink, M. A., Borst, J. W., Visser, A. J. (2003a). Fluorescence correlation spectroscopy of GFP fusion proteins in living plant cells. *Methods Enzymol.* **361**: 93-112.
- Hink, M. A., Visser, N. V., Borst, J. W., van Hoek, A., Visser, A. J. W. G. (2003b). Practical use of corrected fluorescence excitation and emission spectra of fluorescent proteins in Förster resonance energy transfer (FRET) studies. *J. Fluoresc.* **13**: 185-188.
- Honma, T., Goto, K. (2001). Complexes of MADS-box proteins are sufficient to convert leaves into floral organs. *Nature* **409**: 525-529.
- Hoppe, A., Christensen, K., Swanson, J. A. (2002). Fluorescence resonance energy transfer-based stoichiometry in living cells. *Biophys. J.* **83**: 3652-3664.
- Horn, M. A., Heinstein, P. F., Low, P. S. (1989). Receptor-mediated endocytosis in plant cells. *Plant Cell* **1**: 1003-1009.
- Hsieh, R. J., Kinsella, J. E. (1989). Oxidation of PUFA's, mechanisms, products and inhibition with emphasis on fish. *Adv. Food Nutr. Res.* **33**: 233-241.
- Hyun Bae, J., Rubini, M., Jung, G., Wiegand, G., Seifert, M. H. J., Azim, M. K., Kim, J.-S., Zumbusch, A., Holak, T. A., Moroder, L., Huber, R., Budisa, N. (2003). Expansion of the genetic code enables design of a novel "gold" class of green fluorescent proteins. *J. Mol. Biol.* **328**: 1071-1081.
- Immink, R. G., Ferrario, S., Busscher-Lange, J., Kooiker, M., Busscher, M., Angenent, G. C. (2003). Analysis of the petunia MADS-box transcription factor family. *Mol. Genet. Genomics* **268**: 598-606.
- Immink, R. G., Gadella, T. W., Ferrario, S., Busscher, M., Angenent, G. C. (2002). Analysis of MADS box protein-protein interactions in living plant cells. *Proc. Natl. Acad. Sci. USA* **99**: 2416-2421.
- Jalink, K. (2006). Spying on cGMP with FRET. *Nat. Methods* **3**: 11-12.
- Jayaraman, S., Haggie, P., Wachter, R. M., Remington, S. J., Verkman, A. S. (2000). Mechanism and cellular applications of a green fluorescent protein-based halide sensor. *J. Biol. Chem.* **275**: 6047-6050.
- Jin, J. B., Bae, H., Kim, S. J., Jin, Y. H., Goh, C.-H., Kim, D. H., Lee, Y. J., Tse, Y. C., Jiang, L., Hwang, I. (2003). The *Arabidopsis* dynamin-like protein ADL1C and ADL1E play a critical role in mitochondria morphogenesis. *Plant Cell* **15**: 2357-2369.

- Jin, J. B., Kim, Y. A., Kim, S. J., Lee, S. H., Kim, D. H., Cheong, G.-W., Hwang, I. (2001). A new dynamin-like protein, ADL6, is involved in trafficking from the trans-Golgi network to the central vacuole in *Arabidopsis*. *Plant Cell* **13**: 1511-1525.
- Jiskoot, W., Visser, A. J. W. G., Herron, J. N., Sutter, M. (2005). Fluorescence spectroscopy. In: Jiskoot W. and Crommelin D. J. A., editors. *Methods for Structural Analysis of Protein Pharmaceuticals*. Arlington: AAPS Press. pp 83-131.
- Jones, D. L., Kochian, L.V., Gilroy, S. (1998). Aluminium induces a decrease in cytosolic calcium concentration in BY-2 tobacco cell cultures. *Plant Physiol.* **116**: 81-89.
- Joy, D. C., Pawley, J. B. (1992). High-resolution scanning electron microscopy. *Ultramicroscopy* **47**: 80-100.
- Jurgens, G., Geldner, N. (2002). Protein secretion in plants: from the trans-Golgi network to the outer space. *Traffic* **3**: 605-613.
- Karpova, T. S., Baumann, C. T., He, L., Wu, X., Grammer, A., Lipsky, P., Hager, G. L., McNally, J. G. (2003). Fluorescence resonance energy transfer from cyan to yellow fluorescent protein detected by acceptor photobleaching using confocal microscopy and a single laser. *J. Microsc.* **209**: 56-70.
- Keppler, L. D., Baker, C. J. (1989). (O_2^-) initiated lipid-peroxidation in a bacteria-induced hypersensitive reaction in tobacco cell-suspensions. *Phytopathology* **79**: 555-562.
- Keppler, L. D., Baker, C. J., Atkinson, M. M. (1989). Active oxygen production during a bacteria-induced hypersensitive reaction in tobacco suspension cells. *Phytopathology* **79**: 974-978.
- Kim, D. H., Eu, Y. J., Yoo, C. M., Kim, Y. W., Pih, K. T., Jin, J. B., Kim, S. J., Stenmark, H., Hwang, I. (2001). Trafficking of phosphatidylinositol 3-phosphate from the trans-Golgi network to the lumen of the central vacuole in plant cells. *Plant Cell* **13**: 287-301.
- Kitano, H. (2002). Systems biology: A brief overview. *Science* **295**: 1662-1664.
- Koenig, B., Strey, H. H., Gawrisch, K. (1997). Membrane lateral compressibility determined by NMR and X-ray diffraction: effect of acyl chain polyunsaturation. *Biophys. J.* **73**: 1954-1966.
- Koynova, R., Caffrey, M. (1998). Phases and phase transitions of phosphatidylcholines. *Biochim. Biophys. Acta.* **1376**: 91-145.
- Kuypers, F. A., van den Berg J.J., Schalkwijk, C., Roelofsen, B., Op den Kamp, J. A. (1987). Parinaric acid as a sensitive fluorescent probe for the determination of lipid peroxidation. *Biochim. Biophys. Acta.* **921**: 266-274.
- Lakowicz, J. R. (1999). *Principles of Fluorescence Spectroscopy*. 2nd edition. New York, Kluwer Academic/Plenum Publishers.
- Lamb, C., Dixon, R. A. (1997). The oxidative burst in plant disease resistance. *Annu. Rev. Plant Physiol. Plant Mol. Biol.* **48**: 251-275.
- Lasic, D. D. (1995). Applications of liposomes. In: Lipowsky R., Sackmann E., editors. *Structure and dynamics of membranes. From cells to vesicles*: Elsevier. pp 491-519.
- Lentz, B. R. (1993). Use of fluorescence probes to monitor molecular order and motions within liposome bilayers. *Chem. Phys. Lipids.* **64**: 99-116.
- Levine, A., Tenhaken, R., Dixon, R., Lamb, C. (1994). H_2O_2 from the oxidative burst orchestrates the plant hypersensitive disease resistance response. *Cell* **79**: 583-593.
- Li, J., Chory, J. (1997). A putative leucine-rich repeat receptor kinase involved in brassinosteroid signal transduction. *Cell* **90**: 929-938.
- Li, J., Wen, J., Lease, K. A., Doke, J. T., Tax, F. E., Walker, J. C. (2002). BAK1, an *Arabidopsis* LRR receptor-like protein kinase, interacts with BRI1 and modulates brassinosteroid signaling. *Cell* **110**: 213-222.
- Li, J. (2003). Brassinosteroids signal through two receptor-like kinases. *Curr. Opin. Plant Biol.* **6**: 494-499.
- Li, Y. M., Casida, J. E. (1992). Cantharidin-binding protein: identification as protein phosphatase 2A. *Proc. Natl. Acad. Sci. USA* **89**: 11867-70.
- Linsmaier, E. M., Skoog F. (1965). Organic growth factor requirements of tobacco tissue cultures. *Physiol. Plant* **18**: 100-127.

- Lippincott-Schwartz, J., Snapp, E., Kenworthy, A. (2001). Studying protein dynamics in living cells. *Nat. Rev. Mol. Cell Biol.* **2**: 444-456.
- Maiti, S., Haupts, U., Webb, W. W. (1997). Fluorescence correlation spectroscopy: Diagnostics for sparse molecules. *Proc. Natl. Acad. Sci. USA* **94**: 11753-11757.
- Mank, M., Reiff, D. F., Heim, N., Friedrich, M. W., Borst, A., Griesbeck, O. (2006). A FRET-based calcium biosensor with fast signal kinetics and high fluorescence change. *Biophys. J.* **90**: 1790-1796.
- Martin, B. R., Giepmans, B. N. G., Adams, S. R., Tsien, R. Y. (2005). Mammalian cell-based optimization of the biarsenical-binding tetracysteine motif for improved fluorescence and affinity. *Nat. Biotechnol.* **23**: 1308-1314.
- Matz, M. V., Fradkov, A. F., Labas, Y. A., Savitsky, A. P., Zaraisky, A. G., Markelov, M. L., Lukyanov, S. A. (1999). Fluorescent proteins from nonbioluminescent *Anthozoa* species. *Nat. Biotechnol.* **17**: 969-973.
- McGuire, S. O., Jameskracke, M. R., Sun, G. Y., Fritsche, K. L. (1997). An esterification protocol for cis parinaric acid determined lipid peroxidation in immune cells. *Lipids* **32**: 219-226.
- Michalet, X., Pinaud, F. F., Bentolila, L. A., Tsay, J. M., Doose, S., Li, J. J., Sundaresan, G., Wu, A. M., Gambhir, S. S., Weiss, S. (2005). Quantum dots for live cells, in vivo imaging, and diagnostics. *Science* **307**: 538-44.
- Mitchell, D. C., Litman, B. J. (1998). Molecular order and dynamics in bilayers consisting of highly polyunsaturated phospholipids. *Biophys. J.* **74**: 879-891.
- Mithofer, A., Daxberger, A., Fromhold Treu, D., Ebel, J. (1997). Involvement of an NAD(P)H oxidase in the elicitor-inducible oxidative burst of soybean. *Phytochemistry* **45**: 1101-1107.
- Miyawaki, A., Llopis, J., Heim, R., McCaffery, J. M., Adams, J. A., Ikura, M., Tsien, R. Y. (1997). Fluorescent indicators for Ca^{2+} based on green fluorescent proteins and calmodulin. *Nature* **388**: 882-887.
- Miyawaki, A., Griesbeck, O., Heim, R., Tsien, R. Y. (1999). Dynamic and quantitative Ca^{2+} measurements using improved cameleons. *Proc. Natl. Acad. Sci. USA* **96**: 2135-2140.
- Miyawaki, A., Sawano, A., Kogure, T. (2003). Lighting up cells: labelling proteins with fluorophores. *Nat. Cell Biol.* S1-S7.
- Nagai, T., Ibata, K., Park, E. S., Kubota, M., Mikoshiba, K., Miyawaki, A. (2002). A variant of yellow fluorescent protein with fast and efficient maturation for cell-biological applications. *Nat. Biotechnol.* **20**: 87-90.
- Nagai, T., Yamada, S., Tominaga, T., Ichikawa, M., Miyawaki, A. (2004). Expanded dynamic range of fluorescent indicators for Ca^{2+} by circularly permuted yellow fluorescent proteins. *Proc. Natl. Acad. Sci. USA* **101**: 10554-10559.
- Nagata, T., Nemoto, Y., Hasezawa, S. (1992). Tobacco BY-2 cell line as the "HeLa" cell in the cell biology of higher plants. *Int. Rev. Cytol.* **132**: 1-30.
- Naguib, Y. M. A. (1998). A fluorometric method for measurement of peroxyl radical scavenging activities of lipophilic antioxidants. *Anal. Biochem.* **265**: 290-298.
- Nakamura, O. (1999). Fundamental of two-photon microscopy. *Microsc. Res. Tech.* **47**: 165-171.
- Nam, K. H., Li, J. (2002). BRI1/BAK1, a receptor kinase pair mediating brassinosteroid signaling. *Cell* **110**: 203-212.
- Nikolaev, V. O., Gambaryan, S., Lohse, M. J. (2006). Fluorescent sensors for rapid monitoring of intracellular cGMP. *Nat. Methods* **3**: 23-25.
- Nougalli-Tonaco, I. A., Borst, J. W., de Vries, S. C., Angenent, G. C., Immink, R. G. (2006). *In vivo* imaging of MADS box transcription factor interactions. *J. Exp. Bot.* **57**: 33-42.
- O'Connor, D. V., Phillips, D. (1984). Time-Correlated Single Photon Counting. London, Academic Press.
- Offterdinger, M., Georget, V., Girod, A., Bastiaens, P. I. (2004). Imaging phosphorylation dynamics of the epidermal growth factor receptor. *J. Biol. Chem.* **279**: 36972-36981.

- Oja, V. V., Savchenko, G., Jakob, B., Heber, U. (1999). pH and buffer capacities of apoplastic and cytoplasmic cell compartments in leaves. *Planta* **209**: 239-249.
- Pap, E. H. W., Hanicak, A., van Hoek, A., Wirtz, K. W. A., Visser, A. J. W. G. (1995). Quantitative analysis of lipid-lipid and lipid-protein interactions in membranes by use of pyrene-labeled phosphoinositides. *Biochemistry* **34**: 9118-9125.
- Pap, E. H. W., Ketelaars, M., Borst, J. W., van Hoek, A., Visser, A. J. W. G. (1996). Reorientational properties of fluorescent analogues of the protein kinase C cofactors diacylglycerol and phorbol ester. *Biophys. Chem.* **58**: 255-266.
- Pap, E. H., Drummen, G. P., Winter, V. J., Kooij, T. W., Rijken, P., Wirtz, K. W., Op den Kamp, J. A., Hage, W. J., Post, J. A. (1999). Ratio-fluorescence microscopy of lipid oxidation in living cells using C11-BODIPY(581/591). *FEBS Lett.* **453**: 278-282.
- Pap, E. H., Drummen, G. P., Post, J. A., Rijken, P. J., Wirtz, K. W. A. (2000). Fluorescent fatty acid to monitor reactive oxygen in single cells. *Methods Enzymol.* **319**: 603-612.
- Park, M., Kim, S. J., Vitale, A., Hwang, I. (2004). Identification of the protein storage vacuole and protein targeting to the vacuole in leaf cells of three plant species. *Plant Physiol.* **134**: 625-639.
- Patterson, G. H., Lippincott-Schwartz, J. (2002). A photoactivatable GFP for selective photolabeling of proteins and cells. *Science* **297**: 1873-1877.
- Pellegrini, L., Tan, S., Richmond, T. J. (1995). Structure of serum response factor core bound to DNA. *Nature* **376**: 490-498.
- Peter, M., Ameer-Beg, S. M., Hughes, M. K., Keppler, M. D., Prag, S., Marsh, M., Vojnovic, B., Ng, T. (2005). Multiphoton-FLIM quantification of the EGFP-mRFP1 FRET pair for localization of membrane receptor-kinase interactions. *Biophys. J.* **88**: 1224-1237.
- Piston, D. W. (1999). Imaging living cells and tissues by two-photon excitation microscopy. *Trends Cell Biol.* **9**: 66-69.
- Post, J. N., Lidke, K. A., Rieger, B., Arndt-Jovin, D. J. (2005). One- and two-photon photoactivation of a paGFP-fusion protein in live *Drosophila* embryos. *FEBS Lett.* **579**: 325-330.
- Provencher, S. W. (1982). A general purpose constrained regularization program for inverting noisy linear algebraic and integral equations. *Comp. Phys. Commun.* **27**: 229-242.
- Riechmann, J. L., Meyerowitz, E. M. (1997). MADS domain proteins in plant development. *Biol. Chem.* **378**: 1079-1101.
- Rigler, R. (1995). Fluorescence correlations, single molecule detection and large number screening. Applications in biotechnology. *J. Biotechnol.* **41**: 177-186.
- Rigler, R., Elson, E. (eds) (2001). Fluorescence correlation spectroscopy. Theory and applications. Berlin, Springer.
- Rizzo, M. A., Springer, G. H., Granada, B., Piston, D. W. (2004). An improved cyan fluorescent protein variant useful for FRET. *Nat. Biotechnol.* **22**: 445-449.
- Rogers, K. R., Albert, F., Anderson, A. J. (1988). Lipid-peroxidation is a consequence of elicitor activity. *Plant Physiol.* **86**: 547-553.
- Rosell, F. I., Boxer, S. G. (2003). Polarized absorption spectra of green fluorescent protein single crystals: Transition dipole moment directions. *Biochemistry* **42**: 177-183.
- Rouser, G., Fleischer, S., Yamamoto, A. (1970). Two dimensional thin layer chromatographic separation of polar lipids and determination of phospholipids by phosphorus analysis of spots. *Lipids* **5**: 494-496.
- Russinova, E., Borst, J. W., Kwaaitaal, M., Cano-Delgado, A., Yin, Y., Chory, J., de Vries, S. C. (2004). Heterodimerization and endocytosis of *Arabidopsis* brassinosteroid receptors BRI1 and AtSERK3 (BAK1). *Plant Cell* **16**: 3216-3229.
- Rusterucci C., Stallaert V., Milat M.-L., Pugin A., Ricci P., J.-P., B. (1996). Relationship between active oxygen species, lipid peroxidation, necrosis, and phytoalexin production induced by elicitors in *Nicotiana*. *Plant Physiol.* **111**: 885-891.
- Sassaroli, M., Vauhkonen, M., Perry, D., Eisinger, J. (1990). Lateral diffusivity of lipid analogue excimeric probes in dimyristoylphosphatidylcholine bilayers. *Biophys. J.* **57**: 281-290.

- Sassaroli, M., Vauhkonen, M., Somerharju, P., Scarlata, S. (1993). Dipyrrenylphosphatidylcholines as membrane fluidity probes: Pressure and temperature dependence of the intramolecular excimer formation rate. *Biophys. J.* **64**: 137-149.
- Schwille, P., Haustein, E. (2002). Fluorescence correlation spectroscopy: A tutorial for the biophysics textbook online.
- Seifert, M. H., Ksiazek, D., Azim, M. K., Smialowski, P., Budisa, N., Holak, T. A. (2002). Slow exchange in the chromophore of a green fluorescent protein variant. *J. Am. Chem. Soc.* **124**: 7932-7942.
- Separovic, F., Gawrisch, K. (1996). Effect of unsaturation on the chain order of phosphatidylcholines in a dioleoylphosphatidylethanolamine matrix. *Biophys. J.* **71**: 274-282.
- Shah, K., Gadella, T. W., van Erp, H., Hecht, V., de Vries, S. C. (2001). Subcellular localization and oligomerization of the *Arabidopsis thaliana* somatic embryogenesis receptor kinase 1 protein. *J. Mol. Biol.* **309**: 641-655.
- Shah, K., Russinova, E., Gadella, T. W., Willemse, J., De Vries, S. C. (2002). The *Arabidopsis* kinase-associated protein phosphatase controls internalization of the somatic embryogenesis receptor kinase 1. *Genes Dev.* **16**: 1707-1720.
- Shaner, N. C., Campbell, R. E., Steinbach, P. A., Giepmans, B. N., Palmer, A. E., Tsien, R. Y. (2004). Improved monomeric red, orange and yellow fluorescent proteins derived from *Discosoma* sp. red fluorescent protein. *Nat. Biotechnol.* **22**: 1567-1572.
- Shaner, N. C., Steinbach, P. A., Tsien, R. Y. (2005). A guide to choosing fluorescent proteins. *Nat. Methods* **2**: 905-909.
- Sheen, J. (2001). Signal transduction in maize and *Arabidopsis* mesophyll protoplasts. *Plant Physiol.* **127**: 1466-1475.
- Shore, P., Sharrocks, A. D. (1995). The MADS-box family of transcription factors. *Eur. J. Biochem.* **229**: 1-13.
- Skakun, V. V., Hink, M. A., Digris, A. V., Engel, R., Novikov, E. G., Apanasovich, V. V., Visser, A. J. (2005). Global analysis of fluorescence fluctuation data. *Eur. Biophys. J.* **34**: 323-334.
- Smith, D. B., Johnson, K. S. (1988). Single-Step Purification of Polypeptides Expressed in *Escherichia-Coli* as Fusions with Glutathione S-Transferase. *Gene* **67**: 31-40.
- Sohn, E. J., Kim, E. S., Zhao, M., Kim, S. J., Kim, H., Kim, Y.-W., Lee, Y. J., Hillmer, S., Sohn, U., Jiang, L., Hwang, I. (2003). Rhal, an *Arabidopsis* Rab5 homolog, plays a critical role in the vacuolar trafficking of soluble cargo proteins. *Plant Cell* **15**: 1057-1070.
- Sorkin, A., McClure, M., Huang, F., Carter, R. (2000). Interaction of EGF receptor and grb2 in living cells visualized by fluorescence resonance energy transfer (FRET) microscopy. *Curr. Biol.* **10**: 1395-1398.
- Stanley, D. W. (1991). Biological membrane deterioration and associated quality losses in food tissues. *Crit. Rev. Food. Sci. Nutr.* **30**: 487-553.
- Stokes, G. G. (1852). On the change of refrangibility of light. . *Philos. Trans. R. Soc. London* **142**: 463-562.
- Strickler, S. J. a. R. A. B. (1962). Relationship between absorption intensity and fluorescence lifetime of molecules. *J. Chem. Phys.* **37**: 814-820
- Suhling, K., Siegel, J., Phillips, D., French, P. M. W., Lévêque-Fort, S., Webb, S. E., Davis, D. M. (2002a). Imaging the environment of green fluorescent protein. *Biophys. J.* **83**: 3589-3595.
- Suhling, K., Davis, D. M., Phillips, D. (2002b). The influence of solvent viscosity on fluorescence decay and time resolved anisotropy of green fluorescent protein. *J. Fluoresc.* **12**: 91-95.
- Suhling, K., French, P. M. W., Phillips, D. (2005). Time-resolved fluorescence microscopy. *Photochem. Photobiol. Sci.* **4**: 13-22.
- Szabo, A. (1984). Theory of fluorescence depolarization in macromolecules and membranes. *J. Chem. Phys.* **81**: 150-167.
- Takahashi, K., Isobe, M., Muto, S. (1998). Mastoparan induces an increase in cytosolic

- calcium ion concentration and subsequent activation of protein kinases in tobacco suspension culture cells. *Biochim. Biophys. Acta*. **1401**: 339-346.
- Thaler, C., Koushik, S. V., Blank, P. S., Vogel, S. S. (2005). Quantitative multiphoton spectral imaging and its use for measuring resonance energy transfer. *Biophys. J.* **89**: 2736-49.
- Thompson, N. L., Lagerholm, B. C. (1997). Total internal reflection fluorescence: Applications in cellular biophysics. *Curr. Opin. Biotechnol.* **8**: 58-64.
- Toptygin, D., Savtchenko, R. S., Meadow, N. D., Roseman, S., Brand, L. (2002). Effect of the solvent refractive index on the excited-state lifetime of a single tryptophan residue in a protein. *J. Phys. Chem. B* **106**: 3724-3734.
- Toptygin, D. (2003). Effects of the solvent refractive index and its dispersion on the radiative decay rate and extinction coefficient of a fluorescent solute. *J. Fluoresc.* **13**: 201-219.
- Tramier, M., Gautier, I., Piolot, T., Ravalet, S., Kemnitz, K., Coppey, J., Durieux, C., Mignotte, V., Coppey-Moisan, M. (2002). Picosecond-hetero-FRET microscopy to probe protein-protein interactions in live cells. *Biophys. J.* **83**: 3570-3577.
- Truong, K., Sawano, A., Mizuno, H., Hama, H., Tong, K. I., Mal, T. K., Miyawaki, A., Ikura, M. (2001). FRET-based in vivo Ca^{2+} imaging by a new calmodulin-GFP fusion molecule. *Nat. Struct. Biol.* **8**: 1069-1073.
- Tsien, R. Y. (1998). The green fluorescent protein. *Annu. Rev. Biochem.* **67**: 67509-67544.
- Ueda, T., Yamaguchi, M., Uchimiya, H., Nakano, A. (2001). Ara6, a plant-unique novel type Rab GTPase, functions in the endocytic pathway of *Arabidopsis thaliana*. *EMBO J.* **20**: 4730-4741.
- Uskova, M. A., Borst, J. W., Hink, M. A., van Hoek, A., Schots, A., Klyachko, N. L., Visser, A. J. W. G. (2000). Fluorescence dynamics of green fluorescent protein in AOT reversed micelles. *Biophys. Chem.* **87**: 73-84.
- Vaknin, A., Berg, H. C. (2004). Single-cell FRET imaging of phosphatase activity in the *Escherichia coli* chemotaxis system. *Proc. Natl. Acad. Sci. USA* **101**: 17072-17077.
- Valentin, G., Verheggen, C., Piolot, T., Neel, H., Coppey-Moisan, M., Bertrand, E. (2005). Photoconversion of YFP into a CFP-like species during acceptor photobleaching FRET experiments. *Nat. Methods* **2**: 801.
- Valeur, B. (2002). Molecular Fluorescence. Principles and Applications. Weinheim, Wiley-VCH Verlag GmbH.
- van den Berg, J. J., Op den Kamp, J. A., Lubin, B. H., Roelofsen, B., Kuypers, F. A. (1992). Kinetics and site specificity of hydroperoxide induced oxidative damage in red blood cells. *Free Rad. Biol. Med.* **12**: 487-498.
- van den Berg, P. A. W., van Hoek, A., Visser, A. J. W. G. (2004). Evidence for a novel mechanism of time-resolved flavin fluorescence depolarization in glutathione reductase. *Biophys. J.* **87**: 2577-2586.
- van der Heide, U. A., van Ginkel, G., Levine, Y. K. (1996). DPH is localised in two distinct populations in lipid vesicles. *Chem. Phys. Lett.* **253**: 118-122.
- van der Meer, B. W. (2002). Kappa-squared: from nuisance to new sense. *J. Biotechnol.* **82**: 181-196.
- van der Meer, B. W., Pottel, H., Herreman, W., Ameloot, M., Hendrickx, H., Schröder, H. (1984). Effect of orientational order on the decay of the fluorescence anisotropy in membrane suspensions. *Biophys. J.* **46**: 515-523.
- van Gestelen, P., Ledeganck, P., Wynant, I., Caubergs, R.J., Asard, H. (1998). The cantharidin-induced oxidative burst in tobacco BY-2 cell suspension cultures. *Protoplasma* **205**: 83-92.
- van Hoek, A., Visser, A. J. W. G. (1985). Artefact and distortion sources in time correlated single photon counting. *Anal. Instrum.* **14**: 359-378.
- van Hoek, A., Vos, K., Visser, A. J. W. G. (1987). Ultrasensitive time-resolved polarized fluorescence spectroscopy as a tool in biology and medicine. *IEEE J. Quant. Electr.* **QE-23**: 1812-1820.
- Varadi, A., Rutter, G. A. (2002). Green fluorescent protein calcium biosensors. Calcium

- imaging with GFP cameleons. *Methods Mol. Biol.* **183**: 255-264.
- Vauhkonen, M., Sassaroli, M., Somerharju, P., Eisinger, J. (1989). Lateral diffusion of phospholipids in the lipid surface of human low-density lipoprotein measured with a pyrenyl phospholipid probe. *Eur. J. Biochem.* **186**: 465-471.
- Vauhkonen, M., Sassaroli, M., Somerharju, P., Eisinger, J. (1990). Dipyrrenylphosphatidylcholines as membrane fluidity probes. Relationship between intramolecular and intermolecular excimer formation rates. *Biophys. J.* **57**: 291-300.
- Verkhusha, V. V., Lukyanov, K. A. (2004). The molecular properties and applications of Anthozoa fluorescent proteins and chromoproteins. *Nat. Biotechnol.* **22**: 289-96.
- Verveer, P. J., Wouters, F. S., Reynolds, A. R., Bastiaens, P. I. H. (2000). Quantitative imaging of lateral ErbB1 receptor signal propagation in the plasma membrane. *Science* **290**: 1567-1570.
- Vigo-Pelfrey, C., Nguyen, N. (1991). Modulation of lipid peroxidation of liposomes and micelles by antioxidants and chelating agents. In: Vigo-Pelfrey C., editor. *Membrane Lipid Oxidation*. CRC Press, Boca Raton. p pp 135-149.
- Visser, N. V., Hink, M. A., Borst, J. W., van der Krogt, G. N. M., Visser, A. J. W. G. (2002). Circular dichroism spectroscopy of fluorescent proteins. *FEBS Lett.* **521**: 31-35.
- Visser, N. V., Borst, J. W., Hink, M. A., van Hoek, A., Visser, A. J. W. G. (2005). Direct observation of resonance tryptophan-to-chromophore energy transfer in visible fluorescent proteins. *Biophys. Chem.* **116**: 207-212.
- Volkmer, A., Subramaniam, V., Birch, D. J. S., Jovin, T. M. (2000). One- and two-photon excited fluorescence lifetimes and anisotropy decay of green fluorescent proteins. *Biophys. J.* **78**: 1589-1598.
- Vos, K., van Hoek, A., Visser, A. J. W. G. (1987). Application of a reference deconvolution method to tryptophan fluorescence in proteins. A refined description of rotational dynamics. *Eur. J. Biochem.* **165**: 55-63.
- Voss, T. C., Demarco, I. A., Day, R. N. (2005). Quantitative imaging of protein interactions in the cell nucleus. *Biotechniques* **38**: 413-424.
- Wallrabe, H., Elangovan, M., Burchard, A., Periasamy, A., Barroso, M. (2003). Confocal FRET microscopy to measure clustering of ligand-receptor complexes in endocytic membranes. *Biophys. J.* **85**: 559-571.
- Wang, Z. Y., Seto, H., Fujioka, S., Yoshida, S., Chory, J. (2001). BRI1 is a critical component of a plasma-membrane receptor for plant steroids. *Nature* **410**: 380-383.
- Wiley, H. S. (2003). Trafficking of the ErbB receptors and its influence on signaling. *Exp. Cell Res.* **284**: 78-88.
- Wouters, F. S., Bastiaens, P. I. (1999). Fluorescence lifetime imaging of receptor tyrosine kinase activity in cells. *Curr. Biol.* **9**: 1127-1130.
- Wouters, F. S., Verveer, P. J., Bastiaens, P. I. H. (2001). Imaging biochemistry inside cells. *Trends Cell Biol.* **11**: 203-211.
- Wysocka-Diller, J. W., Helariutta, Y., Fukaki, H., Malamy, J. E., Benfey, P. N. (2000). Molecular analysis of SCARECROW function reveals a radial patterning mechanism common to root and shoot. *Development* **127**: 595-603.
- Xia, Z. P., Liu, Y. H. (2001). Reliable and global measurement of fluorescence resonance energy transfer using fluorescence microscopes. *Biophys. J.* **81**: 2395-2402.
- Xu, X., Gerard, A. L., Huang, B. C., Anderson, D. C., Payan, D. G., Luo, Y. (1998). Detection of programmed cell death using fluorescence energy transfer. *Nucleic Acids Res.* **26**: 2034-2035.
- Yin, Y., Wu, D., Chory, J. (2002). Plant receptor kinases: systemin receptor identified. *Proc. Natl. Acad. Sci. USA* **99**: 9090-9092.
- Zacharias, D. A., Violin, J. D., Newton, A. C., Tsien, R. Y. (2002). Partitioning of lipid-modified monomeric GFPs into membrane microdomains of live cells. *Science* **296**: 913-916.
- Zhang, J., Campbell, R. E., Ting, A. Y., Tsien, R. Y. (2002). Creating new fluorescent probes for cell biology. *Nat. Rev. Mol. Cell Biol.* **3**: 906-918.
- Zipfel, W. R., Williams, R. M., Webb, W. W. (2003). Nonlinear magic: multiphoton microscopy in the biosciences. *Nat. Biotechnol.* **21**: 1368-1376.

Nederlandse Samenvatting

Een levende cel bestaat uit een ingewikkeld netwerk van moleculen. Om meer inzicht te krijgen in het reageren van levende cellen op externe stimuli hebben we informatie nodig waar en wanneer in de cel die netwerken worden geactiveerd. Hoe die moleculen van het netwerk onderling met elkaar communiceren is één van de grootste uitdagingen van hedendaags celbiologisch onderzoek. Voor het functioneren van een cel zijn processen zoals het ontvangen en uitwisselen van stoffen en signalen met zijn omgeving essentieel. In levende cellen vinden deze processen vaak plaats door het aangaan van eiwit-eiwit interacties of door binding van liganden aan membraan receptoren. De samenwerking van eiwitmoleculen in de cel kan op verschillende manieren onderzocht worden. Enkele voorbeelden van biochemische en moleculair biologische technieken die hiervoor gebruikt worden zijn DNA sequentie analyse, hybride gist experimenten, eiwit chromatografie, massaspectrometrie of toepassingen van DNA/eiwit arrays. Bioinformatica methoden hebben eveneens hun diensten bewezen in de onderzoeksgebieden genomics en proteomics. Hoewel al deze technieken en methoden waardevolle informatie opleveren, geven ze geen informatie over hoe het bio-moleculaire netwerk in de levende cel opereert. Daarom zijn er verschillende microspectroscopische technieken, gebaseerd op fluorescentie, ontwikkeld om deze informatie aan te dragen. Microspectroscopie kan het best worden omschreven als de combinatie van fluorescentie spectroscopie met microscopie. Met microspectroscopie kunnen moleculen zichtbaar gemaakt worden in de cel. Tegelijkertijd kunnen fysische parameters worden verkregen, die iets zeggen over de toestand waarin een cel verkeert. Zo kunnen bijvoorbeeld de zuurgraad, afstanden tussen moleculen, moleculaire bewegelijkheid of lokale calciumconcentraties worden bepaald. Fluorescentie is het sleutelwoord in dit proefschrift en het principe werkt als volgt. Wanneer een aromatisch molecuul licht opneemt, kan het molecuul in een aangeslagen toestand van hogere energie terecht komen. Het molecuul wil het liefst van deze energie af en kan bijvoorbeeld naar het laagste energienivo terugvallen door licht (fluorescentie) uit te zenden. Met behulp van fluorescentie kunnen eiwitten die van belang zijn voor een bepaald proces zichtbaar gemaakt worden in levende cellen. Er zijn talloze fluorescente indicatoren gesynthetiseerd, die zijn ontworpen om specifieke cellulaire processen te observeren. Er zijn ook fluorescente indicatoren die in de natuur voorkomen. In het begin van de jaren negentig is een eiwit uit een bepaalde kwal geïsoleerd, dat groene fluorescentie vertoont. Dit is het bekende groen fluorescerende eiwit (in het Engels: Green Fluorescent Protein of GFP). In de celbiologie wordt zeer veel gebruik gemaakt van de GFP technologie, omdat het eiwit in verschillende celsystemen tot expressie gebracht kan worden. Daarbij produceert de cel zelf deze groen fluorescerende eiwitten, die genetisch gekoppeld kunnen worden aan een te bestuderen eiwit. Inmiddels zijn er allerlei eiwitten met verschillende kleuren fluorescentie beschikbaar (ook geïsoleerd uit koraal), die veelal ook voor FRET experimenten (zie later) gebruikt kunnen worden. Eén van de meest gebruikte FRET paren is cyaan fluorescerend eiwit (donor) en geel fluorescerend eiwit (acceptor).

De afmetingen van eiwitten en eiwitcomplexen liggen in de orde van grootte van 5 tot 50 nm. Deze moleculen kunnen afgebeeld worden met behulp van bijvoorbeeld electronenmicroscopie. Deze techniek heeft een ruimtelijke resolutie van enkele nanometers

(1 nanometer is 1 miljardste meter). Conventionele lichtmicroscopie daarentegen heeft een ruimtelijk oplossend vermogen van enkele honderden nanometers, veel groter dan de afmetingen van eiwitcomplexen. Echter voor elektronenmicroscopie moet het te bestuderen object speciaal geprepareerd worden en kunnen dynamische processen in de cel met deze techniek niet gevolgd worden. Daarom heeft lichtmicroscopie en in het bijzonder fluorescentiemicroscopie een groot voordeel boven elektronenmicroscopie, omdat fluorescente moleculen in levende cellen op de voet kunnen worden gevolgd. In dit proefschrift worden verschillende microspectroscopische toepassingen beschreven om kwantitatieve informatie over bio-moleculaire netwerken te verkrijgen. Het onderzoek heeft zich zowel op biochemische model systemen als op levende plantencellen gericht.

Na een algemene inleiding (Hoofdstuk 1) worden in de volgende twee hoofdstukken van dit proefschrift de effecten van oxidatie van onverzadigde lipidemoleculen zowel in kunstmatige membraan systemen (Hoofdstuk 2) als in levende plantencellen beschreven (Hoofdstuk 3). Een levende cel wordt omgeven door een wand van fosfolipide-membranen, die bestaan uit polaire kopgroepen en apolaire vetzuurketens. Oxidatie van de onverzadigde vetzuurketens in deze lipiden heeft een groot effect op membraaneigenschappen hetgeen grote gevolgen heeft voor allerlei cellulaire processen. Oxidatie-experimenten, uitgevoerd met een van kleur verschietende fluorescente indicator die is opgenomen in bolvormige membraanvesicles, wijzen uit dat hoe hoger de onverzadigingsgraad in de vesicles is, hoe sneller het oxidatieproces plaatsvindt. Een verklaring voor deze waarneming is, dat de membraanstructuur verandert als gevolg van de onverzadigingsgraad. Wanneer de onverzadigingsgraad hoog is, wordt de pakking van de lipidemoleculen minder dicht. Hierdoor wordt de afstand tussen de kopgroepen groter, zodat de toegankelijkheid van de oxidant voor de onverzadigde vetzuurketens gemakkelijker is. Dit verklaart de snellere oxidatie. Ook de vloeibaarheid van de membraan is onderzocht met andere, specifieke fluorescente indicatoren. Oxidatie van onverzadigde vetzuurketens leidt tot een meer rigide membraanstructuur, doordat de vetzuurketens verzadigd worden en de lipidepakking dichter wordt.

Het oxidatieonderzoek is ook uitgevoerd in levende plantencellen. Plantencellen hebben een verdedigingsmechanisme om zich te verweren tegen pathogene moleculen en andere indringers. Eén van de reacties die volgen op het indringen van vreemde moleculen is de productie van reactieve zuurstof moleculen. Lipideoxidatie in plantencellen is gevolgd met behulp van dezelfde fluorescente indicator als gebruikt voor de kunstmatige membranen. Een opmerkelijke waarneming is de veel lagere oxidatiesnelheid dan eerder gerapporteerd voor dierlijke cellen. Deze lagere oxidatiesnelheid kan worden veroorzaakt door een verschil in lipide-samenstelling van dierlijke en plant membranen. Ook kunnen in plantencellen andere enzymsystemen worden geactiveerd, die mogelijk de lagere oxidatiesnelheden kunnen verklaren.

In Hoofdstukken 4 en 5 staat de technische ontwikkeling van de combinatie van fluorescentie microscopie met spectroscopie centraal. Het succes van deze ontwikkeling wordt geïllustreerd met een tweetal voorbeelden van eiwit-eiwit interacties in plantencellen. Doordat specifieke eiwitten gekoppeld met fluorescente eiwitten in levend plantenweefsel kunnen worden geobserveerd, krijgt men een beter inzicht in signaaltransductie routes. Plantenweefsel bestaat echter uit materialen van hoge brekingsindex (bijvoorbeeld de

celwand), die veel licht kunnen verstrooien. Om deze fluorescente eiwitten toch zichtbaar te maken is gebruik gemaakt van een infrarood laser. Er zijn twee belangrijke voordelen van het gebruik dit type laser aan te voeren. We kunnen nu fluorescente moleculen ook exciteren met twee fotonen infrarood licht (two-photon excitation), mits die op precies dezelfde tijd en plaats het molecuul bereiken. Verder wordt infrarood licht in weefsels veel minder verstrooid dan zichtbaar en ultraviolet licht. Met behulp van deze laser is het dus mogelijk om licht dieper in de weefsels te laten binnendringen. Zo kunnen dieper liggende (fluorescente) eiwitten met twee fotonen worden geëxciteerd en hun fluorescentie met een conventionele optische microscoop worden gemeten.

Omdat de twee-foton excitatie laser het licht afgeeft in de vorm van zich repeterende, korte lichtpulsjes (200 femtoseconden; 1 femtoseconde is een miljoenste van een miljardste seconde), kunnen ook fluorescentie levensduren worden gemeten. De fluorescentie levensduur kan worden omschreven als de gemiddelde tijd die een molecuul nodig heeft om van een aangeslagen toestand naar de grondtoestand te gaan onder uitzending van fluorescentie fotonen. De fluorescentie levensduur is afhankelijk van de moleculaire omgeving. Voor het meten van fluorescentie levensduren kunnen de monsters zowel in cuvetten als op coverslips van een microscoop worden geplaatst. In beide gevallen wordt met gevoelige detectietechnieken ('single photon timing') de fluorescentie intensiteit direct als functie van de tijd bepaald. In geval van microscopie wordt de techniek fluorescentie levensduur microscopie genoemd. In het Engels spreken we van FLIM, dat een acronym is voor Fluorescence Lifetime IMaging of Fluorescence Lifetime Imaging Microscopy. FLIM heeft de meerwaarde dat fluorescentie levensduren ruimtelijk kunnen worden gemeten met de resolutie van een lichtmicroscoop.

FLIM wordt vaak in combinatie met FRET toegepast en wordt dan aangeduid als FRET-FLIM. FRET is een acronym voor Fluorescence Resonance Energy Transfer. Het is het proces waarbij een aangeslagen donor molecuul de energie stralingsloos afgeeft aan een acceptor molecuul. Theodor Förster heeft ongeveer 60 jaar geleden dit proces kwantitatief beschreven. De wisselwerking tussen donor en acceptor moleculen berust op zwakke dipool-dipool interacties, die merkbaar zijn wanneer de moleculen dicht in elkaars buurt zijn (afstand: enkele nanometers). Wanneer FRET optreedt wordt de fluorescentie levensduur van de donor korter. Met FRET-FLIM metingen kunnen eiwit-eiwit interacties in levende cellen worden aangetoond, omdat het proces van energieoverdracht alleen kan plaatsvinden, wanneer de afstand tussen donor en acceptor moleculen enkele nanometers bedraagt. Het ene eiwit wordt dan genetisch uitgerust met een donor (b.v. cyaan) fluorescerend eiwit en het andere eiwit met een acceptor (b.v. geel) fluorescerend eiwit.

In Hoofdstukken 4 en 5 worden twee voorbeelden besproken waarmee eiwit-eiwit interacties in een cel bepaald kunnen worden met behulp van FRET-FLIM. De beperking van de ruimtelijke resolutie van optische microscopie wordt doorbroken door gebruik te maken van FRET omdat dit proces nanometer resolutie heeft. In Hoofdstuk 4 wordt een studie beschreven van interacties tussen transcriptiefactoren (FLORAL BINDING PROTEINS (FBP)) in plantencellen. Er was al eerder aangetoond in hybride gist experimenten dat verscheidende transcriptiefactoren een interactie met elkaar aangingen. Twee van die FBP's gaven echter een negatief resultaat in gist. Met FRET-FLIM metingen kon juist wel een specifieke interactie in plantencellen worden aangetoond. FRET-FLIM metingen *in vivo*

bieden dus belangrijke voordelen boven klassieke *in vitro* methoden. In Hoofdstuk 5 wordt een FRET-FLIM studie gepresenteerd waarbij de dimeervorming (homogeen of heterogeen) van membraanreceptoren betrokken bij somatische embryogenese centraal staat. Deze dimeervorming blijkt op specifieke plaatsen aan het celmembraan plaats te vinden, hetgeen het startsein kan zijn voor het aanschakelen van bepaalde signaaltransductie routes.

In Hoofdstuk 6 zijn verschillende GFP varianten in detail bestudeerd met tijdopgeloste fluorescentie. In deze experimenten is het effect van de lokale omgeving op de fluorescentie levensduur van cyaan en geel fluorescerende eiwitten onderzocht. Wanneer de fluorescente eiwitten zich in een medium met hoge brekingsindex bevinden neemt de fluorescentie levensduur af. Het meten van fluorescentie levensduren van gezuiverde eiwitten in een goed gedefinieerde omgeving levert informatie op die gebruikt kan worden bij *in vivo* experimenten.

In Hoofdstuk 7 worden tijdopgeloste fluorescentie experimenten aan een speciale GFP combinatie, de cameleon, beschreven. De cameleon is een FRET sensor die in staat is intracellulaire calcium concentraties te meten. De sensor bestaat uit een cyaan fluorescerend eiwit en een geel fluorescerend eiwit, die zijn verbonden door een schakeleiwit, dat in staat is calcium moleculen te binden en van structuur te veranderen. Bij binding van calcium aan de sensor neemt de mate van energieoverdracht van donor naar acceptor sterk toe. De toename is evenredig met de lokale calcium concentratie. De fluorescentie van de sensor verschiet dus van kleur als calcium bindt, vandaar de bijnaam cameleon. In dit onderzoek is voor de eerste keer opgehelderd hoe het donoreiwit ten opzichte van het acceptoreiwit is georiënteerd. Dit is gedaan met experimenten, die FRET met gepolariseerde fluorescentie combineren.

De resultaten die zijn beschreven in dit proefschrift geven een goed inzicht hoe microspectroscopie gebruikt kan worden. Dit onderzoek toont eveneens aan dat cellulaire biochemie een toegevoegde waarde krijgt door celbiologische en biofysische technieken te combineren. Dankzij deze multidisciplinaire aanpak wordt het inzicht in signaaltransductie routes vergroot.

List of Abbreviations

APB	Acceptor photobleaching
AtSERK	<i>Arabidopsis thaliana</i> Somatic Embryogenesis Receptor Kinase
BAK1	Bri1-Associated Receptor Kinase 1
BCU	Beam-conditioning unit
BP-C11	4,4-difluoro-5-(4-phenyl-1,3-butadienyl)-4-bora-3a,4a-diaza-s-indacene-3-undecanoic acid: BP-C11
BRI1	Brassinosteroid Insensitive 1
BR	Brassinosteroid
BY2	Bright Yellow 2 tobacco cell
CFP	Cyan Fluorescent Protein
DiPyr ₄ -PC	1,2-bis-(1-pyrenebutanoyl) -sn-glycero-3-phosphocholine
DiPyr ₁₀ -PC	1,2-bis-(1-pyrenedecanoyl) -sn-glycero-3-phosphocholine
DMPC	1,2-dimyristoyl-sn-glycero-3-phosphocholine
DOPC	1,2-dioleoyl-sn-glycero-3-phosphocholine
DPH-HPC	2-(3-(diphenylhexatrienyl)propanoyl)-1-hexadecanoyl-sn-glycero-3-phosphocholine
E/M	Excimer and monomer fluorescence intensity ratio's
FRET	Förster (Fluorescence) Resonance Energy Transfer
FLIM	Fluorescence Lifetime Imaging Microscopy
FCS	Fluorescence Correlation Spectroscopy
FBP	Floral Binding Protein
FRAP	Fluorescence Recovery After Photobleaching
FWHM	Full with half maximum
GFP	Green Fluorescent Protein
H ₂ O ₂	Hydrogenperoxide
K _{AP} P	Kinase Associated Protein Phosphatase
LRR	Leucine Rich Repeat
MonoPyr ₁₀ -HPC	1-hexadecanoyl-2-(1-pyrenedecanoyl)-sn-glycero-3-phosphocholine
OPE	One Photon Excitation
PA-GFP	Photo-Activatable GFP
PBS	Phosphate Buffered Saline
PC	sn-glycero-3-phosphocholine
PMT	Photo Multiplier Tube
ROI	Regions Of Interest
ROS	Reactive Oxygen Species
RFP	Red Fluorescent Protein
RLK	Receptor-Like Kinase
SAPC	1-stearoyl-2-arachidonoyl- sn-glycero-3-phosphocholine
SUV's	Small Unilamellar Vesicles
TIR	Total Internal Reflection
TPE	Two-Photon Excitation
TRFA	Time-Resolved Fluorescence Anisotropy
TCSPC	Time-Correlated Single Photon Counting
VFP	Visible Fluorescent Protein
YFP	Yellow Fluorescent Protein
YC3.60	Yellow Cameleon 3.60

Dankwoord

Vanuit de kuip, dobberend op de Waddenzee, geniet ik van de ondergaande zon en het feit dat het grootste gedeelte van mijn proefschrift af is. Iedereen die een proefschrift geschreven heeft, weet dat zoiets niet vanzelf tot stand komt, maar dat daar vaak verschillende mensen aan meegewerkt hebben.

Het was september 1991 toen ik bij Ton Visser als analist op een KWF project werd aangesteld. Ton, vanaf het eerste moment dat we samenwerken heb je me op een onafhankelijke wijze de wereld van de fluorescentie MicroSpectroscopie weten bij te brengen. Toen ik eind 1995 gedwongen was de leerstoelgroep te verlaten, memoreerde je in je afscheidsspeech over een hopelijk snelle terugkomst welke 2 jaar later gerealiseerd werd. Toen wist ik nog niet dat dit het begin van mijn promotieonderzoek zou zijn. Je vermogen om de juiste mensen om je heen te plaatsen en de interesse voor de wetenschap aan jonge onderzoekers over te brengen, is van wereldklasse. Ik ben je zeer dankbaar voor de jarenlange prettige samenwerking en ik ben er trots op onder jouw vleugels te promoveren. Ik hoop nog jaren met je samen te werken en nog mooie publicaties te schrijven. Ook Sacco de Vries wil ik graag bedanken voor de mogelijkheid die hij mij geboden heeft om te promoveren. Ik hoop op een prettige samenwerking die nog vele jaren mag duren.

My companion during the EU project was Nina Visser. Nina, thanks for all your contributions in several papers including the figures in chapter 1. I am sure that our friendship will last forever. Verder wil ik mijn maatje, Arie van Hoek, uit de kelder ook niet ongenoemd laten. Arie, wij bestieren het MSC nu een aantal jaren en die samenwerking nam in sterke mate toe toen we het 'NWO-Groot' project invulling moesten geven. Ik heb in een zeer korte periode enorm veel van je geleerd en het resultaat in 'the Orange room' mag er wezen. Verscheidene jaren was ook Mark Hink het gezicht van het MSC. Helaas heeft onze samenwerking vanaf jou promotie maar 3.5 jaar mogen duren. Gelukkig heb je in Dortmund een nieuwe uitdagende werkplek gevonden. Mark, aan jouw spectroscopische kennis heb ik veel steun gehad en je wordt in het MSC erg gemist. Verder is Boudewijn van Veen ook één van de aanspreekpunten binnen het MSC. Boudewijn, bedankt voor de prettige samenwerking en de hulp bij de layout van dit boekje.

Andere direct betrokken collega's Ruchira, Adrie, Sergey, Rodrigo, Jose, Sanne, en Carlo wil ik graag bedanken voor de prettige samenwerking en stimulerende werkbesprekingen. Ook wil ik Laura van Egmond niet onvermeld laten. Laura, bedankt voor al je han en span diensten en af en toe een gezellig praatje. Mijn kamergenoot Willy wil ik bedanken voor alle wetenschappelijke en niet wetenschappelijke discussies. Daarnaast wil ik alle collega's en oud-collega's van de leerstoelgroep Biochemie die ik niet persoonlijk genoemd heb, bedanken voor een goede sfeer op de werkvloer.

Furthermore I would like to thank Jenny Russinova, Isabella Nougalli-Tonaco and Richard Immink for the fruitful collaborations. The FRET-FLIM data gave us new insights in protein-protein interactions in plant cells, which resulted in interesting papers. Verder heb ik de afgelopen jaren verschillende studenten op diverse projecten mogen begeleiden. Marsha, Olga, Nicoline, Maarten en Johanna, ik ben jullie erg dankbaar voor al het werk wat jullie hebben verricht. Het MSC versterkt de samenwerking tussen celbiologen en biofysici. Ik heb

met veel collega's leuke boeiende projecten kunnen initiëren welke geresulteerd hebben in diverse publicaties. Ik wil iedereen met wie ik heb samengewerkt, hartelijk danken.

Dit proefschrift is mede tot stand gekomen door de steun van mijn familie. Pa, Ma, Bas en Marion, jullie bijdrage in welke vorm dan ook is van grote waarde geweest. Jullie waren en zijn nog steeds een uitstekend klankbord om mijn wetenschappelijke inzicht in een breder perspectief te plaatsen. Mam, dat ik een van je schilderijen heb mogen gebruiken als omslag maakt het proefschrift helemaal compleet. Frits en Bas, fijn dat jullie mijn paranimfen willen zijn.

Als laatste wil ik mijn gezin in het zonnetje zetten. Tanja, zonder jouw onvoorwaardelijke steun had ik deze promotie niet kunnen realiseren. Door je vreugdevolle levenswijze en het altijd klaar staan voor iedereen, heb je voor mij en ons gezin een solide thuisbasis gevormd. Jij bent samen met Anne en Thomas een grote inspiratiebron en zonder jullie liefde was dit boekje niet tot stand gekomen.

A handwritten signature consisting of the letters 'J' and 'W' in a cursive, stylized font.

Curriculum Vitae

Jan Willem Borst werd op 18 april 1966 geboren te Renkum. Zijn HAVO diploma behaalde hij in 1985 aan de Rijksscholengemeenschap te Amersfoort. Vervolgens volgde hij de studie voor laborant aan de Internationale Hogeschool Larenstein te Wageningen. Tijdens deze studie voerde hij een stage uit bij het ATO Wageningen onder de begeleiding van Dr. P. Klaassen. Vervolgens werd een afstudeervak bij de vakgroep Biochemie aan de Landbouwniversiteit Wageningen onder de begeleiding van Dr Ir I.M.C.M Rietjens voltooid. In juni 1991 studeerde hij af en in september van dat jaar kreeg hij een aanstelling als analist bij de vakgroep Biochemie aan de Landbouwniversiteit Wageningen. Dit project werd gesubsidieerd door het Koningin Wilhelmina Fonds (KWF) en stond onder de supervisie van Dr Ir P.I.H. Bastiaens en Dr A.J.W.G. Visser. In 1996 kreeg hij een aanstelling als analist in de groep van Dr. M.H.T. Timmers bij de vakgroep Fysiologische Chemie aan de Universiteit van Utrecht. In november 1997 keerde hij terug naar de vakgroep Biochemie van de Landbouwniversiteit Wageningen. Op een EU-FAIR project in de groep van Dr A.J.W.G. Visser bestudeerde hij de rol van lipidenoxidatie op onverzadigde vetzuren met behulp van spectroscopische technieken. In januari 1999 werden de werkzaamheden voortgezet op een project Stichting Technische Wetenschappen (STW) aan de leerstoelgroep Biochemie van de Wageningen Universiteit in samenwerking met het Laboratorium voor Monoklonale Antilichamen (LMA) onder begeleiding van Prof Dr A.J.W.G. Visser en Dr Ir A. Schots. In december 2001 kreeg hij een vaste aanstelling bij de leerstoelgroep Biochemie in het MicroSpectroscopisch Centrum aan de Wageningen Universiteit. Hij heeft geavanceerde microspectroscopische apparatuur opgezet, welke was gefinancierd uit een NWO-Groot subsidie. De resultaten van de afgelopen 6 jaar onderzoek hebben geleid tot dit proefschrift. Hij vervolgt zijn werkzaamheden bij de leerstoelgroep Biochemie in het MicroSpectroscopisch Centrum aan de Wageningen Universiteit met het toepassen van microspectroscopische technieken in biologisch onderzoek.

List of Publications

Aker, J., Borst, J.W., Karlova, R., S. C. de Vries. (2006) The *Arabidopsis thaliana* AAA protein CDC48A interacts *in vivo* with the somatic embryogenesis receptor-like kinase 1 receptor at the plasma membrane. *J. Struct. Biol.* (in press)

Westphal, A.H., Matorin, A., Hink, M.A., Borst, J.W., van Berkel, W.J., Visser, A.J. (2006) Real-time enzyme dynamics illustrated with fluorescence spectroscopy of p-hydroxybenzoate hydroxylase. *J. Biol. Chem.* **281**: 11074-11081

Borst, J.W., Laptinok, S., Westphal, A.H., Visser, N.V., Aker, J., Hink, M.A., van Hoek, A., Visser, A.J.W.G. Polarized resonance energy transfer spectroscopy reveals both distance and orientation of calcium sensor YC3.60 (submitted)

Borst, J.W., Nougalli-Tonaco, I., Hink, M.A., van Hoek, A., Immink, R.G.H., Visser, A.J.W.G. Protein-Protein Interactions *In Vivo*: Use of Biosensors Based on FRET. Reviews in Fluorescence 2006. Geddes, C. D. and Lakowicz, J. R., Eds. Kluwer Academic/Plenum Publishers. New York pp 341-355.

Companjen, A.R., Florack, D.E.A., Slootweg, T., Borst, J.W., Rombout, J.H.W.M. (2006) Improved uptake of plant derived LTB-linked proteins in carp gut and induction of specific humoral immune responses upon infeed delivery. *Fish Shellfish Immunol.* **21**: 251-260

Vaganova, E., Yitzchaik, S., Sigalov, M., Borst, J.W., Visser, A.J., Ovadia, H., Khodorkovsky, V. (2005) Time-resolved emission upon two-photon excitation of bis-N-carbazolyl-distyrylbenzene: mapping of water molecule distribution in the mouse brain. *New J. Chem.* **29**: 1044-1048

Nougalli-Tonaco, I.A., Borst, J.W., de Vries, S. C., Angenent, G. C., Immink, R.G. (2005) *In vivo* imaging of MADS-box transcription factor interactions. *J. Exp. Bot.* **57**: 33-42

Visser, N.V., Borst, J.W., Hink, M.A., van Hoek, A., Visser, A.J. (2005) Direct observation of resonance tryptophan-to-chromophore energy transfer in visible fluorescent proteins. *Biophys. Chem.* **116**: 207-212.

Borst, J.W., Hink, M.A., van Hoek, A. Visser, A.J. (2005) Effects of refractive index and viscosity on fluorescence and anisotropy decays of enhanced cyan and yellow fluorescent proteins. *J. Fluoresc.* **15**: 153-160.

Snippe, M., Borst, J.W., Goldbach, R., Kormelink, R. (2005) The use of fluorescence microscopy to visualise homotypic interactions of tomato spotted wilt virus nucleocapsid protein in living cells. *J. Virol. Methods.* **125**: 15-22.

Bhat, R.A., Borst, J.W., Riehl, M., Thompson, R.D. (2004) Interaction of maize Opaque-2 and the transcriptional co-activators GCN5 and ADA2, in the modulation of transcriptional activity. *Plant Mol Biol.* **55**: 239-252.

Rienties, I.M., Vink, J., Borst, J.W., Russinova, E., de Vries, S.C. (2005) The *Arabidopsis* SERK1 protein interacts with the AAA-ATPase AtCDC48, the 14-3-3 protein GF14lambda and the PP2C phosphatase KAPP. *Planta*. **221**: 394-405.

Pouwels, J., van der Velden, T., Willemse, J., Borst, J.W., van Lent, J., Bisseling, T., Wellink, J. (2004) Studies on the origin and structure of tubules made by the movement protein of Cowpea mosaic virus. *J. Gen. Virol.* **85**: 3787-3796.

Russinova, E., Borst, J.W., Kwaaitaal, M., Cano-Delgado, A., Yin, Y., Chory, J., de Vries, S.C. (2004) Heterodimerization and endocytosis of *Arabidopsis* brassinosteroid receptors BRI1 and AtSERK3 (BAK1). *Plant Cell*. **16**: 3216-3229.

Hink, M.A., Visser, N.V., Borst, J.W., van Hoek, A., Visser, A.J.W.G. (2003) Practical use of corrected fluorescence excitation and emission spectra of fluorescent proteins in Förster Resonance Energy Transfer (FRET) studies. *J. Fluoresc.* **13**: 185-188

Verkhusha, V.V., Pozhitkov, A.E., Smirnov, S.A., Borst, J.W., van Hoek, A., Klyachko, N.L., Levashov, A.V., Visser, A.J. (2003) Effect of high pressure and reversed micelles on the fluorescent proteins. *Biochim. Biophys. Acta*. **1622**: 192-195.

Hink, M.A., Borst, J.W., Visser, A.J. (2003) Fluorescence correlation spectroscopy of GFP fusion proteins in living plant cells. *Methods Enzymol.* **361**: 93-112.

Borst, J.W., Hink, M.A., van Hoek A., Visser, A.J.W.G. (2003) Multiphoton microspectroscopy in living plant cells. *Proc. SPIE* **4963**: 231-238.

Borst, J.W., Uskova, M.A., Visser, N.V., Visser, A.J.W.G. (2002) Imaging of oxidative stress in plant cells by quantitative fluorescence microscopy and spectroscopy. In: *Fluorescence Spectroscopy, Imaging and Probes, New Tools in Chemical, Physical and Life Sciences* (Kraayenhof, R., Visser, A.J.W.G., and Gerritsen, H.C., Eds.) Springer Series on Fluorescence, Methods and Applications, Vol. 2, Springer Verlag, Heidelberg, pp. 337-348

Visser, N.V., Hink, M.A., Borst, J.W., van der Krogt, G.N., Visser, A.J. (2002) Circular dichroism spectroscopy of fluorescent proteins. *FEBS Lett.* **521**: 31-35.

Uskova, M.A., Borst, J.W., Hink, M.A., van Hoek, A., Schots, A., Klyachko, N.L., Visser, A.J. (2000) Fluorescence dynamics of green fluorescent protein in AOT reversed micelles. *Biophys. Chem.* **87**: 73-84.

Borst, J.W., Visser, N.V., Kouptsova, O., Visser, A.J.W.G. (2000) Oxidation of unsaturated phospholipids in membrane bilayer mixtures is accompanied by membrane fluidity changes. *Biochim Biophys Acta*. **1487**: 61-73.

Hink, M.A., Griep, R.A., Borst, J.W., van Hoek, A., Eppink, M.H., Schots, A., Visser, A.J. (2000) Structural dynamics of green fluorescent protein alone and fused with a single chain Fv protein. *J. Biol. Chem.* **275**: 17556-17560.

van der Knaap, J.A., Borst, J.W., van der Vliet, P.C., Gentz, R., Timmers, H.T.(1997) Cloning of the cDNA for the TATA-binding protein-associated factorIII170 subunit of transcription factor B-TFIID reveals homology to global transcription regulators in yeast and *Drosophila*. *EMBO J.* **94**: 11827-11832.

Pap, E.H., Ketelaars, M., Borst, J.W., van Hoek, A., Visser, A.J. (1996) Reorientational properties of fluorescent analogues of the protein kinase C cofactors diacylglycerol and phorbol ester. *Biophys. Chem.* **58**: 255-266.

Pap, E.H., van den Berg, P.A., Borst, J.W., Visser, A.J. (1995) The interaction between protein kinase C and lipid cofactors studied by simultaneous observation of lipid and protein fluorescence. *J. Biol. Chem.* **270**: 1254-1260.

Cnubben, N.H., Peelen, S., Borst, J.W., Vervoort, J., Veeger, C., Rietjens, I.M. (1994) Molecular orbital-based quantitative structure-activity relationship for the cytochrome P450-catalyzed 4-hydroxylation of halogenated anilines. *Chem. Res. Toxicol.* **7**: 590-598.

Pap, E.H., Bastiaens, P.I., Borst, J.W., van den Berg, P.A., van Hoek, A., Snoek, G.T., Wirtz, K.W., Visser, A.J. (1993) Quantitation of the interaction of protein kinase C with diacylglycerol and phosphoinositides by time-resolved detection of resonance energy transfer. *Biochemistry.* **32**: 13310-13317.

Bastiaens, P.I., Pap, E.H., Borst, J.W., van Hoek, A., Kulinski, T., Rigler, R., Visser, A.J. (1993) The interaction of pyrene labeled diacylglycerol with protein kinase C in mixed micelles. *Biophys. Chem.* **48**: 183-191.